ELSEVIER

open access

materialstoday

www.materialstoday.com

JULY/AUGUST 2013 | VOLUME 16 | NUMBERS 7–8

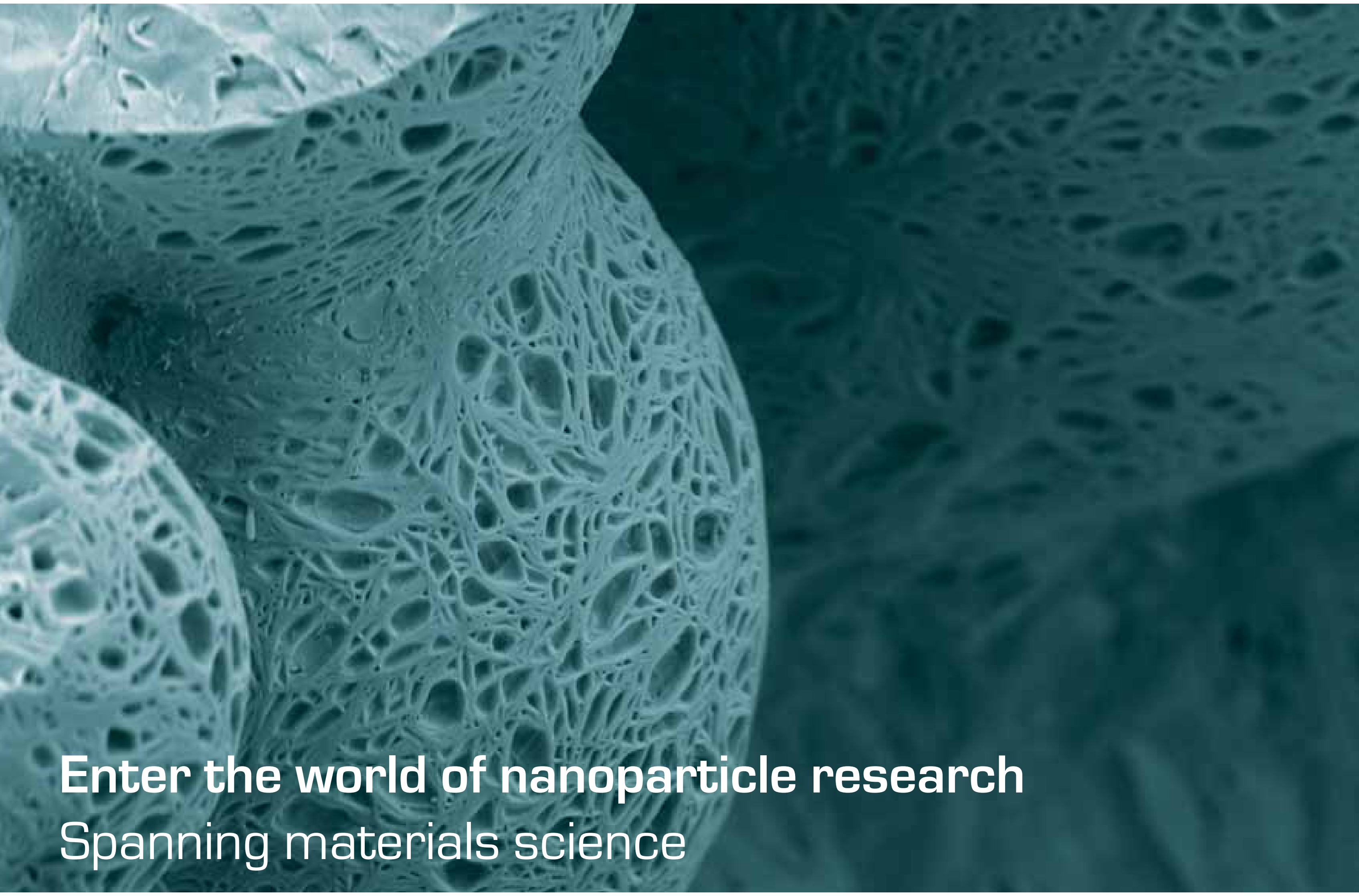

Enter the world of nanoparticle research

Spanning materials science

Liming Dai on high–performance supercapacitors

An introduction to modern "plastic" solar cells

Jennifer Cha discusses applications of DNA

ELSEVIER
keeping you informed...
materialstoday
Up close and personal with atoms and molecules
Probing more than the surface
materialstoday
www.materialstoday.com SEPTEMBER 2009 | VOLUME 12 | NUMBER 9
Nano biosensors
Now you see them, now you don't
materialstoday
www.materialstoday.com OCTOBER 2009 | VOLUME 12 | NUMBER 10
Materials for sensing and diagnosis
Towards a miniaturized mechanical surgeon
materialstoday
www.materialstoday.com NOVEMBER 2009 | VOLUME 12 | NUMBER 11
Energy uncovered
Reactor design and modelling, the new blue print
ScienceDirect

ELSEVIER

materialstoday

July/August 2013
Volume 16 Numbers 7–8
pp. 253–300

Read more about the cover image in this issue's *Uncovered* article. This year's cover competition is brought to you in association with Carl Zeiss. Visit www.zeiss.com/microscopy

REGULARS

ScienceDirect

MATERIALS TODAY
Published By
Elsevier Ltd.
The Boulevard, Langford Lane,
Kidlington, OX5 1GB, UK
Editorial
Editor: Stewart Bland
E-mail: s.bland@elsevier.com
Associate Editor: Mike Weir
E-mail: m.weir@elsevier.com
Editorial Assistant: Zara Preston
E-mail: z.preston@elsevier.com
Advertising
Advertising
Commercial sales
commercialsales@elsevier.com
Circulation enquiries
Lucy Rodzynska
E-mail: lucyrodzynska@elsevier.com
Elsevier Ltd.
The Boulevard, Langford Lane,
Kidlington, OX5 1GB, UK
Print subscription orders and payments
Materials Today (ISSN 1369-7021) is published 10 times per year by Elsevier Ltd. The Boulevard, Langford Lane, Kidlington, OX5 1GB, UK
Europe/ROW Tel: (+44) 1865 843434
USA Tel: (+1) 314 447 8878
Online: www.materialstoday.com/magazine-subscription

© 2013 Elsevier Ltd. All rights reserved

This journal and the individual contributions contained in it are protected under copyright by Elsevier Ltd, and the following terms and conditions apply to their use:

User rights
Articles published in this journal are made freely available on Elsevier's publishing platforms including ScienceDirect. Articles are protected by copyright and may be used for non-commercial purposes. Users may access, download, copy, display, redistribute, adapt, translate, text mine and data mine the articles provided that:

- They cite the article using an appropriate bibliographic citation (i.e. author(s), journal, article title, volume, issue, page numbers, DOI and the link to the definitive published version on ScienceDirect).
- They maintain the integrity of the article.
- They retain copyright notices and links to these terms and conditions so it is clear to other users what can and cannot be done with the article.
- They ensure that, for any content in the article that is identified as belonging to a third party, any re-use complies with the copyright policies of that third party.
- Any translations, for which a prior translation agreement with Elsevier has not been established, must prominently display the statement: "This is an unofficial translation of an article that appeared in an Elsevier publication. Elsevier has not endorsed this translation."

Use of published articles for commercial purposes is prohibited without permission. For permission to use published articles beyond the uses permitted here, visit www.elsevier.com/permissions.

Annual subscription price in the USA US$325 (valid in North, Central and South America), including air speed delivery.
Periodical postage paid at Rahway NJ and additional mailing offices.
Please send payment to: Materials Today
USA Postmaster send all USA address corrections to:
Orders, claims, and journal inquiries: please contact the Elsevier Customer Service Department nearest you:
St. Louis: Elsevier Customer Service Department, 3251 Riverport Lane, Maryland Heights, MO 63043, USA; phone: (877) 8397126 [toll free within the USA]; (+1) (314) 4478878 [outside the USA]; fax: (+1) (314) 4478077; e-mail: JournalCustomerService-usa@elsevier.com
Oxford: Elsevier Customer Service Department, The Boulevard, Langford Lane, Kidlington, Oxford OX5 1GB, UK; phone: (+44) (1865) 843434; fax: (+44) (1865) 843970; e-mail: JournalsCustomerServiceEMEA@elsevier.com
Tokyo: Elsevier Customer Service Department, 4F Higashi-Azabu, 1-Chome Bldg, 1-9-15 Higashi-Azabu, Minato-ku, Tokyo 106-0044, Japan; phone: (+81) (3) 5561 5037; fax: (+81) (3) 5561 5047; e-mail: JournalsCustomerServiceJapan@elsevier.com
Singapore: Elsevier Customer Service Department, 3 Killiney Road, #08-01 Winsland House I, Singapore 239519; phone: (+65) 63490222; fax: (+65) 67331510; e-mail: JournalsCustomerServiceAPAC@elsevier.com
Missing issues: Claims for missing issues should be made within six months of the date of dispatch. Responsibility cannot be accepted by the publisher after six months.

Notice
No responsibility is assumed by the Publisher for any injury and/or damage to persons or property as a matter of products liability, negligence or otherwise, or from any use or operation of any methods, products, instructions or ideas contained in the material herein. Because of rapid advances in the medical sciences, in particular, independent verification of diagnoses and drug dosages should be made. Although all advertising material is expected to conform to ethical (medical) standards, inclusion in this publication does not constitute a guarantee or endorsement of the quality or value of such product or of the claims made of it by its manufacturer.

Printed by Henry Ling, The Dorset Press, Dorchester, UK.
ISSN 1369-7021
Journal Number:03069

ScienceDirect

materialstoday

RESEARCH

Editorial Advisory Panel

Caroline Baillie
Queen's University, Canada
Zhenan Bao
Stanford University, USA
Alejandro Lopez Briseno
University of Massachsetts, USA
Chris Ewels
CNRS, France
Alan Heeger
University of California, USA
Suwan Jayasinghe
University College London, UK
Mark Johnson
Naval Research Laboratory, USA
David Kisailus
University of California, USA
Frederik Krebs
Technical University of Denmark, Denmark
Steven Lenhert
Florida State University, USA
Dan Luo
Cornell University, USA
Valeria Nicolosi
Trinity College, Dublin, Ireland
Tae Won Noh
The Korean Physical Society, South Korea
Aleksandr Noy
University of California, USA
Steve Pearton
University of Florida, USA
David Seidman
Northwestern University, USA
Yugang Sun
Argonne National Laboratory, USA
Helen Van Swygenhoven
Paul Scherrer Institute, Switzerland
George Whitesides
Harvard University, USA
Jackie Yi-Ru Ying
Institute of Bioengineering and Nanotechnology, Singapore

Materials Today • Volume 16, Numbers 7/8 • July/August 2013

Editorial

Stewart Bland

s.bland@elsevier.com

The call of the lab

Back to the benchtop

I would like to begin this issue's Editorial on somewhat of a mixed note, as I announce that Dr. Mike Weir, the Associate Editor of *Materials Today* has decided to step down from his role on the publication and return to the lab. I say this is a mixed note, as although all of us on *Materials Today* will miss Mike, our loss is academia's gain. I hope you will join me in thanking Mike for his work with us on *Materials Today*, particularly our webinar program, as well as his wider role as a publisher for a collection of our other titles here at Elsevier.

And so it seems appropriate to say a little about our recent and upcoming webinars, where you can hear a little bit more from Mike, before he heads back to the lab. If you didn't catch Part 1 of our series on New Innovations in Materials Characterization, then don't worry: you can find the first part here http://tinyurl.com/lo3tf3y, and the second part over here http://tinyurl.com/pdww7s7. The rest of the year is also now packed with upcoming webinars, so keep an eye on the website for our official announcements over at http://www.materialstoday.com/webinars/.

By the time you're reading this, I will likely be on my way to the 2013 ACS National Meeting in Indianapolis. If you will be attending, do drop by the Elsevier booth. And speaking of conferences, I'm happy to announce that the next *Materials Today Virtual Conference* has now been scheduled for the 19th–21st November 2013, focusing on Biomaterials http://www.materialstoday.com/virtual conference/materials-today-virtual-conference-biomaterials-2013. This is our first Virtual Conference to look specifically at biomaterials, so be sure to head over to the website now to register and submit your poster – remember, there's no fee to attend, so I hope to see you there!

But back to this issue, where we begin with a look at how collaborations between materials scientists and computer scientists are required to bring about the next generation of interactive devices. Moving on to review; we enter the fascinating world of nanoparticle research with Florian Heiligtag and Markus Niederberger, taking us on a journey through current research in this rapidly developing field. Second up, Chiechi, Havenith, Hummelen et al. provide us with an introduction to modern ''plastic'' solar cells, a broad topic that spans materials science, physics, and chemistry. Thirdly, Tao Chen and Liming Dai summarize recent progress on the development of high-performance supercapacitors based on carbon nanomaterials. And finally Jennifer Cha and colleagues discuss recent progress in how DNA has brought unmatched function to materials, focusing specifically on new advances in delivery agents, devices, and sensors.

Until next time, we hope you enjoy this issue of *Materials Today*.

Stewart Bland

1369-7021/06/$ - see front matter © 2013 Elsevier Ltd. All rights reserved. http://dx.doi.org/10.1016/j.mattod.2013.07.019

Comment

Anne Roudaut
University of Bristol, UK
roudauta@gmail.com

Sriram Subramanian
University of Bristol, UK
sriramable@gmail.com

Creating the future of interactive devices, together

Science fiction becomes a reality when materials science meets computer science

Envision a future in which the shape of interactive devices is not fixed but can dynamically reconfigure. Imagine downloading a game on your mobile phone and watching the device automatically reshape into a console by curling to facilitate grasping or by producing *pop-up* physical joysticks on its surface. Although one might expect to encounter such a future in science fiction, recent trends in research have shown that it is close to becoming science fact. The days of smartphones, and other interactive devices, looking like bricks is coming to an end and we are now entering an age where they are malleable and able to transform into arbitrary shapes on demand.

Shape-changing devices are not just for entertainment, they also enhance the interaction between the physical and digital world. Consider, for example, a shape-changing map in the classroom of the future. When learning about the formation of continents, mountain ranges or river systems, students will be able to physically interact with and mold surfaces in order to experience the effect of geological and environmental forces. At the heart of these capabilities is the emergent affordances and analytical reasoning that shape-changing devices provide. In everyday life we interact with objects of various forms (water bottles, pens, door handles and so on) whose specific shapes give us cues on where and how to grip, operate and interact with them. This is a notion that is often referred to as 'affordance' [1], meaning the properties of an object that tell us how it wants to be used or helps us to use it. Shape-changing devices provide emergent affordances by dynamically adapting the shape of an interactive device to generate appropriate physical cues for the user.

Currently there are several researchers within the Human Computer Interaction (HCI) community that are interested in designing, prototyping and evaluating such shape-changing devices to make this vision a reality. The Interaction and Graphics group of the University of Bristol has been exploring this through prototypes such as Morphees [2] or the TiltDisplay [3] that have been created as part of an on-going EU funded FET-Open project [4]. Realizing this vision, however, requires tackling lots of research challenges in materials science, engineering and HCI. For example, on the materials science side, breakthroughs in stable and accessible materials are required to create novel proof-of-concept devices; while on the HCI side, we need to have a deep appreciation for the material's properties, and thoroughly consider how those properties can provide affordances that unleash the human interaction potential. While these challenges are interesting for the respective research communities we believe that the true power of shape-changing devices can be magnified many-fold by bringing together the two communities. Through communication, collaboration and coordination of research, we can reach further and faster resulting in an acceleration of research that proves that both together can be much greater than the sum of their parts.

For example, smart memory alloys and electro-active polymer research in Europe have been developing apace, particularly in

1369-7021/06/$ - see front matter © 2013 Elsevier Ltd. All rights reserved. http://dx.doi.org/10.1016/j.mattod.2013.07.005

laboratory-based experiments that develop our understanding of the underlying fundamentals of such materials and showcase their abilities in proof-of-principle experiments. But most of the requirements for materials properties are derived from industrial requirements (like automation and transportation), which are very different from interactive device requirements. Typical proof-of-principle experiments from materials science often fail to consider the rich plethora of interaction possibilities afforded by the user. For instance, electro-active polymers have been shown to have high strain when actuated but typically suffer from low strength. While this may be a limitation in some industrial requirements, with good design they can be harnessed to create prototypes of interactive devices. But creating these designs requires the use of a user-centered design process (UCD), a research skill that is typical of HCI groups.

UCD involves end-users during the entire design, implementation and evaluation process and gathers device and material requirements not through a single requirement-gathering phase but through an iterative design process. This allows us to expose end-users to novel materials and elicit design suggestions by not only drawing on the benefits of new materials but also exposing the user to its potential limitations. These material properties which are seen as limitations can then be turned into strong design benefits of the device. Such is the case of the famous Post-it® Notes. The adhesive, created by Dr. Spence Silver at 3M, was too weak for any industrial applications, but a UCD process resulted in the creation of an application that turned the adhesive's limitation into a benefit.

In summary, starting from the vision of the ultimate display technology by Sutherland in 1965 [5], there has been a growing amount of literature on shape changing objects. The practical implementation of shape-changing interfaces is still far off (estimates range from 15 to 20 years) due to a lack of fundamental knowledge in creating interactive systems and in understanding the basic science of supporting interactions with such systems. We strongly believe that we have reached a point in the design of these devices where we need a real synergy between research teams from multiple fields, all involved to accelerate the realization of this vision. In other words our message is 'let's talk and work together!'.

Further reading

[1] Don A. Norman, The Psychology of Everyday Things. Basic Books, New York, 1988. In paperback as The Design of Everyday Things. Doubleday, New York, 1990.

[2] A. Roudaut, A. Karnik, M. Löchtefeld, S. Subramanian, Morphees: toward high "shape resolution" in self-actuated flexible mobile devices, in: Proceedings of the SIGCHI Conference on Human Factors in Computing Systems (CHI'13), ACM, New York, NY, USA, 2013, pp. 593–602.

[3] J. Alexander, A. Lucero, S. Subramanian, Tilt display demonstration: a display surface with multi-axis tilt & actuation, in: Proceedings of the 14th International Conference on Human–Computer Interaction with Mobile Devices and Services Companion (MobileHCI'12), ACM, New York, NY, USA, 2012, pp. 213–214.

[4] http://www.ghost-fet.com/.

[5] Ivan E. Sutherland, The ultimate display, in: Proceedings of IFIP Congress, 1965, pp. 506–508 (Retrieved 22.09.11).

News

Printing a tiny 3D battery

Tiny lithium-ion batteries, approximately the size of a grain of sand, that can be made layer by layer using a 3D printer could be used in microelectromechanical systems (MEMS), biomedical sensors and miniaturized medical implants, compact electronics, tiny robots and other applications, thanks to work by US teams.

The work by Jennifer Lewis, Shen Dillon and their colleagues at Harvard University and the University of Illinois at Urbana-Champaign could allow miniature devices previously constrained to the laboratory bench for lack of a powerful built-in power supply to become entirely portable [Sun et al., Adv. Mater. (2013) doi:10.1002/adma.201301036].

To print their three-dimensional electrodes, Lewis' group first created and tested several specialized 'inks' that would emerge from the printer nozzles as extruded material rather than a fine mist of droplets as with a conventional inkjet printer. The inks are based on nanoparticulate suspensions of lithium metal oxide compounds – lithium titanate (LTO) and lithium iron phosphate (LFP), for the anode and cathode respectively. Both of these substances show minimal volumetric expansion in use, the team points out. The extrudable inks are produced by suspending LTO and LFP particles in a solution composed of deionized water, ethylene glycol, glycerol, and cellulose-based thickening agents. The resulting inks not only solidify rapidly after exiting the nozzle they also have all the requisite electrochemical properties to create functional electrodes.

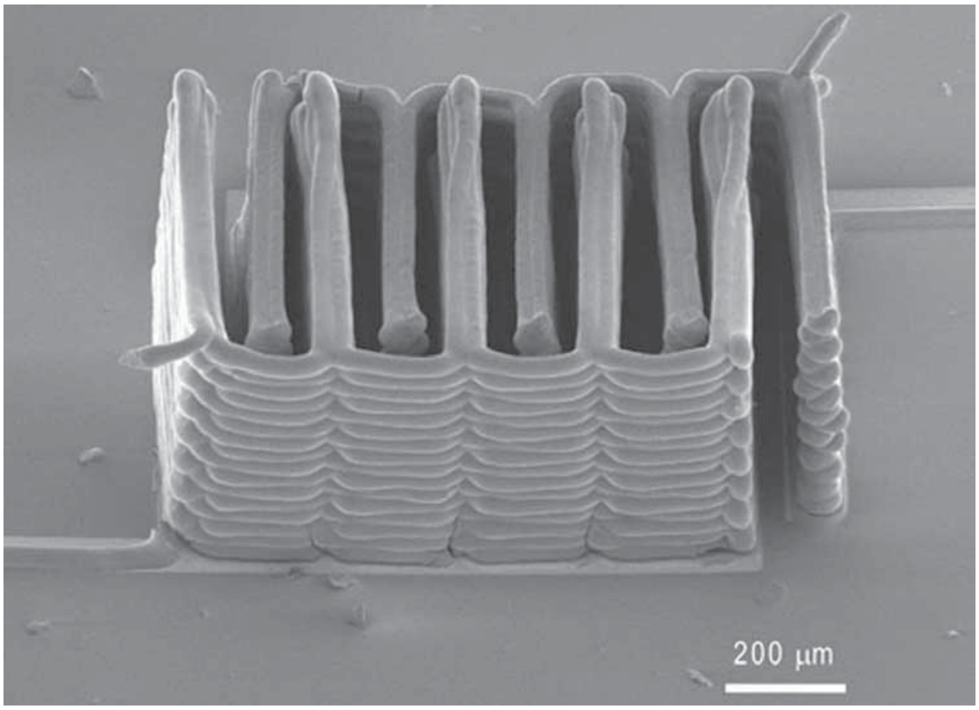

3D printing a battery. Credit: Ke Sun, Teng-Sing Wei, Bok Ahn, Shen J. Dillon, Jennifer Lewis.

'To print high aspect ratio electrode architectures, the composition and rheology of each ink must be optimized to ensure reliable flow through fine deposition nozzles, promote adhesion between the printed features, and provide the structural integrity needed to withstand drying and sintering without delamination or distortion', the team explains.

The 3D printer deposits the inks on to the teeth of two gold combs through 30 μm nozzles, creating a tightly interlaced stack of anodes and cathodes layer by layer. The microelectrode arrays are heated at 600°C in an inert gas to remove any organic residues and to promote sintering of the nanoparticles. The researchers could then package up this device into an insulating container and fill it with electrolyte solution to build a complete, but tiny rechargeable battery.

The team demonstrated that their batteries were comparable in electrochemical performance to commercial batteries in terms of charge and discharge rate, cycle life and energy densities. They big difference being only that these 3D printed batteries are 1000× smaller than the smallest commercial rechargeable battery on the market today.

David Bradley

1369-7021/06/$ - see front matter http://dx.doi.org/10.1016/j.mattod.2013.07.009

Poison gas puts a new spin on quantum computers

Researchers at the University of New South Wales, in Sydney, Australia have proposed a novel technique to distinguish between quantum bits, qubits, separated by only a few nanometers on a silicon substrate. The researchers are hoping that this finding might ultimately allow scientists to construct the first large-scale quantum computer.

Michelle Simmons explains that qubits based on the electron spin of phosphorus atoms on a silicon substrate represents a promising system for building a practical quantum computer, given that the technology for manipulating silicon is already in place thanks to half a century of the microelectronics industry. Moreover, such qubits have previously been shown to have remarkably long coherence and relaxation times. 'However, to be able to couple electron-spins on single atom qubits, the qubits need to be placed with atomic precision, within just a few tens of nanometers of each other,' Simmons says. 'This poses a technical problem in how to make them, and an operational problem in how to control them independently when they are so close together.'

Now, Simmons' team working with theorists at Sandia National Laboratories in New Mexico, USA, have found a way to overcome the various problems and have demonstrated that they can 'read' the spins of individual electrons on a cluster of phosphorus atoms placed precisely in silicon. First, to construct their device, they deposit a layer of hydrogen atoms on a silicon wafer and then create a pattern in this layer to expose the underlying silicon using a scanning tunneling microscope (STM) under ultra-high vacuum. They then exposed this patterned surface to phosphine gas (PH3) and annealed the device at 350°C to allow the phosphorus atoms to be incorporated precisely into the silicon surface. They then cover the patterned layer with a silicon encapsulation layer.

Distinguishing between the spins in each qubit separately is no mean feat but lead author Holger Büch suggests that if each electron is hosted by a different number of phosphorus atoms, then the qubits will respond to different electromagnetic fields – and each qubit can be distinguished from its neighbors. The team reports fidelity of 93%. However, they also point out that the difference in hyperfine coupling between the spin transitions in a single phosphorus atom compared with a pair of atoms clustered in the same qubit gives a read out error rate of about 1 in 10 000. This, they suggest, opens up the possibility of individual qubit addressability in a completely different way to previously thought possible [Büch et al., Nat. Commun. (2013) doi:10.1038/ncomms3017].

'This first demonstration where we can maintain long spin lifetimes of electrons on multi-donor systems is very powerful. It offers a new method for addressing individual qubits, putting us one step closer to realizing a practical, large-scale quantum computer,' Büch explains.

Simmons told *Materials Today* that, 'The next major step for silicon quantum computing is the development of a two qubit gate. Here we need to be able to read out two individual electron spin qubits and control their entanglement to perform a gate operation. There is an international race to realize this milestone.'

David Bradley

Volcanic drug delivery

US researchers have used three-dimensional nanolithography based on light scattering from colloidal particles to build what they refer to as nano-volcanoes that might be used to contain precise quantities of other materials, including pharmaceuticals.

Xu Zhang and colleagues at North Carolina State University have made their nano-volcanoes by first depositing spherical, transparent polystyrene particles (of a specific size between 350 and 1900 nm) directly on to a photoactive, spin-coated thin film of photoresist (Sumitomo PFi88A7) supported on a silicon substrate with an anti-reflection coating. They then shine ultraviolet light through the transparent spheres, which is scattered to form a pattern on the thin film. A quick rinse with a developer solution (Microposit CD-26) washes away parts of the film exposed to UV leaving behind the volcanic peaks.

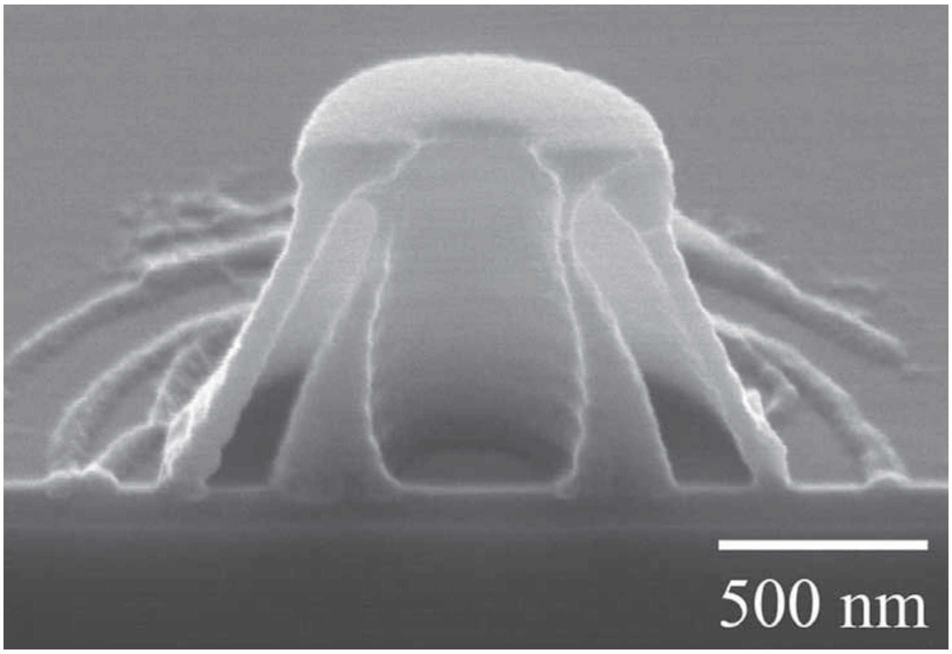

Carving 'nano volcanoes' by scattering light through polymer spheres. Credit: Chih-Hao Chang, North Carolina State University.

'We can control the pattern of light by changing the diameter of the nanoparticle spheres, or by changing the wavelength,' explains Zhang. 'That means we can control the shape and geometry of these structures, such as how big the cavity of the nano-volcano will be. Computer modeling allows them to predict with some precision the shape and size of the nano-volcanoes that will form based on these two factors – nanoparticle size and radiation wavelength.

Importantly, the hollow cores are precisely defined as are the openings to the nano-volcanoes, which means they can be selective for specific guest molecules, with release rate also controlled by these factors. The team is currently investigating the kinetics of the processes involved, and have trapped 50 nm silica nanoparticles as a model system. The nano-volcanoes can also be fabricated with layered, multiple-shell structures. However, their thickness is limited ultimately by how thick the thin layer can be made and allow UV light to penetrate adequately.

'The materials used in this process are relatively inexpensive, and the process can be easily scaled up,' adds team leader Chih-Hao Chang. 'In addition, we can produce the nano-volcanoes in a uniformly patterned array, which may also be useful for controlling drug delivery' [Zhang et al., ACS Nano (2013) doi:10.1021/nn402637a].

The same approach to light carving nano-volcanoes might also find use in creating other high surface area-to-volume ratio 3D structures for solar energy conversion, high-speed battery electrodes, photonic and phononic crystals as well as anti-reflection and self-cleaning surfaces.

Critically, the scattering particles need not be spherical. The use of other colloidal elements, of cubic, tetrahedral, and rod shape could be exploited to create a wide range of possible 3D nanostructures other than the sloping peaks of nano-volcanoes.

David Bradley

The heat is on for superconductors

A European team has at long last found an explanation for the apparently mysterious effect of the 'pseudogap' observed with high-temperature superconductors [K.B. Efetov et al., Nat. Phys. 9 (2013) 442–446].

Decades of research has yet to design such materials that work at ambient temperature but there are several 'high-temperature' superconductors that based on ceramic copper oxides rather than metals that are nudging the critical temperature higher and higher as the research develops. Konstantin Efetov and Hendrik Meier at Ruhr-Universität Bochum and Catherine Pépin of the Institute for Theoretical Physics in Saclay near Paris have calculated that there are two coexisting electron orders in such materials, which could explain why the threshold temperatures of these superconductors is so much farther from absolute zero – at around 138 K – than that seen in the metallic superconductors.

In the superconducting state, electrons travel in so-called Cooper pairs through the crystal lattice of the material. Energy is required to free the electrons from these couplings – the energy gap. In cuprate superconductors, with copper oxide bonds, there is an additional energy gap that exists above the critical, transition temperature, this is the pseudogap. The team points out that this pseudogap is usually only observed for electrons with certain velocity directions. Their new model offers insights into why this should be and offers hope of taking materials scientists another small to warmer climes in superconductor research.

According to the model, the pseudogap state simultaneously contains two electron orders: d-wave superconductivity, in which the electrons of a Cooper pair revolve around each other in a cloverleaf shape, and a quadrupole density wave. The latter is an electrostatic structure in which a quadrupole moment is induced on every copper atom in the two-dimensional crystal lattice has a quadrupole moment. The two – d-wave superconductivity and quadrupole density wave – compete with each other in the pseudogap state. However, thermal fluctuations mean that neither can predominate in the long range unless the system is cooled at which point one of the two systems prevails and superconductivity arises. This, according to the team, could happen at a balmier temperature than the standard transition temperatures for metallic superconductors.

'This phenomenon may help to explain the origin of the mysterious pseudogap state and of the high-temperature transition into the superconducting state in the cuprates. In particular, we show that spectroscopic probes on the oxygen and copper sites reveal chequerboard order,' the team concludes.

David Bradley

Polymer 'stars' for high-quality nanocrystals

A new way to produce high-quality nanocrystals using tiny star-shaped reaction vessels has been developed by researchers at Georgia Tech in the US [Nat. Nanotechnol. (2013) doi:10.1038/NNano.2013.85].

Over the past decade, colloidal nanocrystals have found applications in many fields including drug delivery, electronics and catalysis, and so efforts to produce high-quality crystals have gained momentum. Existing techniques are reliable, but often time-consuming, requiring tightly defined experimental conditions such as multistep reactions and purifications. And each of the established techniques, such as sol–gel processes, can only produce a single type of nanocrystal, limiting their applicability.

A *Nature Nanotechnology* paper from a team of materials scientists at Georgia Tech has reported on a new route to producing high-quality nanocrystals using star-shaped block co-polymer structures as reaction vessels. The team have produced nearly monodisperse magnetic, metallic, ferroelectric, semiconductor and luminescent colloidal nanocrystals, all using these tiny star-shaped vessels.

The co-polymer 'stars' consist of a central beta-cyclodextrin core to which multiple "arms" – as many as 21 linear chains of poly(acrylic) acid (PAA) – are covalently bonded. Together, they form the aggregate of molecules that serve as a reaction vessel and template for the formation of the nanocrystals.

In this technique, the size of the nanocrystals (between a few nanometers and tens of nanometers) is determined by the length of the hydrophilic PAA chain. More surprisingly was the team's finding that the volume ratio of the two solvents – dimethlformamide and benzyl alcohol – had a profound influence on the shape uniformity of the nanocrystals. For lead titanate (PbTiO3), a solvent ratio of 9:1 was found to produce a dispersion with a size distribution within 5% of the average size.

Zhiqun Lin and his team further tailored the technique to produce plain, core–shell and hollow nanoparticles that can be made soluble either in organic solvents or water – leading to an interest from biomedical researchers. The colloidal dispersions of these nanocrystals were also found to be stable and homogenous over long durations – as much as two years – without any sign of precipitation

The versatility and robustness of this technique, and the stability of the nanocrystals produced has already won the team wide acclaim, but Ling hopes to extend it further to include more complex structures such as nanorods and crystals with multifunctional shells.

Laurie Winkless

Atomic circuitry for electronic sandwiches

US scientists at Rice University and Oak Ridge National Laboratory (ORNL) have grown uniform atomic layers of molybdenum disulfide paving the way for two-dimensional electronics.

Jun Lou, Pulickel Ajayan and Boris Yakobson of Rice and colleagues Wu Zhou and Juan-Carlos Idrobo at ORNL used chemical vapor deposition (CVD) to grow an atomic layer of the material on silicon oxide. The resulting material can then be transferred to the well-known zero-band carbon material graphene and insulating hexagonal boron nitride with the potential for fabricating tiny field-effect transistors [Lou et al., Nat. Mater. doi:10.1038/nmat3673].

Previously, Lou and Ajayan intertwined graphene and hexagonal boron nitride, but to produce a working electronic sandwich they needed a semiconductor layer, which is where molybdenum disulfide offers a tasty solution.

''Two-dimensional materials have taken off,'' Ajayan explains. ''The study of graphene prompted research into a lot of 2D materials; molybdenum disulfide is just one of them. Essentially, we are trying to span the whole range of band gaps between graphene, which is a semi-metal, and the boron nitride insulator.''

MDS distinguishes itself from graphene and boron nitride in that viewed from ''above'' it looks like a flat layer of hexagons, however, the molybdenum atoms form a layer between two layers of sulfur atoms.

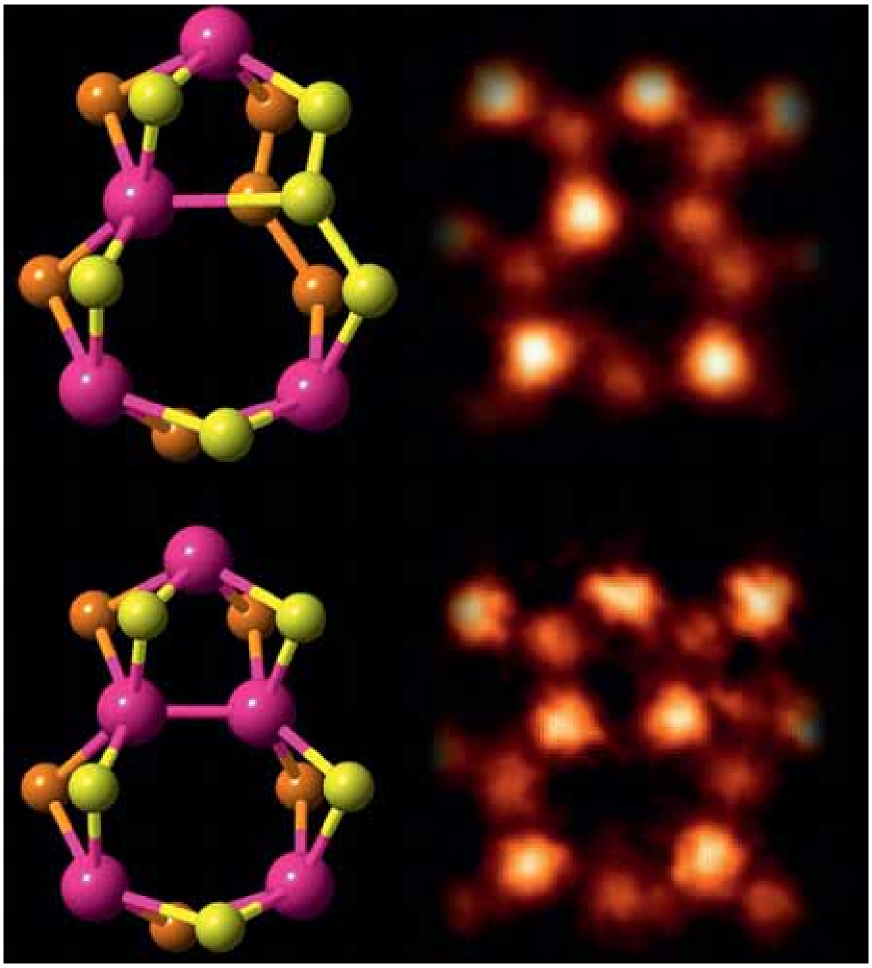

Schematics and experimental images show defects in two-dimensional samples of molybdenum disulfide. Credit: Oak Ridge National Laboratory.

Nevertheless, a monolayer of this material would not detract from the 2D aims of the team. The difficulty arises in that all three components the team would like to sandwich together are grown in very different environments. The team noticed that in the CVD furnace patches of molybdenum disulfide form as ''islands'' even where defects or impurities are present on the substrate. ''The material is difficult to nucleate, in other words, unlike hexagonal boron nitride or graphene,'' Najmaei explains. ''We started learning that we could control that nucleation by adding artificial edges to the substrate, and now it's growing a lot better between these structures.'' With this knowledge the team has thus been able to grow grain sizes as large as 100 μm across.

The ORNL team then used aberration-corrected scanning transmission electron microscopy to obtain images of these islands. Theoretical physicist Yakobson and his team then analyzed the atomic energy levels to examine the impact of defects and impurities on the characteristics of the molybdenum sulfide islands. While the initial aim is to create 2D electronic devices, the team also recognizes that these unique materials, with their varied electronic properties and band gaps might also be stacked together to form ''van der Waals solids''. ''We could put them together in whatever stacking order we need, which would be an interesting new approach in materials science,'' Ajayan adds. ''Creating hetero structures of these 2D materials is exactly what we are focusing on right now,'' Lou told *Materials Today*.

David Bradley

Nanostructured catalyst to improve fuel cells

Scientists in Germany have developed a robust catalyst material that could be incorporated into new devices for stationary, portable or automotive hydrogen-powered fuel cells, potentially leading to a range of innovations in energy conversion and storage. The metallic catalyst particles used in the conversion process – platinum–nickel nano-octahedra – achieve this from only a tenth of the standard amount of platinum previously required, making the material efficient and relatively cheap to produce.

At the moment, the implementation of the more environmentally friendly hydrogen fuel cells is being constrained by the excessively high cost of platinum, which is needed for the electrodes in the fuel cells at which the chemical conversion processes take place. The catalytic effect of the platinum is necessary to achieve the required conversion rates. However, the team, from Forschungszentrum Jülich and Technische Universität Berlin, suspected that platinum–nickel alloy nanoparticles could be an ideal catalyst for fuel cells due to their predicted high activity for the conversion of hydrogen and oxygen to water.

The study, which was published in the journal Nature Materials [Cui et al., Nat. Mater. (2013) doi:10.1038/nmat3668], used ultrahigh-resolution electron microscopy to show that the function of the nanometer-scale catalyst particles is determined by both their geometric shape and atomic structure. When a beam from the microscope was sent through a specimen and, due to interactions, loses some of its energy, and the identification of the location of each element becomes possible, with atomic precision. Standard electron microscopes cannot detect these chemical signatures so accurately.

With catalysis happening only at the surface of the platinum, the material can be retained and also, significantly, the efficiency of the electrodes is improved through the use of the platinum nanoparticles – which in turn increases the ratio of platinum surface to material required. In addition, further amounts of platinum can be saved if it is combined with less valuable metals, such as nickel or copper.

As researcher Professor Peter Strasser of the Technische Universität Berlin claims, the study 'provides direct evidence. . .that the choice of the correct geometric shape for the catalyst particles is as important for optimizing their function as the choice of their composition and size. This provides researchers with new possibilities for further improving functional materials, especially catalysts, for energy storage.' Going forward, it is now crucial for the team to improve the stability of such catalysts.

Laurie Donaldson

Bioadhesive nanoparticles show promise for drug delivery

A newly developed bioadhesive coating for nanoparticles can substantially improve their intestinal absorption into the bloodstream, offering potential for protein-based medicines such as insulin to be taken orally rather than by injection, according to a new study from Brown University. It was shown that, if the bioerodible nanoparticles are coated correctly, it can enhance their uptake, potentially leading to tailored particles that move to specific tissues in the body and paving the way for targeted oral medicines.

To achieve this feat, it is crucial the nanoparticles can move safely through the acidity of stomach to the small intestine so that they can be absorbed and then deliver their drug load into the bloodstream. The bioadhesive coating was found to significantly increase the intestinal uptake of polymer nanoparticles in the laboratory.

The study, reported in the *Journal of Controlled Release* [Reineke et al., J. Controlled Release (2013) doi:10.1016/j.jconrel.2013.05.043], used a coating of a chemical called PBMAD that had been shown to have bioadhesive properties and could withstand the acids in the stomach before dissolving. To test the coating, particles made of two separate plastics were used: polystyrene and PMMA. Doses of each particle were injected into the intestines of rats to gauge if they would be absorbed and where they would end up if they did so. Around two-thirds of the PBMAD-coated particles were absorbed, just under half of the polystyrene particles and only 1.9% of the uncoated PMMA particles.

The nanoparticles also spread differently about the body, with the majority of the polystyrene particles absorbed going to the liver, while another 10% went to the kidneys. Both coated and uncoated PMMA particles went to a much wider variety of tissues, although in different distributions.

The good uptake of the polymeric carrier means they would expect the drugs to have good oral bioavailability as well. As study leader, Edith Mathiowitz, points out, this shows they have ''developed safe and reproducible methods to encapsulate proteins in tiny nanoparticles without compromising their biological activity.''

However, the group still need to show the actual delivery of protein-based medicines in high enough quantities to desired tissues. The group has applied for a patent related to the work, and now intend to repeat the studies with drugs that have been encapsulated into bioadhesive particles to gain a better understanding of how the body takes up these particles.

Laurie Donaldson

New mapping approach identifies defects in solar cells

A team of researchers from Ludwig-Maximilians-Universität München (LMU) in Germany has developed a new method for visualizing material defects in organic thin-film solar cells. It works by functionally characterizing the active layer with the aid of laser light to achieve localized excitation of the semiconducting material.

Their new approach used raster scanning with a laser, with the focused beam being modulated in different ways; such as a rotating attenuator which enabled them to directly map the spatial distribution of defects in organic thin films, something never previously achieved.

Solar cells convert sunlight into electrical power based on the ability of light to excite molecules, thereby producing free electrons and positively charged 'holes', with the length of time it takes for the holes to be extracted by the electrodes being dependent on the structure of the active layer of the cell. If there are defects in the arrangement of the atoms, it behaves like a short-term trap for the charge carriers, reducing the size of the available current.

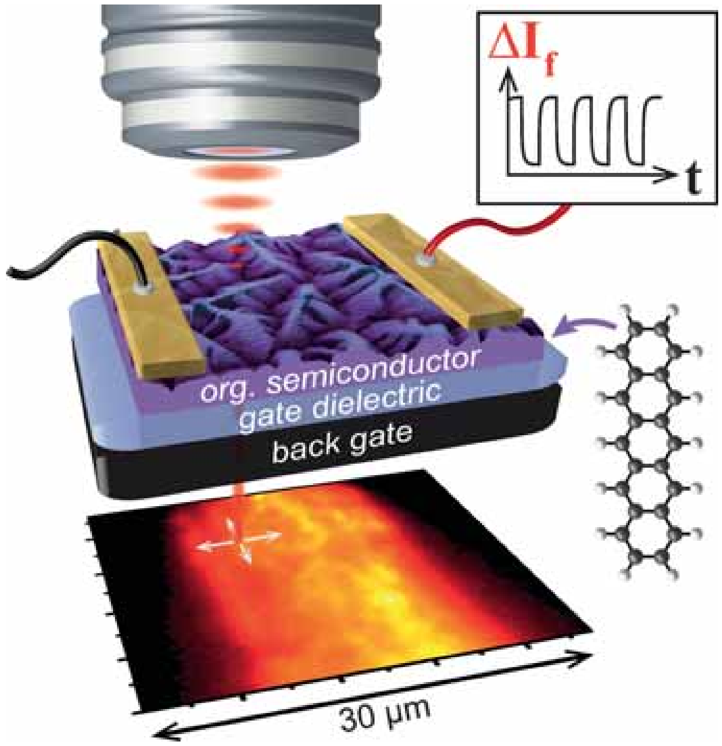

Mapping the distribution of defect density in organic thin films. Source: Christian Westermeier.

This study, reported in the journal Advanced Materials [Westermeier et al., Adv. Mater. (2013) doi:10.1002/adma.201300958], examined a thin pentacene layer in which the majority of charge carriers are positively charged holes, showing how changes in current flow by the localized excitation of defects from laser light can be identified. When a voltage was applied to a metallic back contact, the traps in the material are either filled or emptied in a controllable way, via the field effect. If the frequency of the laser light is modulated, it is possible to determine the temporal dynamics of trap states.

This approach allowed them to image trap states that can interact with the mobile carriers. It is hoped that this will allow them to identify the origin of the traps, or at least help to confirm the effect of the different preparation methods on the distribution of traps. As study leader Bert Nickel points out, 'It would be interesting to know what is special about the surface layer at these hot spots. What produces defects at these sites? They could be due to chemical contaminants or to irregularities in the alignment of the molecules.'

The team now plans to investigate complete solar cells, which consist of a hole-conducting film that is in direct contact with an electron-conducting layer, and organic heterojunctions, the structural backbone of organic solar cells.

Laurie Donaldson

Quantum processor solves optimization problems

A team of scientists from the University of Southern California (USC) in the United States has successfully validated the operational effectiveness of a prototype quantum processor. Their research findings suggest that the device can be used to solve optimization problems, and has the potential for scaling up quantum computing to offer much faster processing power than currently achievable.

The study, which was published in the journal Nature Communications [Boixo et al., Nat. Commun. (2013) doi:10.1038/ncomms3067], confirmed that quantum mechanics plays a functional role in how this first-of-its-kind process or works. The quantum chip, developed by Canadian manufacturer D-Wave, has 108 functional qubits (quantum bits) and is the first commercial quantum optimization processor. Although a variety of such processors have previously been made, they mostly operate on a smaller scale and have fewer qubits. Qubits, a unit of quantum information, are able to encode the digits of one and zero simultaneously, called a "superposition", compared to the distinct coding of either a one or zero carried out by traditional bits.

It is hoped that this superposition and the ability of quantum states to effectively tunnel through energy barriers will be key to the development of a new generation of processors that can carry out faster optimization calculations. Sergio Boixo, first author on the study, said "Our work seems to show that, from a purely physical point of view, quantum effects play a functional role in information processing in the D-Wave processor."

In addition, the device was found not to be constrained by the problem of decoherence, a mechanism which could have prevented it from behaving in a quantum way. Decoherence can be such an issue that the Quantum Computing Center, where D-Wave is housed, uses a magnetically shielded box that is maintained at temperatures near absolute zero to protect the processor against its effects.

Also, as researcher Daniel Lidar points out, they "have verified that the D-Wave processor performs optimization calculations (that is, finds lowest energy solutions) using a procedure that is consistent with quantum annealing and is inconsistent with the predictions of classical annealing." Quantum annealing helps to solve optimization problems with quantum mechanics on a large scale.

The team have undertaken a recent upgrade to the original D-Wave processor and, with a new 512-qubit chip now in place, they are planning to test the new chip to see if it can match up to its predecessor.

Laurie Donaldson

Materials Today • Volume 16, Numbers 7/8 • July/August 2013 RESEARCH

RESEARCH: Review

The fascinating world of nanoparticle research

Florian J. Heiligtag and Markus Niederberger*

Laboratory for Multifunctional Materials, Department of Materials, ETH Zurich, Wolfgang-Pauli-Strasse 10, 8093 Zurich, Switzerland

Nanoparticle research is a fascinating branch of science. The strongly size-related properties of nanoparticles offer uncountable opportunities for surprising discoveries. The often unexpected and unprecedented behavior of nanoparticles bears great potential for innovative technological applications, but also poses great challenges to the scientists. They have to develop highly controllable synthesis approaches, more sensitive characterization tools and finally new models and theories to explain the experimental observations. In this review, we discuss a personal selection of papers dedicated to nanoparticle research, which we believe provide an illustrative overview of current research directions in this rapidly developing field. We have structured the text in five sections: introduction, nanoparticle synthesis, formation mechanisms, nanoparticle assembly, and applications. The chosen examples within these sections are not directly related to each other, but reflect the remarkable broadness of nanoparticle research covering historical aspects, basic and applied science as well as commercial applications.

Introduction

Nanoparticles have a surprisingly long history. Their preparation is neither an exclusive result of modern research nor restricted to man-made materials. Naturally occurring nanoparticles include organic (proteins, polysaccharides, viruses, among others) as well as inorganic compounds (iron oxyhydroxides, aluminosilicates, metals, among others) and are produced by weathering, volcano eruptions, wildfires or microbial processes [1,2]. Nanoparticles are not necessarily produced by modern synthesis laboratories, but have obviously existed in nature for a long time, and therefore their use can be traced back to ancient times. While the application of clay minerals as natural nanomaterials does not seem to be very sophisticated, the controlled reinforcement of a ceramic matrix with natural asbestos nanofibers more than 4500 years ago is more intriguing [3]. However, the most spectacular effects were obtained with metal nanoparticles as color pigments in luster and glass technology [4,5]. Metallic luster decorations of glazed ceramics appeared in Mesopotamia during the 9th century [6]. These decorations showed amazing optical properties due to the presence of separate silver and/or copper nanoparticles dispersed within the outermost layers of the glaze [6]. The example in Fig. 1a displays iridescence under specular reflection with shiny blue and green colors. Transmission electron microscopy (TEM) analysis revealed a double layer of silver nanoparticles with smaller sizes (5–10 nm) in the outer layer and larger ones (5–20 nm) in the inner layer (Fig. 1b). The distance between the two layers is constant at about 430 nm, giving rise to interference effects (Fig. 1c) [6]. The light scattered by the second layer has a phase shift with respect to the one scattered by the first layer, and because the phase shift depends on the wavelength of the incoming light, each wavelength is scattered differently.

Metal nanoparticles are able to color glass in an extraordinary way. Gold has been used for a long time to introduce a striking red color to glass. One of the finest examples of such ruby glass is the Lycurgus Cup in the British Museum (Fig. 2a). Manufactured by Romans in the fourth century it appears with a green color in daylight (Fig. 2a, left), but changes to red (Fig. 2a, right), when illuminated from the inside [7,8]. An interesting fact about the use of gold nanoparticles in ruby glass is that after the Romans the technology was forgotten, and was only rediscovered in Europe in the seventeenth century. Although the birth of gold-based glass and enamel colors is ascribed to Andreas Cassius, who

---

**Corresponding author:*. Niederberger, M. (markus.niederberger@mat.ethz.ch)

1369-7021/06/$ - see front matter © 2013 Elsevier Ltd. All rights reserved. http://dx.doi.org/10.1016/j.mattod.2013.07.004

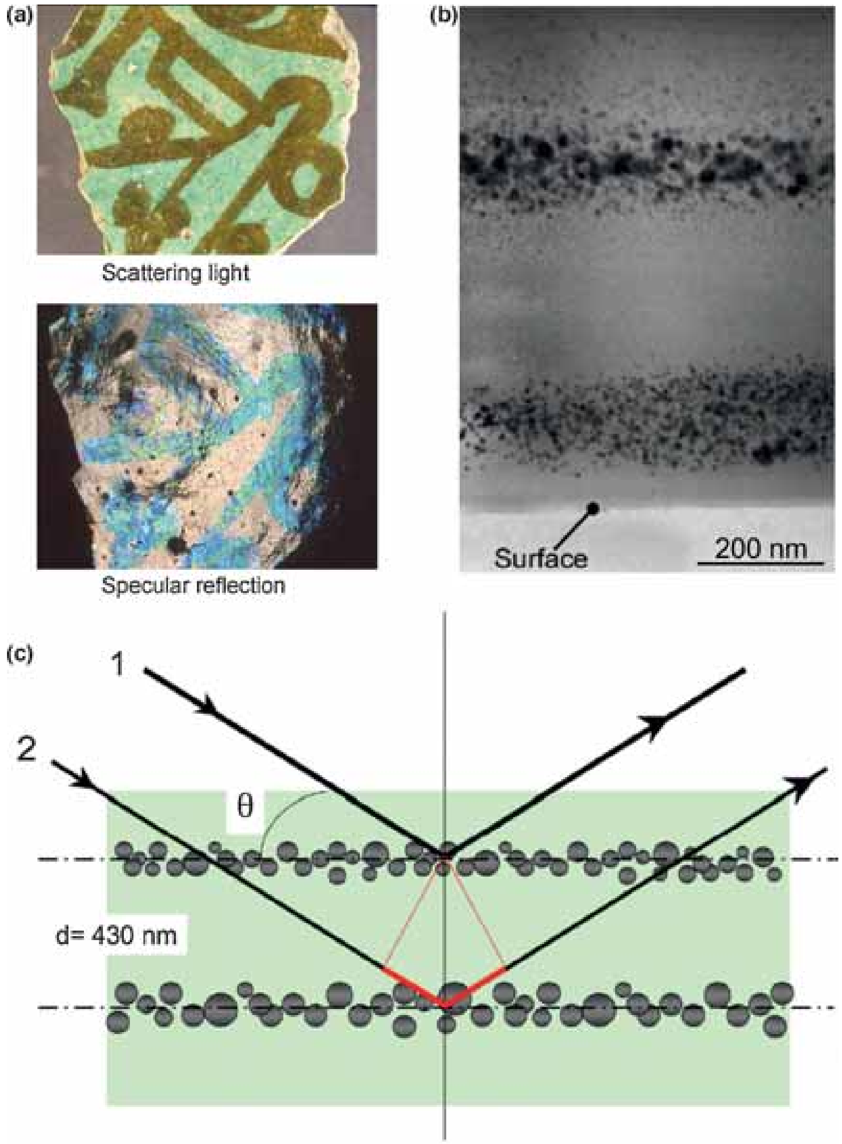

FIGURE 1

(a) Photograph of a medieval piece of a glazed ceramic observed by scattered light and specular reflection. (b) TEM image of the double layer of silver nanoparticles. (c) Schematic representation of interference phenomena due to the double layer. Reproduced from Ref. [6] with permission of Trans Tech Publications and Dr. Philippe Sciau.

subsequently received the name Purple of Cassius, the preparation of colloidal gold with a tin compound had been described several years earlier by Johann Rudolph Glauber [9]. However, there is no evidence that Glauber ever applied his knowledge to the coloring of glass. It was Johann Kunckel, who ran a glass factory in Potsdam between 1679 and 1689, that successfully used the purple precipitate to produce ruby glass (Fig. 2b) [9]. From a scientific point of view, the next big step forward in nanoparticle research was made by Michael Faraday approximately 150 years ago. As a matter of fact, his systematic studies on the interaction of light with metal nanoparticles can be regarded as the beginning of modern colloid chemistry and the emergence of Nanoscience and Nanotechnology [10]. In 1857 he presented his work on 'Experimental Relations of Gold (and other Metals) to Light' to the Royal Society of London [11]. Faraday prepared his colloidal gold dispersions in a two-phase system consisting of an aqueous solution of a gold salt and a solution of phosphorus in carbon disulfide. After a short reaction time the bright yellow color of the $Na[AuCl_4]$ solution turned into a ruby color characteristic of gold nanoparticles (Fig. 2c).

The principle motivation to perform research on nanoparticles is founded in the so-called quantum size effect. Metal and semiconducting nanoparticles just a few nanometers in diameter, and thus with sizes somewhere between single atoms/molecules and bulk materials, show pronounced size- (and also shape-) dependent electronic and optical properties [12–14]. The observation of such size effects raised expectations for the superior performance of nanomaterials compared to their bulk counterparts in many applications, if the size and the shape of the particles can be optimized in a rational way. Systematic work on the photocatalytic properties of colloidal CdS [15,16] resulted in the description of the quantum size effect at the beginning of the 1980s. Brus *et al.* found that CdS crystallites in the size range of a few nanometers did not have the electronic spectra of the bulk material, even though they exhibited the same unit cell and bond length as the

FIGURE 2

(a) The Lycurgus Cup in reflected (left) and in transmitted (right) light. © Trustees of the British Museum. (b) Beaker with lid attributed to Johann Kunckel using the purple preparation of gold chloride and stannous hydroxide later to be associated with the name of Andreas Cassius. *Source*: http://de.wikipedia.org/wiki/Johannes_Kunckel. (c) Five original bottled samples prepared by Michael Faraday. *Source*: http://aveburybooks.com/faraday/catalog.html. Reprinted with permission of Prof. Ryan D. Tweney (Bowling Green State University) and Prof. Frank James (Royal Institution).

bulk material [17]. These findings opened up a new and exciting possibility to tailor the chemical and physical properties of a material: new applications and properties as a result of controlling crystallite size and shape on a nanometer scale rather than by altering the composition [14]. Consequently, the development of advanced synthesis routes not only offering control over the composition, as typically required for traditional bulk synthesis, but also over particle size, size distribution, shape and surface properties became essential on the way to study and apply the size-dependent properties of nanomaterials.

Nanoparticle synthesis

After several decades of intense research effort, it is apparent that a large number of synthesis approaches to a great variety of nanoparticles are available. Here we will exclusively focus on liquid-phase routes. In addition, due to space limitations, we restrict the number of the examples to just a few that are representative for a specific class of materials and that are still frequently used. A more comprehensive overview of solution routes to nanoparticles is given in Ref. [18].

When it comes to the synthesis of gold nanoparticles, probably the most convenient and widely used synthesis technique is the so-called citrate route developed by Turkevich *et al.* more than 60 years ago [19]. The reaction is very simple and involves just gold chloride, sodium citrate as a reducing and stabilizing agent and water as a solvent. The obtained gold nanoparticles exhibit a spherical morphology (Fig. 3a) with a relatively narrow size distribution (20 ± 1.5 nm) [19]. Although the citrate route is still very popular for the preparation of aqueous gold nanoparticle sols, many other approaches have been developed, performed in specific organic solvents or in the presence of different types of surfactants and reducing agents to fine-tune the morphology from nanocubes (Fig. 3b) to hexagonal shapes (Fig. 3c), nanorods (Fig. 3d) and nanostars (Fig. 3e) [20,21]. Interestingly, all these nanoparticles have different optical properties. In the case of gold nanorods with varying aspect ratios (Fig. 3f), this effect is visible to the naked eye [22]. The optical absorption spectra show a shift of the band at longer wavelengths, corresponding to the absorption and scattering of light along the long axis of the nanorods, from the visible to near infrared with increasing lengths, and the color

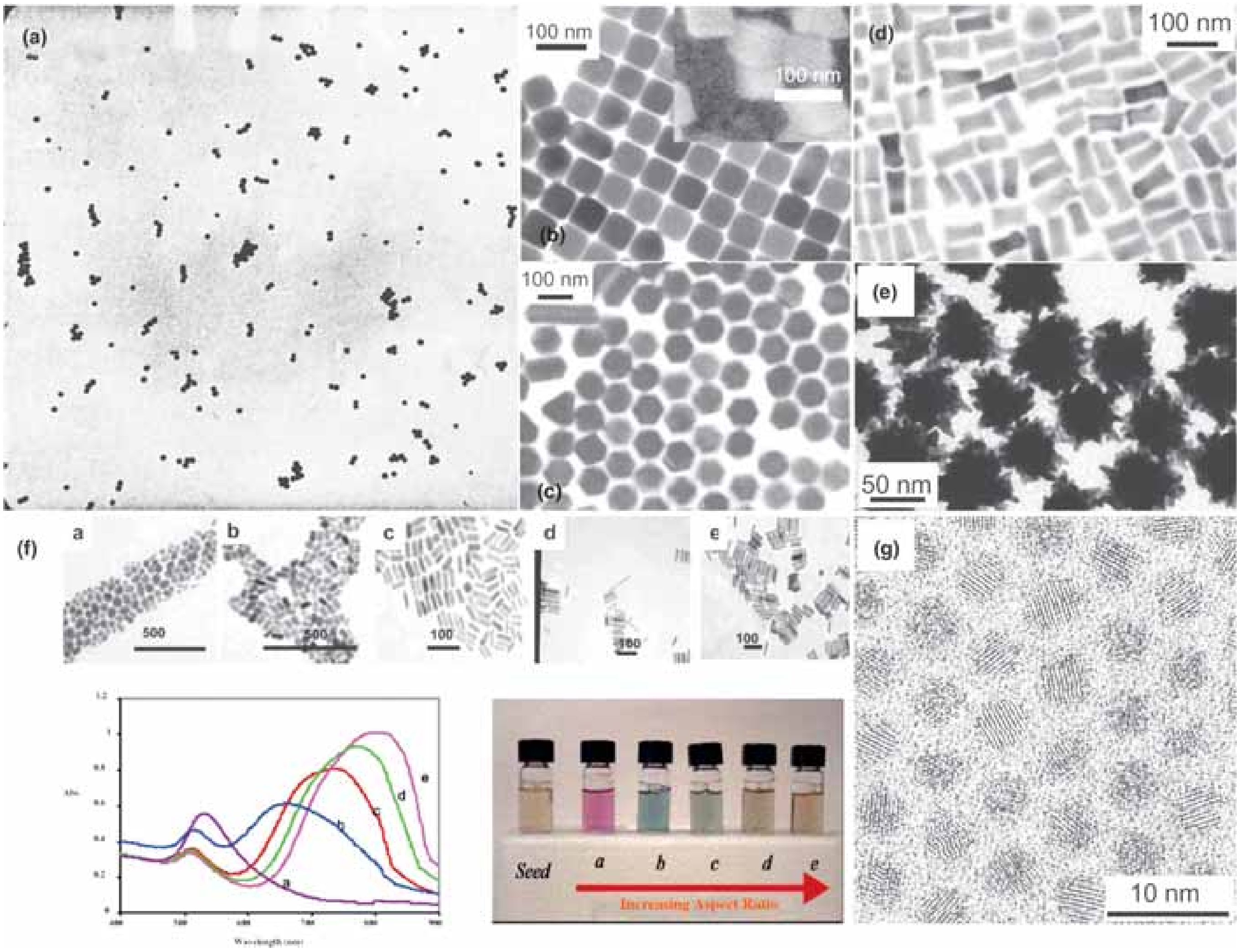

FIGURE 3

(a) Electron micrograph of a gold sol prepared by the citrate route. Reproduced from Ref. [19] with permission from The Royal Society of Chemistry. (b)–(e) TEM images of gold nanoparticles with different shapes. Reprinted with permission from Refs. [20,21]. Copyright 2004/2010 American Chemical Society. (f) TEM images of gold nanoparticles with increasing aspect ratios from a to e, corresponding absorption spectra and photograph of the dispersions. Reprinted with permission from Ref. [22]. Copyright 2005 American Chemical Society. (g) High-resolution TEM image of CdSe nanocrystals. Reproduced from Ref. [23]. Copyright 2001 American Chemical Society.

of the corresponding dispersions change from pink to blue, green and brownish.

Regarding the synthesis of semiconducting nanoparticles with a defined size and size distribution, the introduction of the hot injection method represented a significant milestone. In 1993, Murray, Norris and Bawendi reported a simple route for the production of high quality CdE (E = S, Se, Te) quantum dots in the range of 1.2–11.5 nm [24]. The synthesis involved the rapid injection of an organometallic precursor into a hot coordinating solvent to produce instantaneous nucleation. Further growth of the nuclei into nanocrystals proceeded at a lower temperature, so that new nucleation events were suppressed. The separation of nucleation and growth is an important parameter to achieve a high degree of monodispersity (Fig. 3g) [25]. Nowadays the hot injection method has been adapted to prepare many other nanocrystalline semiconductors [26].

Another important class of materials are metal oxides, which offer a unique variety of structures, compositions and properties. Their potential applications in emerging fields such as energy storage and conversion, catalysis, photocatalysis, sensing and biomedicine makes them a primary focus in nanoparticle research [27]. In addition to organometallic routes [28], heat-up methods [29], and polyol-mediated syntheses [30], hydrolytic [31] and non-hydrolytic/nonaqueous [32] sol–gel approaches have been particularly successful for the preparation of metal oxides. For nanoscale materials, nonaqueous sol–gel methods seem to have some advantages over aqueous processes mainly with respect to the high crystallinity of the particles and the accessibility of a wider range of compositions of the products [33]. Nonaqueous sol–gel routes involve the reaction of various types of molecular precursors (metal halides, metal acetates, metal acetylacetonates, metal alkoxides, among others) with an organic solvent or a mixture of organic solvents with or without any surfactants, followed by heating in the temperature range of typically 50–250°C [34]. Depending on the synthesis temperature, the heating step is performed in an oil bath, in an autoclave or in a microwave reactor (Fig. 4, upper part). There are several advantages connected to these nonaqueous sol–gel methods. Most importantly, the nanoparticles are highly crystalline and a broad range of sizes, shapes and compositions is accessible, covering all types of properties

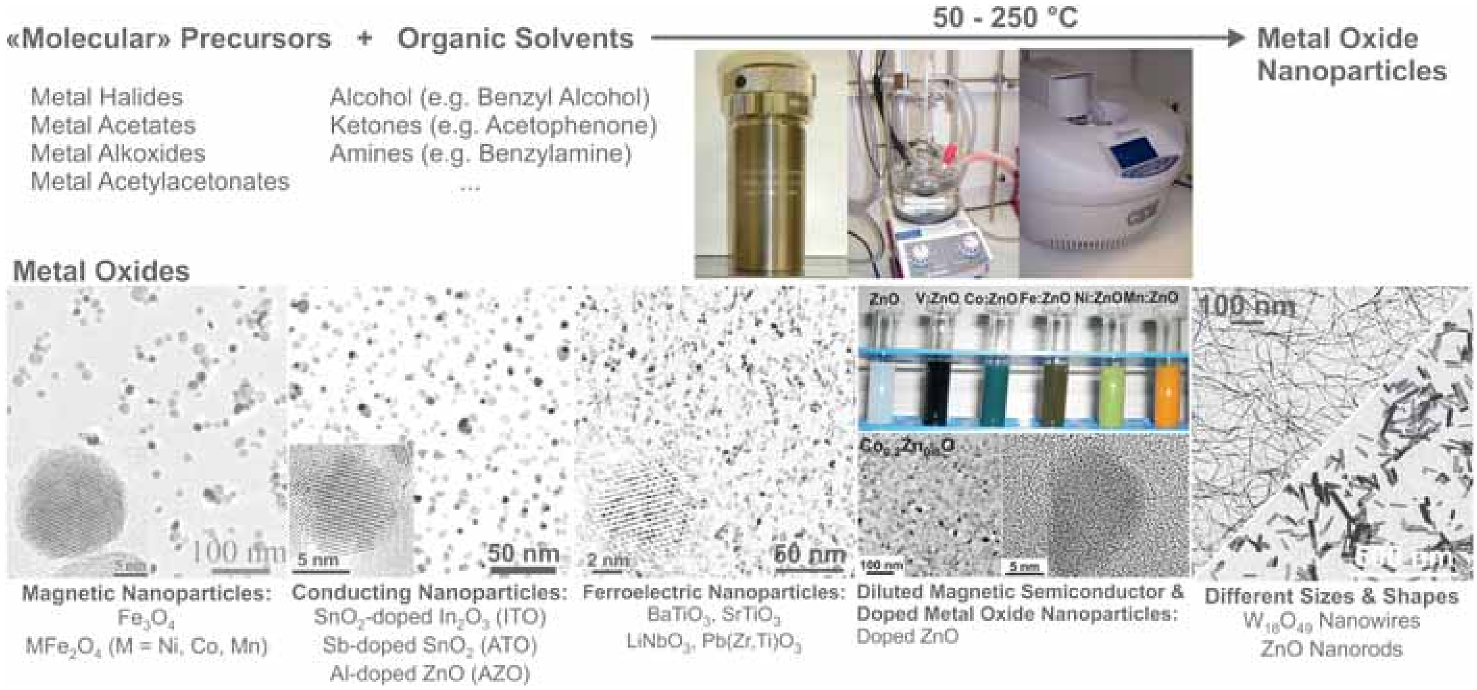

FIGURE 4

Upper part: schematic of the nonaqueous and surfactant-free liquid-phase synthesis approach to metal oxide nanoparticles using autoclave, oil bath or microwave heating. Lower part: TEM images of selected metal oxide nanoparticles synthesized by the nonaqueous approach.

including magnetic, electronically conductive, or ferroelectric materials (Fig. 4, lower part).

Formation mechanisms

Although nanoparticle synthesis has made great progress in the last few years and reached a very high level of sophistication, our understanding of nanoparticle formation lags considerably behind. As a matter of fact, systems that have been known for a long time, such as the preparation of gold nanoparticles by the citrate route, are still not yet completely understood. It is amazing that more than 50 years after the publication of the work of Turkevich *et al.* [19] the role of citrate in the formation of the gold nanoparticles remains an unresolved issue [35]. However, the reasons why the mechanistic aspects of nanoparticle formation are not well understood is not due to a lack of effort within the scientific community, but due to the high complexity of the reaction pathways. Experimental studies have to include all aspects of nanoparticle formation such as pre-nucleation processes [36–38], nucleation and growth [39,40], assembly and agglomeration [41], chemical reaction pathways [42] and the solid–liquid interface [43]. As a matter of fact, the experimental observations often contradict the classical models or the generally accepted understanding and therefore the theoretical concepts have to be continuously adapted to the new findings [44,45].

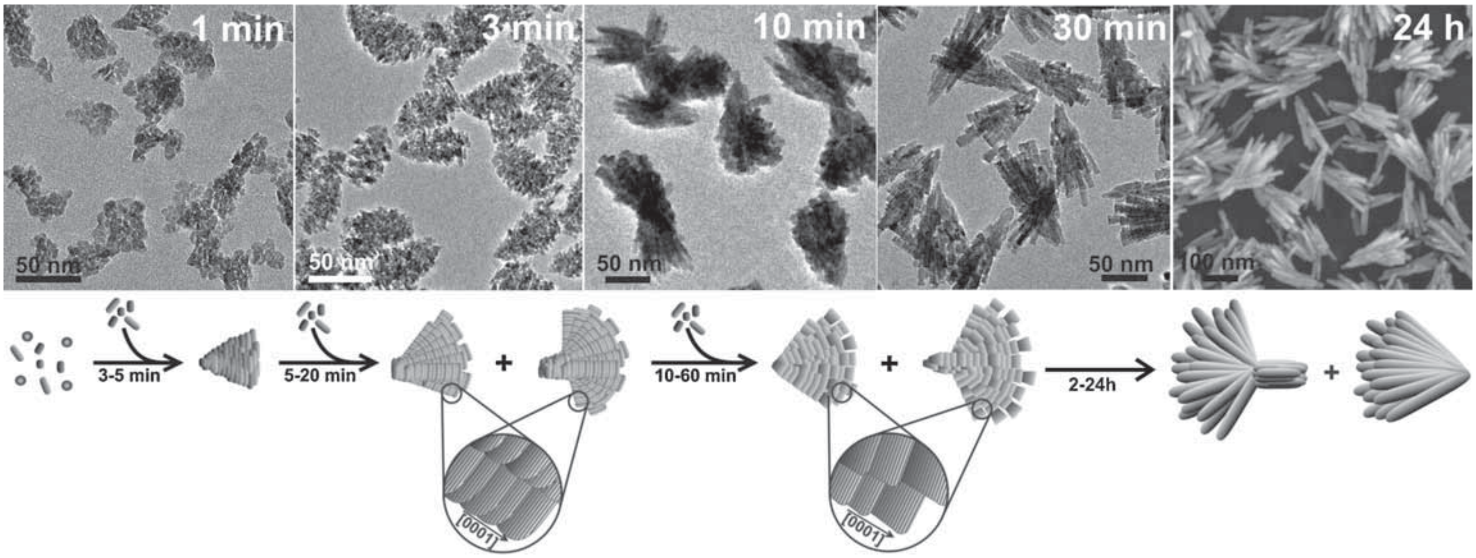

FIGURE 5

TEM and SEM images of ZnO nanostructures grown in benzyl alcohol after different reaction times (upper panels) and the corresponding schematic illustration (lower panel).

One material which has been synthesized in a tremendous variety of nanostructures is ZnO [46]. The corresponding synthesis routes are as manifold as the underlying chemical mechanisms [47], and the complex morphologies are a direct result of the crystallization pathways. One such example is the growth of ZnO nanorods that assemble into fan-like bundles (Fig. 5) [39]. The reaction between zinc acetylacetonate and benzyl alcohol results after 1 min in undefined agglomerates, which transform into particles with a triangular, fir tree-like morphology after 3 min. With continuous reaction time, the shape changes into fan-like structures consisting of angled nanorods (Fig. 5, upper panels). The schematic illustration (Fig. 5, lower part) summarizes these experimental observations. After a first nucleation, the primary particles assemble into triangular nanostructures. Additional nucleation and growth of primary particles continuously provides the building blocks for further attachment to the nanostructures, finally resulting in rod-like nanoparticle stacks. This particle-based growth occurs in a crystallographically controlled way along the *c*-axis. The bottlenecks between adjacent particles are then filled up by surface reconstruction, finally resulting in smooth nanorod surfaces. The unusual aspect of this crystallization mechanism is that several nucleation events occur and that the growth of the nanostructures involves nanoparticle assembly as well as classical growth by incorporation of the monomeric species on the surface of the nanostructures. In spite of such an intricate growth behavior involving several processes occurring in parallel, the final nanostructures are surprisingly uniform in size and shape.

Such complex crystallization mechanisms are of course not at all restricted to ZnO, but have been reported for other oxides, for example tungsten oxide nanoplatelets [48] and molybdenum dioxide nanorods [37]. What is common in all these systems is that despite the apparent simplicity of the synthesis route, typically just involving a precursor and a solvent, the nanostructure generation followed a rather complicated pathway. The study of crystallization mechanisms can be tedious and time-consuming, however it is indispensable on the way to develop concepts for the size- and shape-controlled synthesis of nanoparticles.

Assembly

About 20–30 years ago, the major part of nanoparticle research was clearly focused on the development of synthesis techniques. Nowadays, synthesis work is still important, but additionally, the use of nanoparticles as building blocks, like LEGO bricks, and their assembly into larger structures represents a rapidly growing branch of research [49]. Considering, how many nanoparticles with different compositions and properties are available and how many possibilities one has to mix and arrange them, it is obvious that such a toolbox opens up fascinating options for the preparation of new materials. However, the controlled assembly of nanoparticles crucially depends on the ability to understand and master interparticle interactions such as van der Waals, electrostatic, magnetic, molecular and entropic forces [50]. Unfortunately, on the nanoscale it is very difficult to estimate the relative contributions of the different interactions, because they all fall within the same order of magnitude and it is therefore not acceptable to neglect any parameters [49]. As a consequence, the formation of most nanoparticle assemblies can be modeled and justified only *a posteriori* and very few examples are known where the course of nanoscale self-assembly was predicted prior to the experiment. Therefore we shall not discuss this topic here (the reader is referred to dedicated reviews [50,51]) and just present a few examples on nanoparticle assembly.

In spite of the fact that nanoparticle assembly is currently a hot topic, the first examples were published more than 20 years ago. Bentzon *et al.* prepared 7 nm sized iron oxide nanoparticles by the thermal decomposition of $Fe(CO)_5$ in decalin with oleic acid – one of the standard procedures still used nowadays for iron oxide nanoparticles [52]. Due to the high monodispersity, the nanoparticles formed micrometer-sized ‘supercrystals’ (today called superlattices) stacking in an hcp or fcc structure, just like atoms in crystals [53].

A next step on the way to increase the complexity of nanoparticle assemblies is the usage of binary nanoparticle mixtures, *i.e.*, building blocks of different compositions and sizes [54]. Thereby the stacking behavior basically follows the same rules as for ionic crystals, where the size ratio of the building blocks and the charge

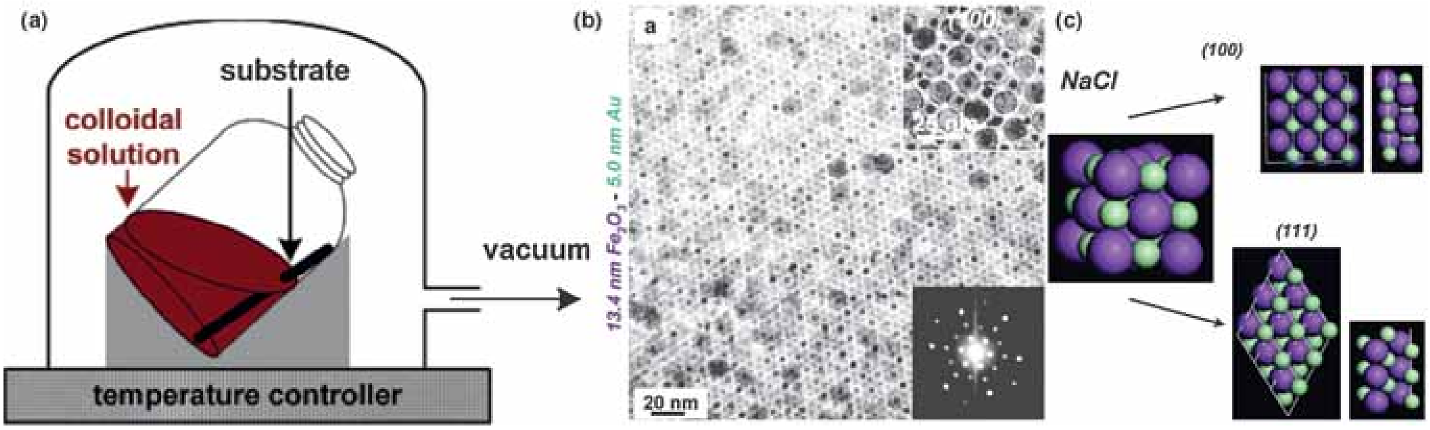

FIGURE 6

(a) A scheme of the low-pressure chamber used for growing ordered binary assemblies. (b) TEM micrograph of 13.4 nm Fe_2O_3 and 5.0 nm Au nanoparticle superlattice, isostructural with NaCl represented by the (1 1 1) projection, (c) three-dimensional sketch of NaCl unit cell, depicting the (1 0 0) and (1 1 1) planes, respectively, and the minimum number of layers in the (1 0 0) and (1 1 1) projections necessary for the formation of the patterns identical with the observed ones. Reprinted with permission from Ref. [54]. Copyright 2006 American Chemical Society.

of the ions are mainly responsible for the resulting structure. Fig. 6a shows schematically, how these assemblies are deposited on a substrate from colloidal solutions. A mixture of 13.4 nm Fe_2O_3 and 5 nm Au nanocrystals of 5 nm pack into a NaCl-type lattice, typically represented by (1 1 1) projections (Fig. 6b and c). These ordered domains extend over several microns, which is impressive for such superlattices, but orders of magnitudes too small for a 'real' material. One way to increase the size of the

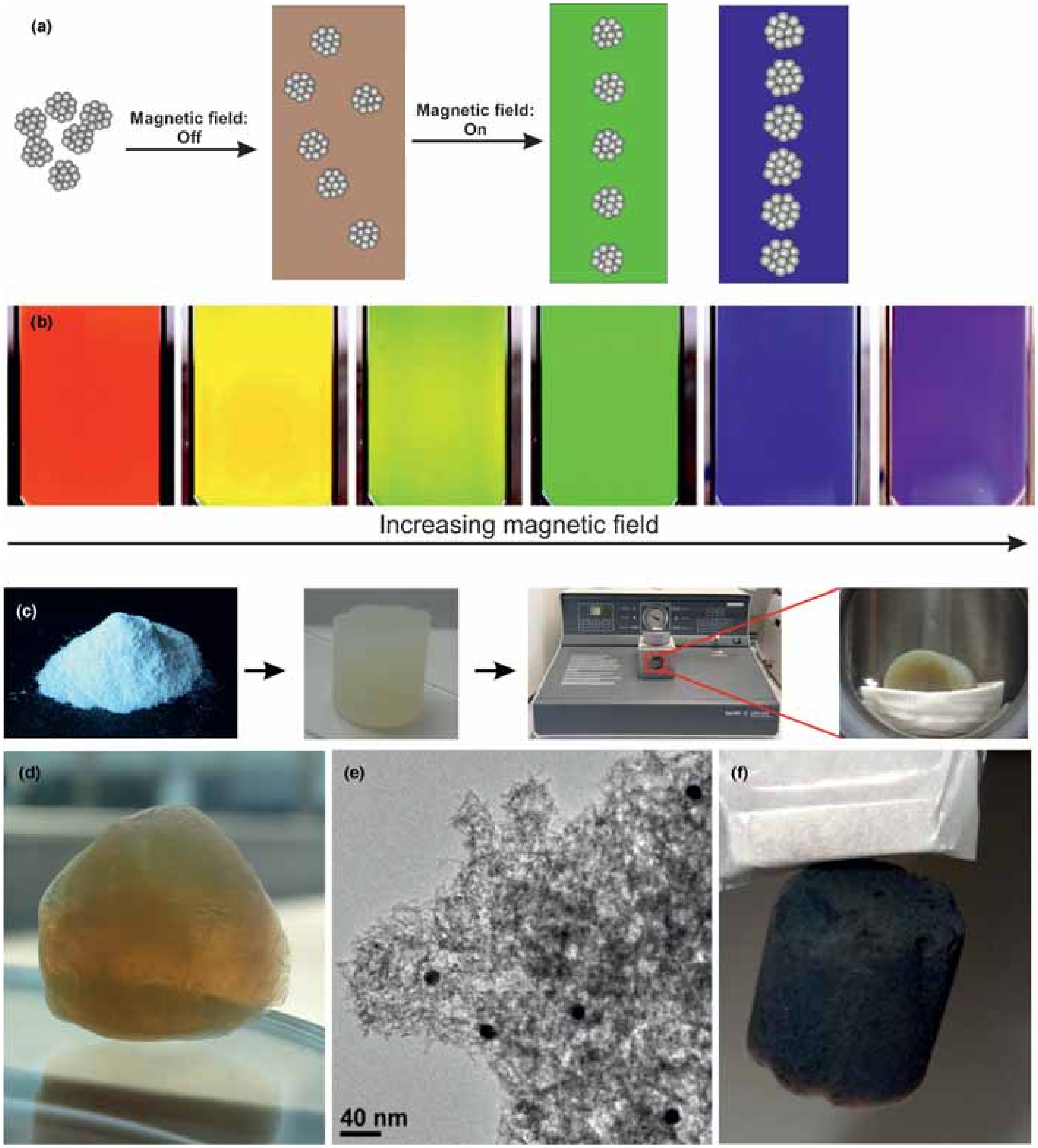

FIGURE 7

(a) Schematic illustration showing the assembly of nanoparticle clusters into one-dimensional periodic structures using a magnetic field. The strength of the magnetic field determines the distance between the clusters and thus the observed color. (b) Photographs of aqueous dispersions of Fe_3O_4 colloidal nanocrystal clusters in response to an increasing magnetic field. Reprinted with permission from Ref. [56]. Copyright 2012 American Chemical Society. (c) Photographs of the different steps to prepare a titania aerogel from the nanoparticle powder: powder – wet gel monolith – supercritical dryer – close-up of the reactor chamber of the supercritical dryer with a gel inside. (d) Photograph of a gold–titania aerogel, (e) TEM image of a gold–titania aerogel, (f) photograph of an iron oxide-titania aerogel attracted by a magnet.

nanoparticle assemblies is the use of external forces. Bergstrom *et al.* applied a magnetic field to assemble nanoparticles on a TEM grid [55]. At the initial stage of the drying process, the dispersion of the magnetic iron oxide nanocubes is shortly exposed to a magnetic field perpendicular to the substrate. This is sufficient to induce the development of small, highly ordered and crystallographically aligned nanocube clusters. During the drying process, the clusters grow in a self-assembly process to nanoparticle superlattices that extend over several micrometers in the lateral dimensions and about 300 nm in height.

One example, which elegantly combines the size-dependent properties of individual nanoparticles with the collective properties of the assemblies are responsive superparamagnetic colloidal photonic crystals [56]. In the first step, superparamagnetic iron oxide nanoparticles are arranged into relatively monodisperse spherical clusters, which are dispersed in a liquid medium as schematically shown in Fig. 7a. At this stage, the color of the dispersion is typically brown. Applying a weak magnetic field makes it possible to assemble these colloidal clusters into ordered particle arrays. The periodicity leads to strong optical diffraction, so that different structural colors (Fig. 7b) can be obtained depending on the strength of the magnetic field (which determines the distance between the particles). The colors can be fixed in a curable polymer matrix. The fascinating aspect in this case is that the nanoparticle clusters, despite their building blocks being just a few nanometers in size, respond to an external stimulus in such a way that an optical effect is produced that can be seen by naked eye.

The only way to produce a macroscopic body from nanoparticles is to assemble them in three dimensions and over several lengths scales. One example, which is solely based on a self-assembly process, is the preparation of titania aerogels from preformed anatase nanoparticles. A powder of surface functionalized titania nanoparticles (3–4 nm in diameter) is dispersed in water and gelled at slightly elevated temperatures (Fig. 7c). The wet monolith is subsequently dried in supercritical CO_2, resulting in a nanocrystalline titania aerogel consisting of nanoparticles that are arranged into a 3-dimensional network from the nano- to the centimeter-scale [57]. These anatase aerogels show outstanding specific surface areas and high porosity. The preparation of nanostructured bulk materials from preformed nanoparticles represents a highly flexible modular approach to a large variety of new materials, as different types of nanoparticle can be co-assembled in this way. For example, a mixture of gold and titania nanoparticles leads to a photocatalytic material (Fig. 7d) active under visible light. TEM images show the fine nanoparticle network with embedded gold nanoparticles (Fig. 7e). If magnetic nanoparticles are incorporated in the aerogel, then a macroscopically magnetic monolith can be produced (Fig. 7f).

Nanoparticle assembly is one of the most fascinating and most rapidly developing sub-areas in nanoparticle research [58]. The targeted architectures range from mesoporous materials [59], to metal and semiconducting aerogels [60], responsive and dynamic nanoparticle assemblies [61,62], macroscopic-scale nanowire films [63] and nanoscale helices [64].

Applications

If one thinks about possible applications of nanoparticles, then the first thought is usually that it has to be sophisticated; some type of high-tech product. Therefore it might be surprising that large scale applications of nanoparticles entered our daily lives decades ago, and they are not particularly spectacular. A prominent example along these lines is carbon black. It is an amorphous powder, consisting of nanoparticles in the size range of typically 20–50 nm. Its annual industrial production amounts to an unbelievable 10 million metric tons, worldwide [65]. Over 90% of carbon black is used for the reinforcement of rubber, mainly car tires. It is produced by the incomplete combustion of heavy aromatic oil or natural gas.

A completely different application of nanoparticles is in food products. Amorphous silica nanoparticles are used as anti-caking agent to maintain the flow properties in powder products (*e.g.*, instant soups) and to thicken pastes [66]. The conventional form of amorphous silica is known as food additive E551. Like in the case of many other nanopowders, it is controversially debated, whether E551 is a nanomaterial or not, because during the production process the nanosized primary particles agglomerate to larger structures [66]. From a characterization point of view, it is often very difficult to distinguish primary particles from aggregates or agglomerates.

Another major application of nanoparticles is in cosmetics, especially in sunscreens. Sunscreens contain titanium dioxide and zinc oxide nanoparticles, because they are colorless and reflect/scatter ultraviolet light more efficiently than larger particles [67]. The small size of nanoparticles provides the benefit of making them transparent, which results in better consumer acceptance and thus improves the protection of human skin against UV-induced damage.

Amazingly, taking advantage of optical effects to improve the appearance of materials is still a major application of nanoparticles, just as in ancient times. A prominent example is automotive coatings, which consist of several layers [68]. The two topmost layers are the colored base coat and the clear coat which protects the paint from the environment. Mercedes-Benz brought nanoparticle-based clearcoat into series production for both metallic and non-metallic paint finishes by the end of 2003. The coating fulfills a practical and an esthetical role. On the one hand it increases the scratch resistance, and on the other hand it visibly enhances the gloss (Fig. 8a).

Liquid magnets, so-called ferrofluids, represents another example of nanoparticles at work. Because ferrofluids are ultrastable suspensions of small magnetic nanoparticles in a liquid, they combine the normal behavior of a liquid with superparamagnetic properties. In the presence of a magnetic field, the magnetic moment of the nanoparticles try to align with the magnetic field direction leading to a macroscopic magnetization of the liquid (Fig. 8b). The possibility to control the flow properties of a ferrofluid as well as its position inside a technical device lead to a countless number of applications in devices such as dynamic seals and dampers [69,70]. But music enthusiasts also appreciate ferrofluids as heat transfer materials in loudspeakers.

In addition to these mass applications, selected nanoparticles have found their way into more sophisticated, high-tech products. However, the timeline from the discovery in the laboratory to a commercial product is typically very long. For example, from the first report on the use of titanium dioxide nanoparticles in a dye-sensitized solar cell [71] it took more than 20 years to develop a

FIGURE 8

Photographs of (a) a Mercedes car with a nanoparticle clearcoat. Copyright Daimler AG. (b) Ferrofluid (picture by Andrew Magill) and (c) solar keyboard folios for iPads. Copyright Logitech.

commercially available product. In summer 2012 the hardware manufacturer Logitech brought an external iPad keyboard on the market (Fig. 8c), which is powered by any light, representing the first major commercial use of dye-sensitized solar cells.

Conclusions

The fascination with nanoparticle research is founded in the observation of unusual, often unexpected effects related to the tiny size of the particles. Although some of these phenomena have been applied in materials technology for several hundreds of years, their systematic study within nanoscience began just a few decades ago, and nanoparticle research is far from being exhaustively explored. New nanomaterials are still being created, new effects discovered and new models and concepts developed to explain and understand the observed experimental results. The high potential of nanoparticles for applications has moved them from basic research, solely driven by scientific curiosity, into the focus of technological interest. As a matter of fact, one of the most interesting aspects of nanoparticle research is that well-known materials like titania, carbon or gold (to mention only a few) demonstrate completely different properties on the nanoscale. As a consequence of these size-dependent properties, completely new fields of applications open up without forcing materials scientists to necessarily develop completely new materials compositions. Variation of size, shape and assembly just does the job.

Acknowledgement

Financial support from ETH Zurich (ETH-07 09-2) is gratefully acknowledged.

References

[1] J.R. Lead, K.J. Wilkinson, Environ. Chem. 3 (2006) 159.
[2] R.M. Hough, R.R.P. Noble, M. Reich, Ore Geol. Rev. 42 (2011) 55.
[3] P. Colomban, G. Gouadec, Ann. Chim. Sci. Mater. 30 (2005) 673.
[4] P. Colomban, J. Nano Res. 8 (2009) 109.
[5] P. Sciau, in: A.A. Hashim (Ed.), The Delivery of Nanoparticles, InTech, Rijeka, Croatia, 2012.
[6] P. Sciau, C. Mirguet, C. Roucau, D. Chabanne, M. Schvoerer, J. Nano Res. 8 (2009) 133.
[7] U. Leonhardt, Nat. Photon. 1 (2007) 207.
[8] I. Freestone, N. Meeks, M. Sax, C. Higgitt, Gold Bull. 40 (2007) 270.
[9] L.B. Hunt, Gold Bull. 9 (1976) 134.
[10] P.P. Edwards, J.M. Thomas, Angew. Chem. Int. Ed. 46 (2007) 5480.
[11] M. Faraday, Philos. Trans. R Soc. Lond. 147 (1857) 145.
[12] A. Henglein, Chem. Rev. 89 (1989) 1861.
[13] A.P. Alivisatos, J. Phys. Chem. 100 (1996) 13226.
[14] C. Burda, et al. Chem. Rev. 105 (2005) 1025.
[15] K. Kalyanasundaram, et al. Angew. Chem. Int. Ed. 20 (1981) 987.
[16] A. Henglein, Ber. Bunsen-Ges. 86 (1982) 301.
[17] R. Rossetti, et al. J. Chem. Phys. 80 (1984) 4464.
[18] B.L. Cushing, V.L. Kolesnichenko, C.J. O'Connor, Chem. Rev. 104 (2004) 3893.
[19] J. Turkevich, P.C. Stevenson, J. Hillier, Discuss. Faraday Soc. 11 (1951) 55.
[20] T.K. Sau, C.J. Murphy, J. Am. Chem. Soc. 126 (2004) 8648.
[21] S. Barbosa, et al. Langmuir 26 (2010) 14943.
[22] C.J. Murphy, et al. J. Phys. Chem. B 109 (2005) 13857.
[23] D.V. Talapin, et al. Nano Lett. 1 (2001) 207.
[24] C.B. Murray, D.J. Norris, M.G. Bawendi, J. Am. Chem. Soc. 115 (1993) 8706.
[25] J. Park, et al. Angew. Chem. Int. Ed. 46 (2007) 4630.
[26] C. de Mello Donega, P. Liljeroth, D. Vanmaekelbergh, Small 1 (2005) 1152.
[27] G.R. Patzke, et al. Angew. Chem. Int. Ed. 50 (2011) 826.
[28] M.L. Kahn, et al. J. Mater. Chem. 19 (2009) 4044.
[29] S.G. Kwon, T. Hyeon, Small 7 (2011) 2685.
[30] C. Feldmann, Adv. Funct. Mater. 13 (2003) 101.
[31] L.L. Hench, J.K. West, Chem. Rev. 90 (1990) 33.
[32] P.H. Mutin, A. Vioux, Chem. Mater. 21 (2009) 582.

[33] M. Niederberger, N. Pinna, Metal Oxide Nanoparticles in Organic Solvents: Synthesis, Formation, Assembly and Application, Springer-Verlag, London, 2009.
[34] M. Niederberger, Acc. Chem. Res. 40 (2007) 793.
[35] X.H. Ji, et al. J. Am. Chem. Soc. 129 (2007) 13939.
[36] D. Gebauer, A. Völkel, H. Cölfen, Science 322 (2008) 1819.
[37] D. Koziej, et al. Small 7 (2011) 377.
[38] I. Olliges-Stadler, et al. Chem. Eur. J. 18 (2012) 2305.
[39] B. Ludi, et al. Nanoscale 4 (2012) 1982.
[40] D. Carriazo, et al. Small 8 (2012) 2231.
[41] J. Ba, et al. Small 3 (2007) 310.
[42] M. Niederberger, G. Garnweitner, Chem. Eur. J. 12 (2006) 7282.
[43] F. Zaera, Chem. Rev. 112 (2012) 2920.
[44] M. Niederberger, H. Cölfen, Phys. Chem. Chem. Phys. 8 (2006) 3271.
[45] D. Gebauer, H. Cölfen, Nano Today 6 (2011) 564.
[46] Z.L. Wang, Mater. Today 7 (2004) 26.
[47] B. Ludi, M. Niederberger, Dalton Trans. (2013), http://dx.doi.org/10.1039/C3DT50610J.
[48] I. Olliges-Stadler, et al. Nanoscale (2013), http://dx.doi.org/10.1039/C3NR02020G.
[49] D.V. Talapin, ACS Nano 2 (2008) 1097.
[50] K.J.M. Bishop, et al. Small 5 (2009) 1600.
[51] Y. Min, et al. Nat. Mater. 7 (2008) 527.
[52] M.D. Bentzon, et al. Philos. Magn. B 60 (1989) 169.
[53] M.D. Bentzon, A.R. Tholen, Ultramicroscopy 38 (1991) 105.
[54] E.V. Shevchenko, et al. J. Am. Chem. Soc. 128 (2006) 3620.
[55] A. Ahniyaz, Y. Sakamoto, L. Bergstrom, Proc. Natl. Acad. Sci. U.S.A. 104 (2007) 17570.
[56] L. He, et al. Acc. Chem. Res. 45 (2012) 1431.
[57] F.J. Heiligtag, et al. J. Mater. Chem. 21 (2011) 16893.
[58] Z.H. Nie, A. Petukhova, E. Kumacheva, Nat. Nanotechnol. 5 (2010) 15.
[59] I.E. Rauda, et al. Acc. Chem. Res. 46 (2013) 1113.
[60] N. Gaponik, A.K. Herrmann, A.J. Eychmuller, Phys. Chem. Lett. 3 (2012) 8.
[61] S.C. Warren, O. Guney-Altay, B.A. Grzybowski, J. Phys. Chem. Lett. 3 (2012) 2103.
[62] L.B. Wang, et al. Acc. Chem. Res. 45 (2012) 1916.
[63] J.W. Liu, H.W. Liang, S.H. Yu, Chem. Rev. 112 (2012) 4770.
[64] M. Yang, N.A. Kotov, J. Mater. Chem. 21 (2011) 6775.
[65] T. Patnaik, B. Brown, Rubber & Plastic News, 2010, December, p. 16.
[66] S. Dekkers, et al. Nanotoxicology 5 (2011) 393.
[67] G.J. Nohynek, et al. Crit. Rev. Toxicol. 37 (2007) 251.
[68] A.H. Tullo, Chem. Eng. News 80 (2002) 27.
[69] S. Odenbach, Colloids Surf., A 217 (2003) 171.
[70] L. Rodriguez-Arco, et al. in: G. Berselli, R. Vertechy, G. Vassura (Eds.), Smart Actuation and Sensing Systems – Recent Advances and Future Challenges, InTech, Rijeka, Croatia, 2012.
[71] B. O'Regan, M. Grätzel, Nature 353 (1991) 737.

Materials Today • Volume 16, Numbers 7/8 • July/August 2013 RESEARCH

Carbon nanomaterials for high-performance supercapacitors

Tao Chen and Liming Dai*

Center of Advanced Science and Engineering for Carbon (Case4Carbon), Department of Macromolecular Science and Engineering, Case Western Reserve University, 10900 Euclid Avenue, Cleveland, OH 44106, USA

Owing to their high energy density and power density, supercapacitors exhibit great potential as high-performance energy sources for advanced technologies. Recently, carbon nanomaterials (especially, carbon nanotubes and graphene) have been widely investigated as effective electrodes in supercapacitors due to their high specific surface area, excellent electrical and mechanical properties. This article summarizes the recent progresses on the development of high-performance supercapacitors based on carbon nanomaterials and provides various rational concepts for materials engineering to improve the device performance for a large variety of potential applications, ranging from consumer electronics through wearable optoelectronics to hybrid electric vehicles.

Introduction

Global energy consumption, along with CO_2 emission, has been accelerating at an alarming rate due to rapid global economic expansion, an increase in the world population, and an ever-increasing human reliance on energy-consuming appliances. It has been estimated that the world will need to double its energy supply by 2050 (see the World Energy Council Website at www.worldenergy.org). The rapid increase in global energy consumption and the environmental impact of traditional energy resources pose serious challenges to human health, energy security, and the environment; and reveal a growing need to develop new types of clean and sustainable energy conversion and storage systems, such as batteries and supercapacitors for electric vehicles with low exhaust emissions.

Supercapacitors, also called as ultracapacitors, are electrochemical energy storage devices that combine the high energy-storage-capability of conventional batteries with the high power-delivery-capability of conventional capacitors [1–4]. Being able to achieve higher power and longer cycle life than conventional dielectric capacitors and batteries, supercapacitors have been developed to provide power pulses for a large variety of applications, ranging from consumer electronics through hybrid electric vehicles (HEVs) to industrial electric utilities [5]. Therefore, supercapacitors play an important role in achieving better fuel economy, decreasing harmful emissions, and reducing the reliance on petroleum sources. The world market for supercapacitors has been growing steadily and rapidly [1]. To improve the performance of state-of-the-art supercapacitors to meet the stringent requirements for the applications mentioned above, and many other advanced applications not discussed (e.g. portable, transparent and wearable electronics), new electrode materials with superior properties over those of current activated carbon electrodes are needed and new device structures (e.g. all-solid state supercapacitors [6,7], optically transparent [8,9], mechanically flexible and stretchable [10–12], and even fiber-shaped [13–15] supercapacitors) are highly desirable.

Nanotechnology has opened up new frontiers by offering unique enabling technologies and new materials for energy storage. In particular, graphitic carbon nanomaterials (e.g. carbon nanotubes, graphene sheets) have been playing a more and more important role in the development of high-performance supercapacitors [4,5]. The aim of this article is to summarize recent progress in the development of supercapacitors (especially electrical double layer capacitors) based on carbon nanomaterials and to provide various rational concepts for materials engineering to improve device performance.

Supercapacitors

A typical supercapacitor consists of three essential components, namely the electrodes, the electrolyte, and the separator. The overall performance of supercapacitors is determined by the

---

*Corresponding author:. Dai, L. (liming.dai@case.edu)

1369-7021/06/$ - see front matter © 2013 Elsevier Ltd. All rights reserved. http://dx.doi.org/10.1016/j.mattod.2013.07.002

physical properties of both the electrode and the electrolyte materials. Nevertheless, the electrode is one of the most important components for charge storage/delivery, and plays a crucial role in determining the energy and power densities of a supercapacitor. The electrochemical performance of a supercapaictor can be characterized by cyclic voltammetry and galvanostatic charge–discharge measurements [1–4]. The capacitance (*C*) is determined from the constant current discharge curves according to Eqn 1:

$$C = \frac{I}{(dV/dt)} \tag{1}$$

where *I* is the discharge current and dV/dt is calculated from the slope of the discharge curve. Then, the specific capacitance (C_{SP}) for one electrode in a supercapacitor can be calculated using the following equation:

$$C_{SP}\,(\mathrm{F\ g^{-1}}) = \frac{4C}{m} \tag{2}$$

where *C* is the measured capacitance for the two-electrode cell and *m* is the total mass of the active materials in both electrodes. The mass can also be replaced by volume or area of the electrodes depending on the nature of the targeted applications. The stored energy (*E*) and the power density (*P*) in a supercapacitor can then be calculated from Eqns 3 and 4, respectively:

$$E = \frac{(CV^2)}{2} \tag{3}$$

$$P = \frac{V^2}{(4R_s)} \tag{4}$$

where *C* ($\mathrm{F\,g^{-1}}$) is the total capacitance of the cell, *V* is the cell voltage, and R_S is the equivalent series resistance.

The principle of energy storage in a supercapacitor can be either (i) electrostatic charge accumulation at the electrode/electrolyte interface (electrical double layer capacitance, EDLC), as schematically shown in Fig. 1, or (ii) charge transfer, via reversible (Faradaic) redox reaction(s), to redox materials (e.g. conductive polymers, metal oxide nanoparticles) on the surface of electrode (pseudo-capacitance). In practical supercapacitors, the two storage mechanisms often work simultaneously [16]. Different charge transfer processes involved in the EDLC and pseudo-capacitance [4,5,16]. In EDLC, the energy is stored through ion adsorption (a purely electrostatic process) at the electrode-electrolyte interface with no charge transfer across the electrodes, suggesting a non-faradic process. By contrast, pseudo-capacitance arises from reversible redox reaction(s) between the electrolyte and active species on the surface of electrodes. Although pseudo-capacitance higher than EDLC capacitance can be achieved, supercapacitors based on pseudo-capacitance often suffer from the poor electrical conductivity of the electroactive species, and hence demonstrate low power density and cycling stability. Therefore, the combination of both EDLC and pseudo-capacitance presents an effective means to improve the overall capacitance of a supercapacitor.

Since both EDLC and pseudocapacitance are surface phenomena, high-surface-area mesoporous carbon and activated carbons (specific surface area: 1000–2000 $\mathrm{m^2\,g^{-1}}$) have been widely used as electrode materials in both academic and commercial supercapacitors [16–19]. Taking a specific surface area of 1000 $\mathrm{m^2\,g^{-1}}$ for carbon as an example, its ideal attainable capacitance could be 200–500 $\mathrm{F\,g^{-1}}$. However, the practically obtained values are of only a few tens of $\mathrm{F\,g^{-1}}$. Activated carbons have a wide pore size distribution, consisting of micropores (<2 nm), mesopores (2–50 nm), and macropores (>50 nm) [17,18], with most of the surface area of activated carbons being on the scale of micropores [20]. Pores of this size are often poorly or non-accessible for electrolyte ions (especially for organic electrolytes), and thus are incapable of supporting an electrical double layer. By contrast, mesopores contribute the most to the capacitance in an electrical double-layer capacitor [21–23]. However, recent experimental and theoretical studies have demonstrated that charge storage in pores 0.5–2 nm in size (smaller than the size of solvated electrolyte ions) increased with decreasing pore size due to the closer approach of the ion center to the electrode surface in the smaller pores [18,24–26]. Pores less than 0.5 nm wide are too small for double layer formation [26]. Currently available activated carbon materials have a high surface area but unfortunately a low mesoporosity, and hence a limited capacitance due to a low electrolyte accessibility [20]. This translates to the limited energy density of the resultant supercapacitors (Eqn 3). The low electrolyte accessibility of activated carbons, coupled with their poor electrical conductivity, produces a high internal resistance and hence a low power density for the capacitors (Eqn 4) [20]. Consequently, a limited energy density (4–5 $\mathrm{Wh\,kg^{-1}}$) and a limited power density

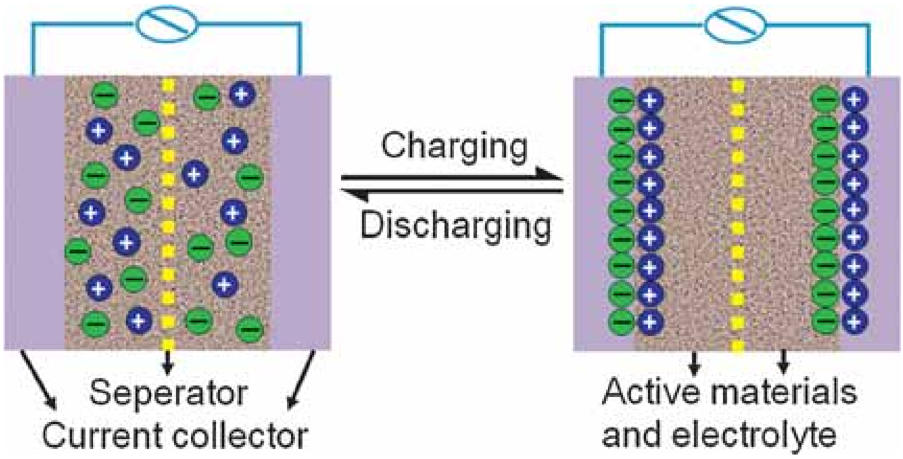

FIGURE 1

Schematic illustration of the charging/discharging process in a supercapacitor.

(1–2 kW kg^{-1}) have been obtained for currently available supercapacitors based on the activated carbon electrodes [20]. Clearly, therefore, new materials are needed to overcome the drawbacks of activated carbon electrode materials to improve the performances for supercapacitors.

Owing to their large surface area, high mesoporosity and electrolyte accessibility, and good electrical properties, carbon nanomaterials, especially graphene and carbon nanotubes (CNTs), are very promising candidates to replace activated carbons as the electrode materials in high-performance supercapacitors [27,28]. Graphene, a single-atom-thick layer of sp^2 carbon atoms densely packed into a two-dimensional (2D) honeycomb lattice, can be viewed as the basic building block for carbon materials of all other dimensionalities, such as 0D fullerene, 1D nanotubes, and 3D graphite (Fig. 2) [27]. For instance, a carbon nanotube (CNT) may be conceptually viewed as a graphene sheet that is rolled into a nanoscale tube form as a single-walled carbon nanotube (SWNT), or as a multiwalled carbon nanotube (MWNT) with additional graphene coaxial tubes around the SWNT core [29].

CNTs with a high aspect ratio, large specific surface area (SWNT >1600 $m^2 g^{-1}$, MWNT >430 $m^2 g^{-1}$) [30,31] as well as good mechanical and electrical (~5000 S cm^{-1}) properties have been widely used as the active electrodes in supercapacitors [28,32–37]. Having many similarities to CNTs in structure and properties, including its high aspect ratio (the ratio of lateral size to thickness), large surface (2630 $m^2 g^{-1}$) [38–40], excellent carrier mobility (15,000 $cm^2 V^{-1} s^{-1}$ for both electrons and holes) [41], and good mechanical properties [42], graphene is an attractive candidate for many potential applications where CNTs have been exploited. Superior to CNTs, one-atom-thick graphene sheets with a 2D planar geometry could offer additional advantages as more effective electrode materials in supercapacitors [43]. Furthermore, the availability of many rational strategies for materials engineering and rich chemistries for controlled functionalization of both CNTs and graphene should facilitate materials engineering for the development of various high-performance supercapacitors based on carbon nanomaterials, as described below.

High-performance supercapacitors by controlling the orientation and tip structure of carbon nanotubes

As mentioned above, CNTs with a high aspect ratio, large specific surface area [30,31] and high electrical conductivity have been widely used as the active electrode in supercapacitors [28,32–37]. For instance, a supercapacitor of a specific capacitance of 102 F g^{-1} with a power density >8 kW kg^{-1} and an energy density of ~1 Wh kg^{-1} has been fabricated from electrodes based on free-standing mats of entangled MWNTs in H_2SO_4 electrolyte [31]. More recently, a higher specific capacitance of 180 F g^{-1} has been

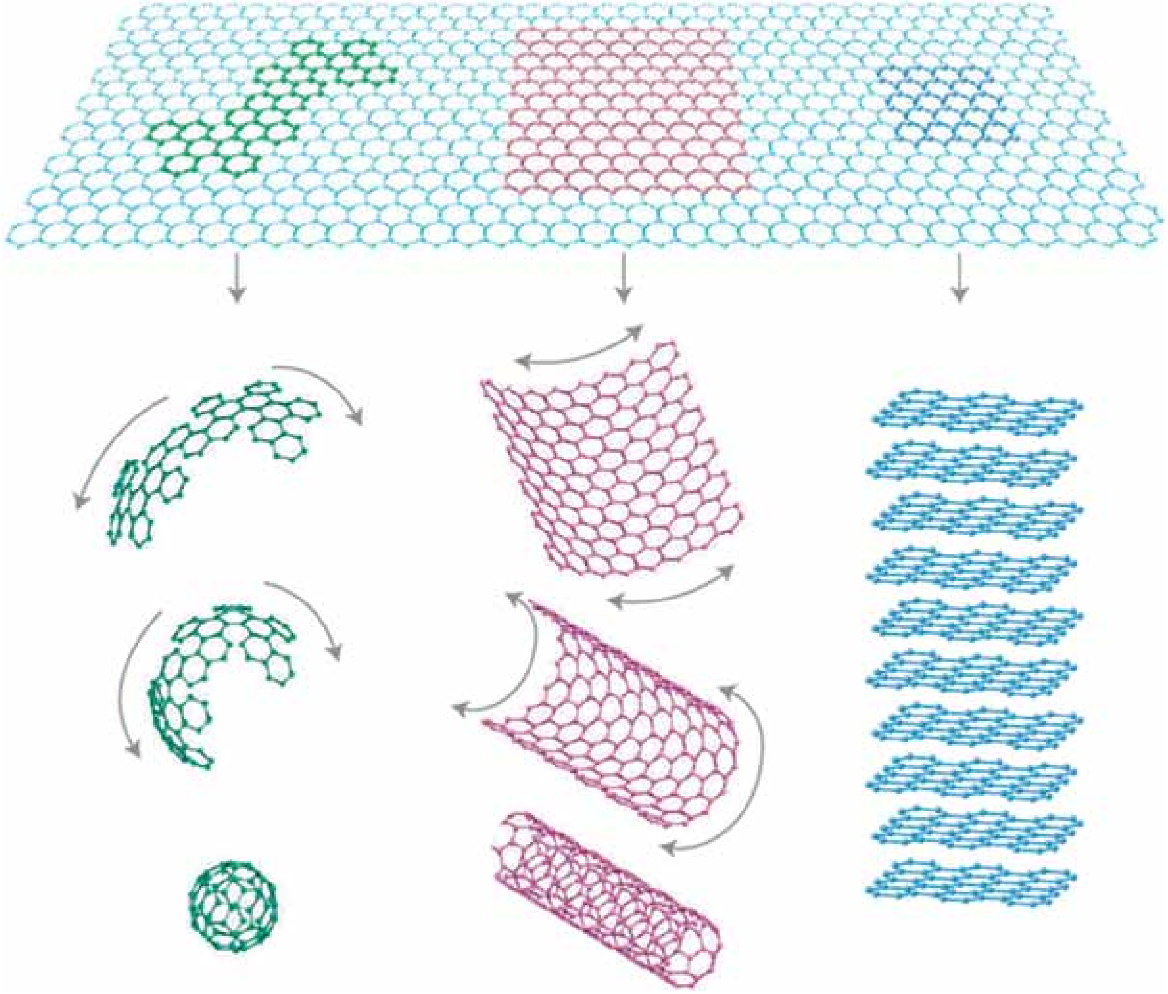

FIGURE 2

The mother of all graphitic forms. Graphene is a 2D building block for carbon materials of all other dimensionalities. It can be wrapped up into 0D buckyballs, rolled into 1D nanotubes or stacked into 3D graphite [27]. Reprinted from Ref. [27] with permission. Copyright 2007, Nature Publishing Group.

achieved when a random SWNT network (Fig. 3a) was used as the electrode in a KOH electrolyte [32]. In this particular case, the maximum power density and energy density approached 20 kW kg^{-1} and 10 Wh kg^{-1}, respectively. This value of power density is higher than those attainable by activated carbon-based commercial capacitors, but the energy density still needs to be improved. The randomly entangled or bundled structure could have significantly reduced the CNT specific area with a concomitant decrease in the electrochemical energy-storage performance [35,44,45].

Compared to their randomly entangled counterparts, vertically-aligned CNT arrays (VA-CNTs) have been demonstrated to be advantageous for supercapacitor applications. Unlike the irregular pore structures of random CNTs (Fig. 3a), the vertically-aligned structure and the well-defined tube-spacing in a VA-CNT array (Fig. 3b,c) can provide a more electrolyte-accessible surface. The aligned structures should also provide improved charge storage/delivery properties as each of the constituent aligned tubes can be connected directly onto a common electrode to allow them to effectively participate in the charging/discharging process (Fig. 3d). Moreover, the top end-caps of the VA-CNTs can be properly opened (e.g. by plasma etching [44,46]) (Fig. 3e–g) to allow the electrolyte access to the otherwise inaccessible inner cavity of the VA-CNTs for charge storage. Indeed, recent research has demonstrated the improved rate capability of VA-CNTs over randomly entangled CNTs [35,44–49], along with enhanced energy density (148 Wh kg^{-1}) and power density (315 kW kg^{-1}) [50–55]. Specifically, a high capacitance has been obtained in 1 M H_2SO_4 for a VA-CNT array electrode (365 F g^{-1}) prepared by template-assisted CVD [56] and in ionic liquid electrolytes [57] for an VA-CNT electrode (440 F g^{-1}) prepared by a template-free CVD approach (Fig. 3e–h) [44,49]. To further optimize the performance of VA-CNT supercapacitors, conductive polymer (e.g. polyaniline [58] and polypyrrole [59]) and metal oxide (e.g. MnO_2 [60], TiO_2 [61] and RuO_2 [62]) can be deposited onto the surface of CNTs to introduce pseudocapacitance.

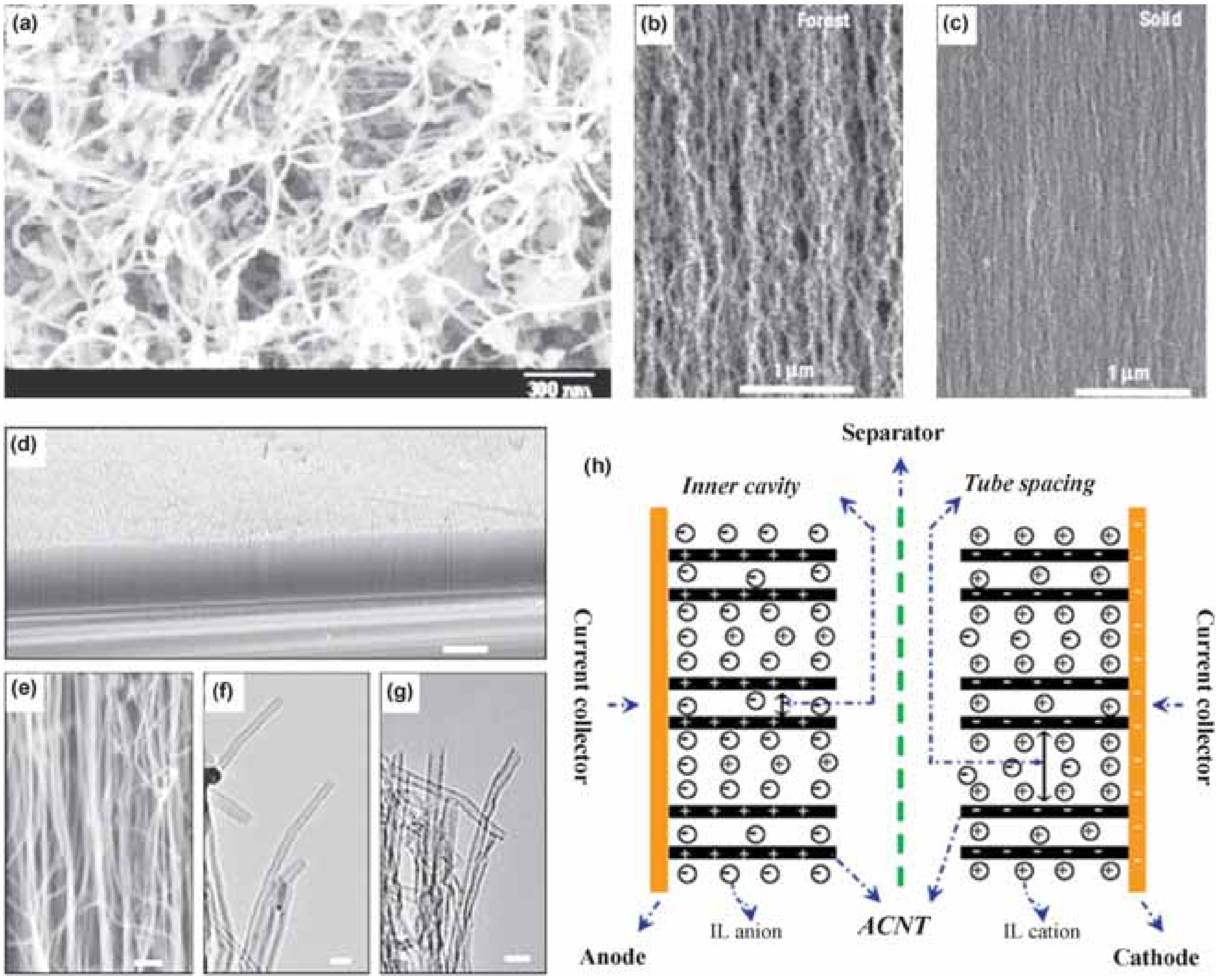

FIGURE 3

Typical structures of random, VA-CNTs and the schematic illumination of VA-CNT based supercapacitors. (a) SEM image of the as -grown randomly entangled SWNTs [32]. Reprinted from Ref. [32] with permission. Copyright 2001, John Wiley and Sons. (b,c) SEM images of the as-grown forest (b) after having been solidified with a droplet of liquid (c) [35]. Reprinted from Ref. [35] with permission. Copyright 2006, Nature Publishing Group. (d) SEM image of a plasma-etched VA-CNT electrode (scale bar: 100 µm). (e) Higher magnification view of the electrode (scale bar: 100 nm). TEM images of the CNTs before (f) and after (g) plasma etching (scale bar: 20 nm) (h) Schematic of an electrochemical capacitor based on plasma-etched VA-CNT electrodes and ionic liquid electrolyte. [44]. Reprinted from Ref. [44] with permission. Copyright 2009, Elsevier.

High-performance supercapacitors by controlling the edge-structure and π–π stacking of graphene sheets

Supercapacitors based on CNT electrodes do not exhibit the expected performance (e.g. specific capacitance below 500 F g^{-1}) due to the high contact resistance between the CNT electrode and current collector and its inefficient interaction with the electrolyte. Besides, it is difficult, if not impossible, to scale up the production of VA-CNTs for the commercialization of supercapacitors [63]. The recent availability of solution-processable graphene oxide (GO) by exfoliation of graphite powder via solution oxidation [64] and edge-functionalized graphene (EFG) sheets via ball milling [65,66] has allowed for the large-scale production of graphene materials at a relatively low cost for various device applications through solution processing [67]. Due to its large surface area, high carrier transport mobility and excellent thermal/mechanical stability, graphene has recently been studied as an alternative carbon based electrode in supercapacitors [68]. Theoretically, the double-layer capacitance value of a graphene electrode can reach up to 550 F g^{-1}, the highest value of intrinsic capacitance among all carbon-based electrodes [69,70]. Using chemically reduced graphene oxide electrodes, a supercapacitor with specific capacitances of 135 and 99 F g^{-1} in aqueous and organic electrolytes, respectively, has been fabricated [39], as was a supercapacitor with ultrahigh specific energy density (85.6 Wh kg^{-1} at room temperature and 136 Wh kg^{-1} at 80 °C) [70]. Recently, supercapacitors with high specific capacitance (276 F g^{-1}), power density (20 W cm^{-3}, 20 times higher than that of the activated carbon counterpart), energy density (1.36 mWh cm^{-3}, 2 times higher than that of the activated carbon counterpart), and excellent stability during bending from 0° to 180° have also been developed by using a standard LightScribe DVD optical drive to directly reduce graphene oxide films to graphene electrodes (Fig. 4a–c) [71]. The performance can be further enhanced by using a conductive polymer [72,73] or metal oxide [74,75] coating to introduce pseudocapacitance.

Recent work on the EFG with various edge groups (e.g. –H, –COOH and –SO_3H) by effective and eco-friendly ball milling of graphite (Fig. 4d) provides an effective means for the development of functionalized graphene materials with tailor-made chemical structures and electronic properties attractive for multifunctional applications [65], including large-area transparent and conducting electrodes for electronics and metal-free catalysts for oxygen reduction reaction in fuel cells [66]. Although EFGs have hardly been exploited for energy-storage application, the use of EFGs, having abundant active sites at the edge and perfect conjugation (conductivity) on its basal plane, as the electrode materials could lead to high-performance supercapacitors with a high rate capability. Through controllable self-assembling, EFGs should also facilitate the formation of hierarchically structured electrodes in supercapacitors for specific applications.

High-performance supercapacitors based on 3D pillared graphene-carbon nanotube networks

Although graphene sheets with a large surface area are ideal electrode materials for energy storage, a large portion of the surface

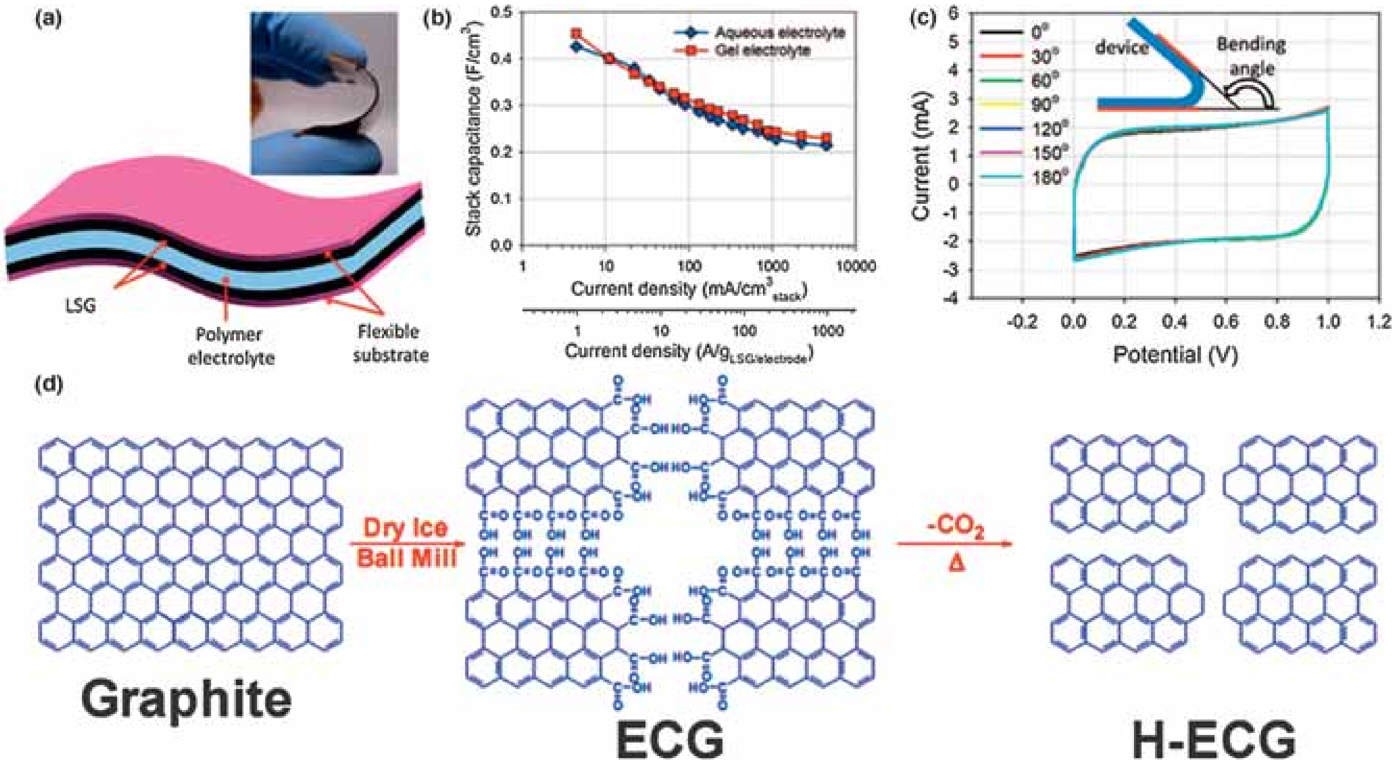

FIGURE 4

Structure and electrochemical properties of an all-solid-state supercapacitor based on laser-scribed graphene (LSG) and the synthetic route to edge-functionalized graphene. (a) Schematic diagram of the supercapacitor based on LSG. Inset is a photograph showing the flexibility of the device. (b) A comparison between performances of LSG-EC using gelled versus aqueous electrolytes. (c) Flexibility of the LSG-based supercapacitor: current–voltage measurements were collected at a scan rate of 1000 mV s^{-1} [71]. Reprinted from Ref. [71] with permission. Copyright 2012, AAAS. (d) Syntheses and proposed structures of edge-carboxylated graphene (ECG) and heat-treated (decarboxylated) ECG (H-ECG) [65]. Reprinted from Ref. [65] with permission. Copyright 2012, the National Academy of Sciences.

area associated with individual graphene sheets in the graphene electrode is inaccessible due to restacking via the strong π–π interaction. Therefore, it is crucial to physically separate 2D graphene sheets to preserve their high surface area, for example by template-assisted construction of 3D graphene foams (Fig. 5a,b) with a porous structure and large surface area [76–79]. In addition, a solution layer-by-layer self-assembling approach to prepare multilayered hybrid carbon films of alternating poly(ethyleneimine)-modified graphene sheets and acid-oxidized MWNT layers was developed to construct supercapacitors with a relatively high specific capacitance of 120 F g^{-1} (higher than those of vertically-aligned [35] and random CNT electrodes [32]) and rate capability since the well-defined interlayers of CNT networks allowed for not only a fast ion diffusion but also efficient electron transport [80]. However, it is difficult to control the porosity and pore distribution within the multilayered CNT/graphene hybrid film as each of the constituent CNT and graphene layers is randomly assembled, and hence it is infeasible to further improve the device performance. To address this issue, 3D pillared VA-CNT/graphene architectures with alternating VA-CNT and graphene layers, whose porous structure and pore distribution can be easily controlled by tuning the length and packing density of VA-CNTs, have been produced [81–83] and investigated as ideal electrode materials for advanced supercapacitors [84–88]. By intercalated growth of VA-CNTs into thermally-expanded highly ordered pyrolytic graphite (HOPG), a 3D pillared VA-CNT/graphene architecture was

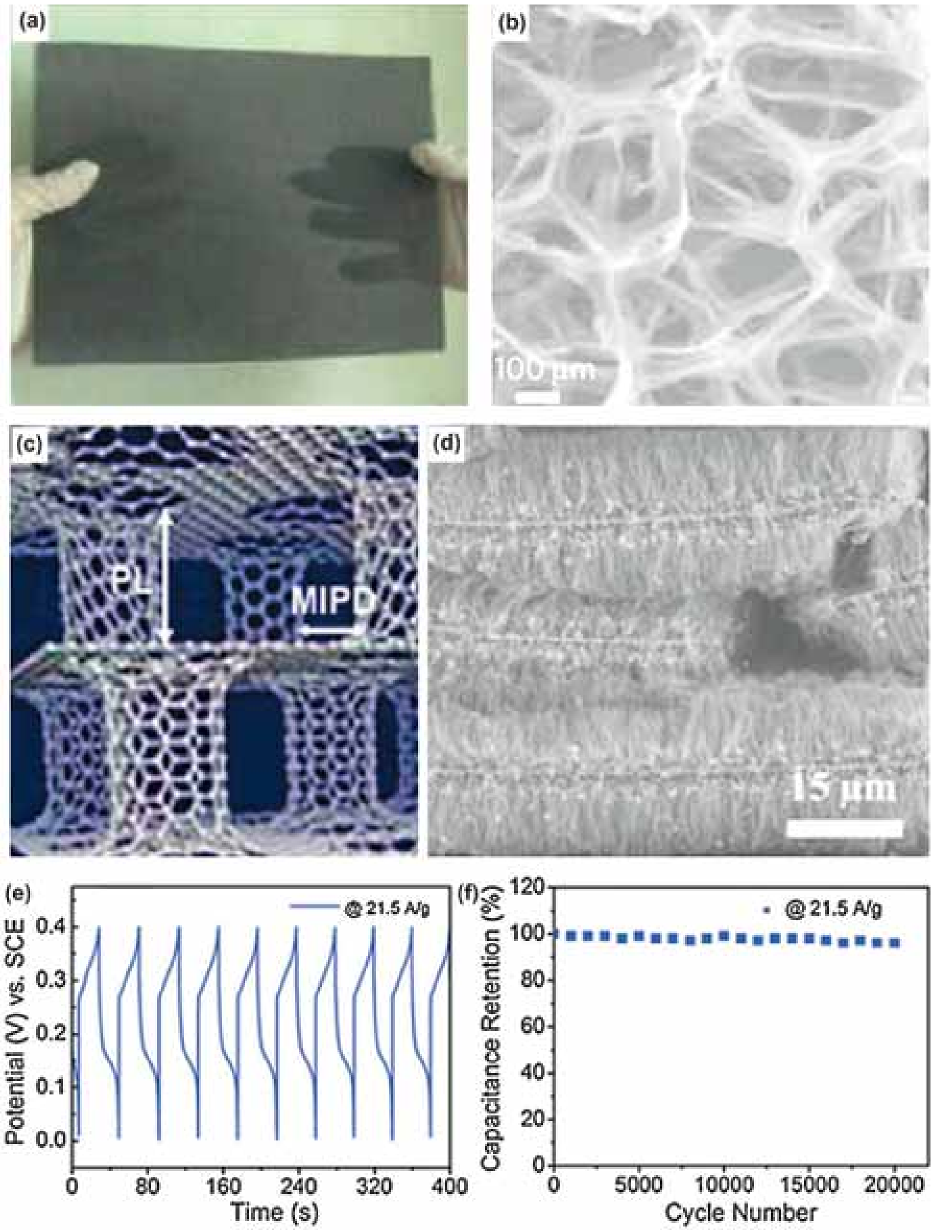

FIGURE 5

Structure of graphene foam, 3D pillared VA-CNT/graphene architecture and the electrochemical properties of its composite with $Ni(OH)_2$. (a) Photograph of a 17 cm × 22 cm free-standing graphene foam. (b) SEM image of a graphene foam [76]. Reprinted from Ref. [76] with permission. Copyright 2011, Nature Publishing Group. (c) Schematic diagram of a 3D pillared VA-CNT/graphene nanostructure. (d) Typical SEM images of the 3D pillared VA-CNT/graphene architectures. (e) Galvanostatic charge and discharge curves for the $Ni(OH)_2$-coated VA-CNT/graphene electrode at a current density of 21.5 A/g. (f) Dependency of the specific capacitance versus cycle number for the $Ni(OH)_2$-coated VA-CNT/graphene electrode at a galvanostatic charge and discharge current density of 21.5 A g^{-1} [89]. Reprinted from Ref. [89] with permission. Copyright 2009, American Chemical Society.

created (Fig. 5c,d) [89], which showed a specific capacitance of about 110 F g^{-1} in an electrical double layer supercapacitor. The resulting 3D pillared structure hybridized with nickel hydroxide coating showed a high specific capacitance (1065 F g^{-1}, Fig. 5e) with a remarkable rate capability and excellent long-term electrochemical stability – only 4% capacity loss after 20,000 charge–discharge cycles (Fig. 5f) [89].

The value of 1065 F g^{-1} is about 10 times that of the high-surface-area activated carbons (<100 F g^{-1}) [90] and within the range of 953–1335 F g^{-1} for graphene-supported single-crystalline nickel hydroxide hexagonal nanoplates [91]. In the 3D hierarchical structure, VA-CNTs can act as not only mechanical supports for the graphene layers but also good conductive paths for electrons and ions, and hence the high capacitance and excellent rate capability.

High-performance supercapacitors with novel structures

As discussed above, significant progress has been achieved with conventional supercapacitors based on liquid electrolytes. However, they cannot satisfy the requirements for certain specific applications, including portable, transparent and wearable electronics. In this regard, recent work on the development of lightweight, flexible, stretchable (Fig. 6a–c) [10–12] and/or transparent (Fig. 6d,e) [8,9] supercapacitors with novel structures (e.g. all-solid [6,7], fiber-shaped [13–15]; Fig. 6f–h) has attracted a great deal of attention. Highly-stretchable supercapacitors based on buckled SWNT macrofilm electrodes have also been developed by coating a thin SWNT film onto a pre-strained elastomeric substrate (polydimethylsiloxane, PDMS) and followed by relaxation of the pre-strained substrate (Fig. 6a) [11]. Even when these supercapacitors

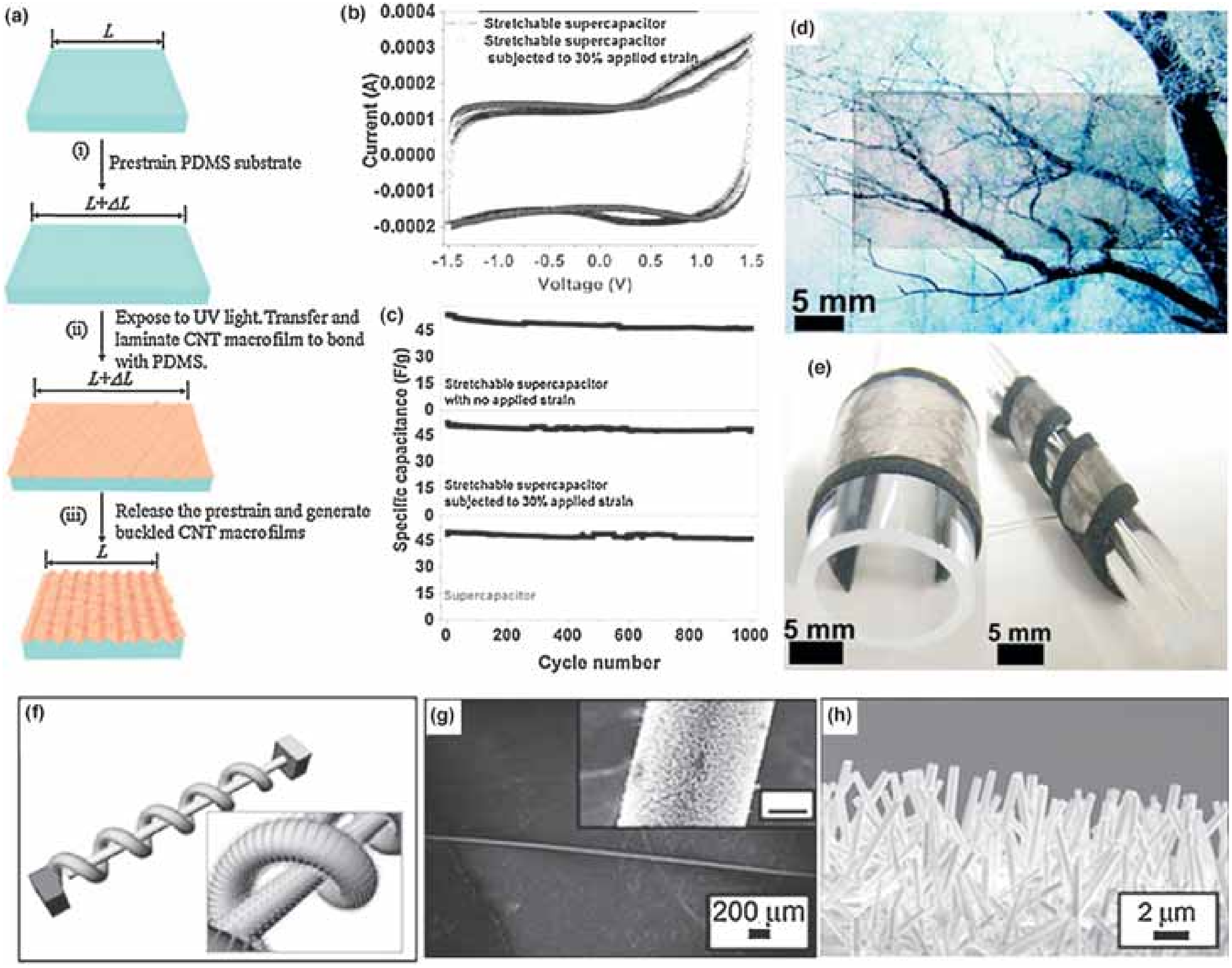

FIGURE 6

Supercapacitors with novel structures and their electrochemical performances: (a) Schematical illustration of the fabrication steps of a buckled SWNT macrofilm on an elastomeric PDMS substrate for stretchable supercapacitor. (b) Cyclic voltammograms of the stretchable supercapacitors measured at scan rates of 100 mV s^{-1}. (c) Long charge–discharge cycling at a constant current density of 1 A g^{-1} demonstrates the stability of the stretchable supercapacitor under 0 and 30% applied tensile strain [10]. Reprinted from Ref. [10] with permission. Copyright 2009, John Wiley and Sons. (d,e) Optical pictures demonstrating transparent (d) and flexible (e) natures of the supercapacitors [8]. Reprinted from Ref. [8] with permission. Copyright 2012, Nature Publishing Group. (f) Schematically illustration of a fiber-based supercapacitor. (g) Low-resolution SEM image of a Kevlar fiber covered with ZnO nanowire arrays. (Inset) A close-up view (scale bar: 10 µm). (h) Higher-magnification SEM image of the plastic wire, showing arrays of NWs [13]. Reprinted from Ref. [13] with permission. Copyright 2012, John Wiley and Sons.

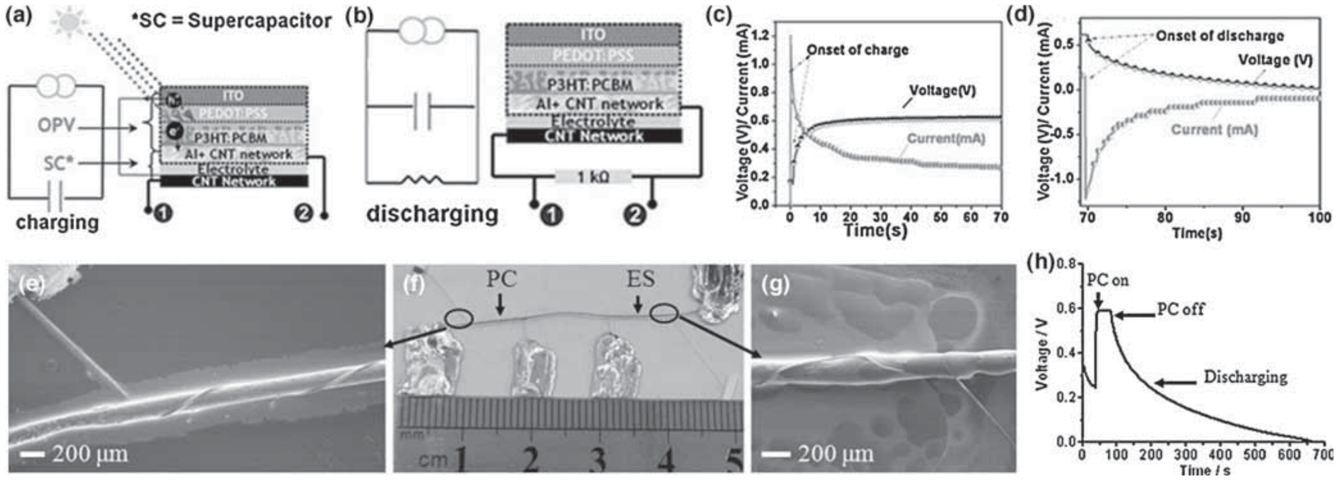

FIGURE 7

Structures and properties of integrated self-powering devices in planar and fiber forms. (a,b) Schematic and circuit illustrations of a PSC during the charging (a) and discharging (b) process. (c,d) The voltage and current profiles versus time for the charging (c) and discharging (d) process of a PSC [95]. Reprinted from Ref. [95] with permission. Copyright 2011, The Royal Society of Chemistry. (e) Photograph of a typical integrated wire-shaped device consisting of photoelectric conversion (PC) and energy storage (ES). (f) SEM image of the end PC part. (g) SEM image of the end ES part. (h) A typical photocharging–discharging curve of the integrated energy wire. The discharging current is 0.1 μA [98]. Reprinted from Ref. [98] with permission. Copyright 2012, John Wiley and Sons.

were stretched up to 30% stains, their electrochemical properties and stabilities remained almost unchanged with respect to the pristine state (Fig. 6b,c). By extension, stretchable electrodes based on graphene or aligned CNT films should be potential candidates for stretchable supercapacitors with a high efficiency [92,93], which can be used as the energy source for stretchable electronics. On the other hand, supercapacitors with high optical transparency (Fig. 6d,e) are useful for personal electronics and energy windows as power sources; they are also crucial components for many other power-integrated devices (e.g. self-powered light-emitting diodes, vide infra). Recently, supercapacitors in a fiber form (Fig. 6f–h) have been demonstrated to show many unique advantages, including being lightweight, wearable and flexible, for use as power sources by integrating them into clothing, bags and other textiles [13–15]. Specific capacitance as high as 38 mF cm^{-2} has been achieved for a fiber-shaped supercapacitor based on the CNT/PANI composite fiber electrodes [15].

Integrated self-powering systems

Self-powering systems with integrated energy conversion (e.g. solar cells) and storage (e.g. supercapacitors) devices have recently attracted more and more attention [94–96]. Using an SWNT network as the integration platform (Fig. 7a,b), for instance, a printable all-solid integrated device consisting of a polymer solar cell (PSC) and a supercapacitor has been developed [95]. The supercapacitor charged when the integrated device was under an illumination of 100 mW cm^{-1}, whereas discharging took place once the light source was switched off and the device was connected to a resistor as a load (Fig. 7a,b). Fig. 7c,d shows the voltage and current profiles versus time of the integrated system during the charging and discharging process, respectively, with a capacitance of 28 F g^{-1} [95]. Integrated devices containing an energy conversion unit and a supercapacitor in a single wire have also been devised for wearable electronics [97,98]. Specifically, Fig. 7e–g shows an integrated self-powering energy wire, consisting of a wire-shaped dye-sensitized solar cell (DSSC) and a supercapacitor both based on an aligned CNT fiber and modified titanium wire as the two electrodes, for simultaneous energy conversion and storage [98]. The supercapacitor in this integrated device can be rapidly charged to a voltage (Fig. 7h) close to the open-circuit voltage of the DSSC upon light irradiation. The entire energy conversion and storage efficiency up to 1.5% was obtained by multiplying the energy conversion efficiency of the solar cell part and the energy storage efficiency of the storage part. We anticipate considerable technical challenges ahead but also believe many more developments will be made over the next few years to advance the fiber-shaped integrated self-powering systems for wearable electronic applications.

Concluding remarks

With global energy consumption and CO_2 emissions increasing exponentially, it is crucial to develop clean and renewable energy systems and advanced energy storage devices. Nanotechnology has opened up new frontiers in materials science and engineering to meet this challenge by creating new materials and technologies for efficient energy conversion and storage. Of particular interest, carbon nanomaterials (e.g. CNTs and graphene) have been shown to be attractive for advanced energy storage applications. Recent research and development clearly indicate that high-performance supercapacitors can be prepared by using electrodes based on vertically-aligned CNTs with opened tips, graphene sheets with tunable through-thickness π–π stacking interactions and/or edge functionalities, and 3D pillared graphene-carbon nanotube networks. Their performance can be further enhanced by coating with conductive polymers and/or metal oxide to introduce pseudocapacitance. However, it is still challenging to further improve the performance of supercapacitors based on carbon nanomaterials. On one hand, the aggregation of CNTs and/or graphene materials tends to result in a loss of surface area, and hence inferior device performance. Carbon nanomaterials with various 3D architectures (such as CNT arrays, graphene foams, and 3D pillared VA-CNT/graphene networks), along with the 2D graphene sheet transferred onto a crumpled structure [99,100], have been developed to prevent the aggregation. On the other hand, the relatively high cost compared to commercial mesoporous and/or activated carbon is another challenge for carbon nanomaterials to be scaled up for practical application in supercapacitors. Therefore, it is highly desirable to develop carbon nanomaterials with high charge capacity at a low cost (e.g. by ball milling).

For potential applications in portable and wearable optoelectronics, conventional supercapacitors are too heavy and bulky. To address these challenges, a few optically transparent, mechanically stretchable, and/or wearable wire-shaped supercapacitors have been developed based on limited electrode materials. The wire-shaped supercapacitors and the integrated self-powering systems play important roles in the development of flexible wearable optoelectronics. Aligned CNTs and/or graphene films with high transparency, stretchability, and charge mobility are promising electrodes for transparent, flexible, and/or stretchable supercapacitors, although it is still in the initial research stage. Continued research efforts in this embryonic field could give birth to a flourishing area of supercapacitor technologies.

Acknowledgement

The authors are grateful for financial support from AFOSR (FA9550-12-1-0037, FA-9550-12-1-0069 NSFC-NSF (DMR-1106160)).

References

1 M. Winter, R.J. Brodd, Chem. Rev. 104 (2004) 4245.
2 P. Simon, Y. Gogotsi, Nat. Mater. 7 (2008) 845.
3 M.D. Stoller, R.S. Ruoff, Energy Environ. Sci. 3 (2010) 1294.
4 L.L. Zhang, X. Zhao, Chem. Soc. Rev. 38 (2009) 2520.
5 W. Lu, L. Dai, in: J.M. Marulanda (Ed.), Carbon Nanotubes, In-Tech, 2010, pp. 563–589.
6 C. Meng, et al. Nano Lett. 10 (2010) 4025.
7 L. Yuan, et al. ACS Nano 6 (2012) 656.
8 H.Y. Jung, et al. Sci. Rep. 2 (2012) 773.
9 Z. Niu, et al. Small 9 (2013) 518.
10 C. Yu, et al. Adv. Mater. 21 (2009) 4793.
11 X. Li, et al. Nano Lett. 12 (2012) 6366.
12 Z. Niu, et al. Adv. Mater. 25 (7) (2013) 1058.
13 J. Bae, et al. Angew. Chem. Int. Ed. 50 (2011) 1683.
14 Z. Cai, et al. J. Mater. Chem. A 1 (2013) 258.
15 K. Wang, et al. Adv. Mater. 25 (2013) 1494.
16 L.L. Zhang, et al. J. Mater. Chem. 20 (2010) 5983.
17 K. Kierzek, et al. Electrochim. Acta 49 (2004) 515.
18 E. Raymundo-Pinero, et al. Carbon 44 (2006) 2498.
19 E. Raymundo-Pinero, et al. Adv. Mater. 18 (2006) 1877.
20 E. Frackowiak, F. Béguin, Carbon 39 (2001) 937.
21 B. Kastening, S. Spinzig, J. Electroanal. Chem. 214 (1986) 295.
22 S.T. Mayer, et al. J. Electrochem. Soc. 140 (1993) 446.
23 I. Tanahashi, et al. J. Electrochem. Soc. 137 (1990) 3052.
24 J. Chmiola, et al. Science 313 (2006) 1760.
25 J. Huang, et al. Angew. Chem. Int. Ed. 47 (2008) 520.
26 T.E. Rufford, et al. J. Phys. Chem. C 113 (2009) 1933.
27 A.K. Geim, K.S. Novoselov, Nat. Mater. 6 (2007) 183.
28 L. Dai, et al. Small 8 (2012) 1130.
29 S. Iijima, Nature 354 (1991) 56.
30 M. Cinke, et al. Chem. Phys. Lett. 365 (2002) 69.
31 C.M. Niu, et al. Appl. Phys. Lett. 70 (1997) 1480.
32 K.H. An, et al. Adv. Funct. Mater. 11 (2001) 387.
33 E. Frackowiak, et al. J. Power Sources 97–98 (2001) 822.
34 R.H. Baughman, et al. Science 297 (2002) 787.
35 D.N. Futaba, et al. Nat. Mater. 5 (2006) 987.
36 M. Kaempgen, et al. Nano Lett. 9 (2009) 1872.
37 A. Izadi-Najafabadi, et al. ACS Nano 5 (2011) 811.
38 C. Liu, et al. Nano Lett. 10 (2010) 4863.
39 M.D. Stoller, et al. Nano Lett. 8 (2008) 3498.
40 Y. Zhu, et al. Science 332 (2011) 1537.
41 K. Novoselov, et al. Nature 438 (2005) 197.
42 C. Lee, et al. Science 321 (2008) 385.
43 J.S. Wu, et al. Chem. Rev. 107 (2007) 718.
44 W. Lu, et al. J. Power Sources 189 (2009) 1270.
45 C.S. Du, et al. Nanotechnology 16 (2005) 350.
46 S.M. Huang, L.M. Dai, J. Phys. Chem. B 106 (2002) 3543.
47 H. Zhang, et al. Nano Lett. 8 (2008) 2664.
48 L.J. Gao, et al. Solid State Commun. 146 (2008) 380.
49 W. Lu, et al. ECS Trans. 6 (2008) 257.
50 H. Chen, et al. Mater. Sci. Eng. R: Rep. 70 (2010) 63.
51 A. Thess, et al. Science 273 (1996) 483.
52 B. Zheng, et al. Nano Lett. 2 (2002) 895.
53 L. Dai, et al. ChemPhysChem 4 (2003) 1150.
54 Y. Yan, et al. Small 3 (2007) 24.
55 L. Qu, L. Dai, J. Mater. Chem. 17 (2007) 3401.
56 Q.L. Chen, et al. Electrochim. Acta 49 (2004) 4157.
57 H. Zhang, et al. J. Electrochem. Soc. 155 (2008) K19.
58 F. Huang, et al. ChemSusChem 5 (2012) 888.
59 Y. Hu, et al. Electrochim. Acta 66 (2012) 279.
60 Y. Hou, et al. Nano Lett. 10 (2010) 2727.
61 Q. Wang, et al. Adv. Funct. Mater. 16 (2006) 2141.
62 Y.T. Kim, et al. J. Mater. Chem. 15 (2005) 4914.
63 R. Van Noorden, Nature 469 (2011) 14.
64 S. Park, R.S. Ruoff, Nat. Nanotechnol. 4 (2009) 217.
65 I.-Y. Jeon, et al. Proc. Natl. Acad. Sci. U. S. A. 109 (2012) 5588.
66 I.-Y. Jeon, et al. J. Am. Chem. Soc. 135 (2012) 1386.
67 L. Dai, Acc. Chem. Res. 46 (2013) 31.
68 J. Liu, et al. MRS Bull. 37 (2012) 1265.
69 J.L. Xia, et al. Nat. Nanotechnol. 4 (2009) 505.
70 C.G. Liu, et al. Nano Lett. 10 (2010) 4863.
71 M.F. El-Kady, et al. Science 335 (2012) 1326.
72 J. Xu, et al. ACS Nano 4 (2010) 5019.
73 Q. Wu, et al. ACS Nano 4 (2010) 1963.
74 X. Dong, et al. Carbon 50 (2012) 4865.
75 S.H. Lee, et al. Adv. Funct. Mater. 21 (2011) 1338.
76 Z.P. Chen, et al. Nat. Mater. 10 (2011) 424.
77 Y.H. Xue, et al. Angew. Chem. Int. Ed. 51 (2012) 12124.
78 X.H. Cao, et al. Small 7 (2011) 3163.
79 Y. Zhao, et al. Adv. Mater. 25 (2013) 591.
80 D. Yu, L. Dai, J. Phys. Chem. Lett. 1 (2010) 467.
81 G.K. Dimitrakakis, et al. Nano Lett. 8 (2008) 3166.
82 Y. Mao, J. Zhong, New J. Phys. 11 (2009) 093002.
83 V. Varshney, et al. ACS Nano 4 (2010) 1153.
84 Z. Fan, et al. Adv. Mater. 22 (2010) 3723.
85 R.K. Paul, et al. Small 6 (2010) 2309.
86 G.-P. Dai, et al. RSC Adv. 2 (2012) 8965.
87 V. Sridhar, et al. ACS Nano 6 (2012) 10562.
88 J. Lin, et al. Nano Lett. 13 (2013) 72.
89 F. Du, et al. Chem. Mater. 23 (2011) 4810.
90 O. Barbieri, et al. Carbon 43 (2005) 1303.
91 H.L. Wang, et al. J. Am. Chem. Soc. 132 (2010) 7472.
92 Y. Zhu, et al. Adv. Mater. 22 (2010) 3906.
93 K.S. Kim, et al. Nature 457 (2009) 706.
94 Z. Yang, et al. J. Mater. Chem. A 1 (2013) 954.
95 G. Wee, et al. Energy Environ. Sci. 4 (2) (2011) 413.
96 W. Guo, et al. Nano Lett. 12 (2012) 2520.
97 J. Bae, et al. Adv. Mater. 23 (2011) 3446.
98 T. Chen, et al. Angew. Chem. Int. Ed. 51 (2012) 11977.
99 J. Luo, et al. ACS Nano 5 (2011) 8943.
100 J. Luo, et al. ACS Nano 7 (2013) 1464.

Materials Today • Volume 16, Numbers 7/8 • July/August 2013

Modern plastic solar cells: materials, mechanisms and modeling

Ryan C. Chiechi[1,2,*], Remco W.A. Havenith[2], Jan C. Hummelen[1,2], L. Jan Anton Koster[2] and Maria A. Loi[2]

[1] Stratingh Institute for Chemistry, University of Groningen, Nijenborgh 4, 9747AG Groningen, The Netherlands
[2] Zernike Institute for Advanced Materials, University of Groningen, Nijenborgh 4, 9747AG Groningen, The Netherlands

We provide a short review of modern 'plastic' solar cells, a broad topic that spans materials science, physics, and chemistry. The aim of this review is to provide a primer for non-experts or researchers in related fields who are curious about this rapidly growing field of interdisciplinary research. We introduce the basic concepts of plastic solar cells and design rules for maximizing their efficiency, including modern quantum chemical calculations that can aide in the design of new materials. We discuss the history of the materials and modern trends in polymeric donor materials and fullerene acceptors, and provide demonstrative data from hybrid polymer/quantum dot devices.

Introduction

This short review provides an overview of research on organic photovoltaic (OPV) devices and many of the materials used in their construction. The sharp rise in societal interest in carbon-neutral, green energy technology in the 21st century has spurred a commensurate rise in research into OPV materials. The volume of this research, which spans chemistry, physics, and materials science, is too great to review in detail in one paper, thus our intent is to give an overview that can serve as an entry point for non-experts into the field or as a guide for researchers in tangential fields who have a general interest in OPV materials research. We focus on two broad categories of OPV devices, 'plastic' solar cells comprising a conjugated polymer and a fullerene acceptor and hybrid organic–inorganic solar cells that blend inorganic semiconductors into organic materials, and the basic principles of designing and understanding new materials and devices. For brevity, we omit small-molecule OPV devices, which are functionally nearly equivalent to polymer-based devices, and direct the reader to recent publications on this topic [1–3].

Photovoltaic cells use the energy of absorbed photons to generate free charge carriers (holes and electrons) which can do electrical work. Organic photovoltaic cells are photovoltaic devices that accomplish this conversion of energy using organic materials – either entirely or as part of a blend [4]. In all cases, at least one of the charge carriers traverses a bulk organic material. Silicon-based (and many other inorganic-based) photovoltaic devices generate free carriers directly from the absorption of a photon, but presently known organic materials do not screen charges as effectively as silicon (because of their lower dielectric constant), which introduces extra steps in the mechanism. In modern OPV devices, the absorption of a photon creates an exciton (i.e. a bound electron-hole pair) which must then be split into free carriers before it decays back to the ground-state, thus OPV devices are 'excitonic' solar cells. This scission process takes place at the interface between the two constituent materials, a donor and an acceptor. These materials are chosen such that energy offsets between the energy levels exist, thus making charge transfer energetically favored (Figure 1a). These materials can be layered or intimately mixed, provided there is a continuous pathway for both holes and electrons to traverse toward the electrodes. Figure 2 is a cartoon of a typical architecture for an OPV device with an inset showing the four basic steps of the exciton scission process at the interface between the donor and acceptor (in reality, many different phases exist in the heterojunction, the cartoon is simplified for clarity). (I) A photon is absorbed by either the donor or the acceptor, creating an exciton. (II) The exciton then diffuses to the interface between the donor and the acceptor. (The distance over which an exciton can travel before decaying is the exciton

---

*Corresponding author: Chiechi, R.C. (r.c.chiechi@rug.nl)

1369-7021/06/$ - see front matter http://dx.doi.org/10.1016/j.mattod.2013.07.003

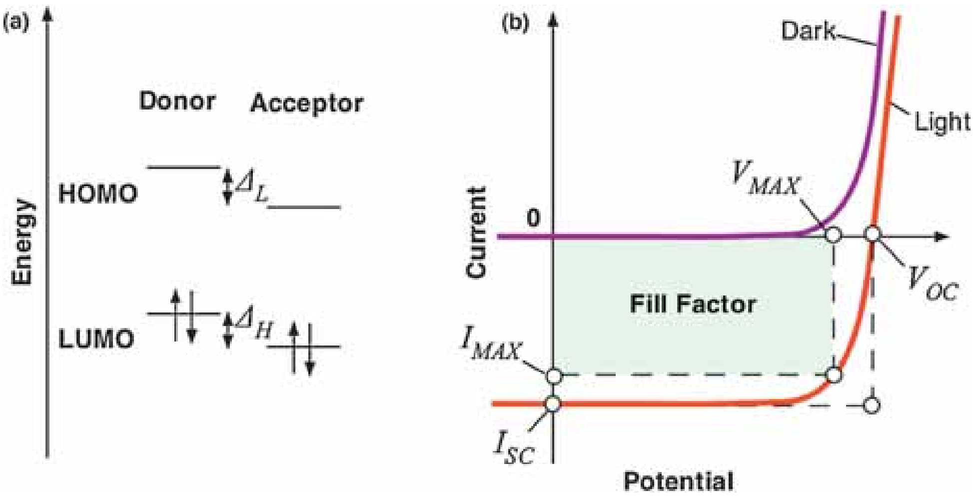

FIGURE 1

(a) Band diagram of a donor–acceptor combination showing HOMO and LUMO offsets. (b) Typical current–voltage characteristics of organic solar cells in dark and under illumination.

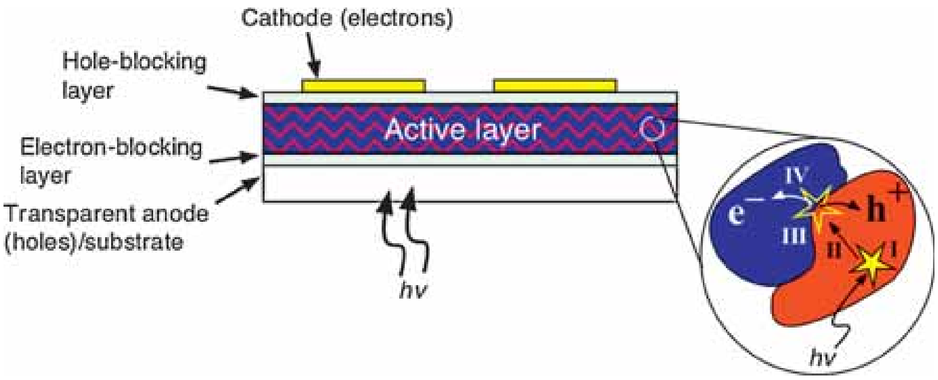

FIGURE 2

A cartoon of an organic photovoltaic device. The active layer comprises the donor and acceptor materials. The inset is a schematic of the scission of an exciton at the interface between the donor (red) and acceptor (blue) materials. (I) The absorption of a photon creates and exciton. (II) The exciton delocalizes to the donor/acceptor interface. (III) A charge-transfer state is created between the two materials. (IV) The charge transfer state dissociates into free carriers which then diffuse into the bulk.

diffusion length.) (III) When the exciton reaches the interface, an electron is transferred to the acceptor (or a hole is transferred onto the donor) creating a so-called charge-transfer (CT) state in which the charges reside on different molecules, but remain bound to each other by coulombic attraction. (IV) The charges overcome this attraction and the CT state dissociates into two free charge-carriers, an electron (e^-) and a hole (h^+), which then travel into the bulk, and eventually into the electrodes. The drift-direction of the charge-carriers is influenced by a difference in work function of the two metallic contacts, which can be further optimized by introducing blocking layers [5]. Hole and electron blocking layers are not present in all OPV devices, but are becoming increasingly common in architectures in which both the donor and the acceptor are in contact with both electrodes. The cathode material has historically been a low work function metal such as Ca or Al and the anode/substrate of a thin film of poly(ethylenedioxythiophene):poly(styrenesulfonate) (PEDOT:PSS) on tin-doped indium oxide (ITO) on glass or a transparent polymer substrate, but neither is particularly well suited for deployment in commercial devices, which require solution-processable electrode materials (e.g. silver inks).

Design rules

It is the excitonic nature of OPV devices that introduces challenges that are not present in silicon-based devices. For example, the nature of the CT state is not fully understood [6], nor is the exact mechanism of dissociation into free carriers. Furthermore, the broadband nature of the solar spectrum can lead to a complex set of charge separation mechanisms that may operate simultaneously, depending on the materials combinations and the morphology of the heterojunction. These challenges are rooted in the complex nature of organic materials for which slight variations in their packing and orientation in the solid-state give rise to substantially different properties. One can design a material with favorable optical properties – a large oscillator strength, broadband absorption, among others. – but current organic materials (usually) form excitons that have a limited lifetime and therefore a limited diffusion length. The relatively low dielectric constants of organic materials that gives rise to the excitonic mechanism also favors charge recombination, either geminate, when formed by absorption of the same photon (i.e. the initial CT state) while they are still weakly bound to each other across the interface or bimolecular (non-geminate), when free carriers annihilate each other.

There are no straightforward design rules for mitigating these losses – at least in terms of the specific chemical structure of the materials – but there are general rules for maximizing the external power conversion efficiency (PCE η) of an OPV device [7].

An OPV device is measured by sweeping a voltage range in the dark and under AM 1.5 G illumination (AM is the standard air mass, $1/\cos\theta$, $\theta = 48^\circ$ relative to the azimuth, and G is global, which accounts for diffuse, off-axis light). A cartoon of these *I/V* curves is shown in Figure 1b. The key parameters derived from these curves are the open-circuit voltage, V_{OC}, the short-circuit current, I_{SC}, and the fill factor, *FF*, from which η can be determined using Eq. (1) where P_{MAX} is the maximum incident power and *A* is the area of the device [8] (Note: Current density, J_{SC}, is often substituted for I_{SC}/A.) The degree to which a device deviates from ideality is captured in *FF*, which is largely a reflection of recombination processes.

$$\eta = FF\frac{I_{SC}V_{OC}}{AP_{MAX}} \quad (1)$$

The current–voltage characteristics and efficiencies of OPV devices are sometimes modeled using an equivalent circuit that places the source of the photocurrent in parallel with a diode and a resistor and in series with another resistor. However, such an approach obscures much of the physics so other models have been developed. Inspired by the observation that many polymer/fullerene solar cells (see below) are characterized by length scales that are smaller than typical device thicknesses (~100–200 nm), a one-dimensional drift-diffusion approach was developed [9]. In this model, the blend of acceptor and donor materials is treated as an effective medium. Despite the neglect of morphology, this modeling approach provided the first quantitative description of organic solar cells in terms of materials properties and basic physics. Several two-dimensional and three-dimensional models have been put forward to deal with morphological issues, both based on drift-diffusion [10–14], as well as, on kinetic Monte-Carlo techniques [15,16]. Finding a suitable description of the morphology is not trivial, but if it is known quantitative agreement can be obtained [14].

Idealized energy offsets for the donor and acceptor are shown in Figure 1a. A very simple approximation of the maximum possible V_{OC} is the difference in energy between the LUMO of the acceptor and the HOMO of the donor. When a photon is absorbed by either material, the resulting exciton will lose an amount of energy equivalent to Δ_H or Δ_L when it dissociates at the donor/acceptor interface however these values cannot be zero because they are the driving force for the dissociation. Empirically, ~0.3 eV is sufficient to drive the scission of excitons [17]. If the difference is smaller, excitons will tend to decay to the ground state. Any excess energy is dissipated and does not contribute to V_{OC}. The upper limit for I_{SC} can be approximated by the overall efficiency of the four steps shown in Figure 2, the transport of the free carriers, and their extraction by the electrodes. It is a reflection of the combined properties of the device, the materials, and the processing and the relaxation of high-energy photons to the band-edge, which is unavoidable. Therefore, V_{OC} is the one parameter that is (nearly) directly relatable to controllable materials properties, that is, the ionization potential and electron affinity of organic materials are synthetically adjustable and can be measured by a variety of means.

Next-generation organic solar cells

Until recently, it was argued that organic solar cells would always be less efficient than inorganic ones with maximum efficiencies of organics limited to 10–11% [7]. These 'design rules' have guided the research in this field for several years. However valuable, the analysis underlying these rules is limited. In a more extended treatment we have recently shown that OSCs can have efficiencies of more than 20% [18]. A key parameter is the screening of charge carriers by using high-ε materials. Light absorption then leads directly to significant numbers of free carriers, avoiding the need to use a large offset between the donor and acceptor energy levels. This mechanism would place organic solar cells on equal footing with their inorganic counterparts.

Donor and acceptor materials

Donors

Although the observation of photoconductivity [19] and eventually the photovoltaic effect in organic molecules [20] dates back to the early 20th century, modern organic photovoltaic began in earnest in 1986 with the 'Tang Cell,' which was a two-layer device comprising a glass/ITO anode supporting a layer of copper phthalocyanine (the donor), a perylene diimide derivative (the acceptor), and a gold cathode [21]. This device yielded $\eta \sim 1\%$ under AM 2 illumination, despite reasonably high values of $FF \sim 0.65$ because it consisted of only a planar donor/acceptor interface; the bulk of the volume of the device carries charges, but does not contribute to I_{PH}. In 1992 a team of researchers at UC Santa Barbara demonstrated photo-induced electron transfer from poly[2-methoxy-5-(2′-ethylhexyloxy)-*p*-phenylene vinylene] (MEH-PPV) to C_{60} [22]. This work demonstrated the principles of the first 'plastic' solar cell an OPV device containing a conjugated organic polymer. A follow-up to this work in 1995 introduced a soluble fullerene derivative, [6,6]-phenyl-C61-butyric acid methyl ester (PCBM) and defined the concept of a (polymer/fullerene) bulk heterojunction (BHJ) an intimate mixture between two materials (usually a conjugated polymer and a fullerene derivative) that creates a high surface area of contact between donor and acceptor materials through spontaneous, nanoscopic phase-segregation, preferably at the scale of the exciton diffusion lengths [23]. That same year, researchers at the University of Cambridge independently observed the formation of BHJs in intimate mixtures of polymers [24]. Virtually all OPV devices – polymer/fullerene, polymer/polymer, hybrid organic/inorganic, among others. – employ the BHJ strategy to optimize the area of the charge-separation interface in the volume of the active layer.

The early plastic solar cells utilized MEH-PPV, which was designed with asymmetric and racemic 2-ethylhexyl side-chains explicitly to make the polymer more glassy (i.e. homogeneous) in the solid state as well as to improve the solubility. That MEH-PPV and a derivative with longer racemic side-chains, poly[2-methoxy-5-(3′,7′-dimethyloctyloxy)-1,4-phenylenevinylene] (MDMO-PPV), performed so well in OPV devices was largely a coincidence that the spacing of the side chains was exactly the right size to allow fullerenes to intercalate, providing close π–π contact between the materials and improved charge transport. Nearly simultaneously McCullough *et al.* developed a straightforward route to regio-regular poly(3-alkylthiophenes) and specifically regio-regular poly(3-hexylthiophene) (rr-P3HT) [25]. Although the band-gap of rr-P3HT is slightly

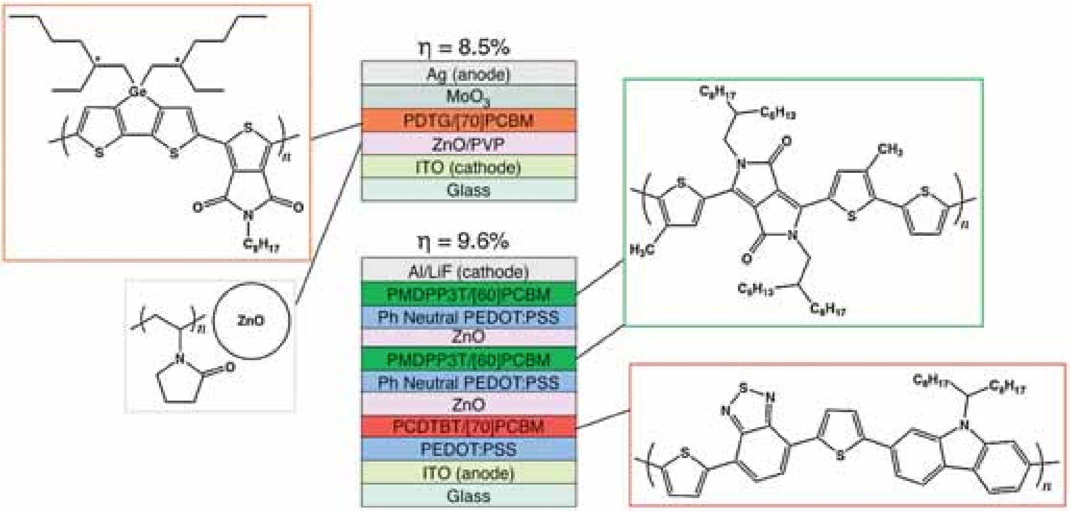

FIGURE 3

A schematic of two exemplary polymer/fullerene OPV devices and the structure of the polymers used in their fabrication from Refs. [29,31]. Top: a single-junction cell in an inverted architecture in which a PVP/ZnO nanoparticle composite serves as an intermediate layer that allows ITO to serve as a cathode. In this configuration, the MoO_3 layer serves the same function as PEDOT:PSS in a non-inverted device. Bottom: a triple-junction device in which three single-layer devices are stacked and wired in series to efficiently harvest a large portion of the visible-to-NIR spectrum.

too large to match the solar spectrum, the Van der Waals interactions of the hexyl side-chains create a strong driving force for the formation of highly crystalline domains and the HOMO and LUMO levels are matched sufficiently (though not perfectly) well to PCBM. The result is an 'ink' of rr-P3HT/PCBM that is capable of producing devices of $\eta \sim 5\%$ with unparalleled reproducibility. Thus it became the benchmark against which materials, fabrication methods, and device architectures are still largely compared [26]. Most modern conjugated polymers pursue the 'weak donor/strong acceptor' strategy combining 'weak donors' with 'strong acceptors' in co-polymers [27]. Here, the terms 'donor' and 'acceptor' are referring to the electron affinities of the co-monomers relative to each other and should not be confused with donors and acceptors in OPV devices; donor/acceptor co-polymers are still hole-carrying, donor materials. The weak (electron) donor pushes the HOMO level up, while the strong acceptor brings the LUMO level down, thus narrowing the band-gap and matching the energy levels of the fullerene acceptor. This strategy has pushed η into the 5–10% range, which recently exceeded 10% in a tandem OPV cell [28].

Figure 3 is a schematic of two exemplary polymer/fullerene OPV devices that capture many of the aspects of modern OPV materials and device design. The top device is inverted, meaning a silver anode collects holes, while the ITO cathode collects electrons [29]. Inverted architectures are desirable for commercialization because they obviate the need for reactive cathode materials, but until recently they have generally lagged behind in efficiency. In this case, efficient inversion is accomplished by using ZnO in poly(vinylpyrrolidone) (PVP) matrix at the cathode and MoO_3 at the anode. This device also incorporates a donor/acceptor co-polymer containing Ge [30]. The use of heteroatoms, particularly the higher chalcogens and carbon group elements, in conjugated polymers is an increasingly common strategy that influences bond lengths and angles and interchain interactions without negatively impacting the electronic properties. The bottom device in Figure 3 shows a triple-junction architecture, where three single-junction OPV cells are stacked and wired in series [31]. Multi-junction OPV devices benefit from being able to capture different portions of the spectrum with different active layers, allowing each material to be tuned for a specific absorbance range and potentially reducing losses from band-edge relaxation however, balancing the annihilation of charges at each interface is non-trivial and requires optimization for each combination of materials. A broad discussion of various polymer solar cell architectures can be found elsewhere [32].

Acceptors

Despite the recognition of the active role of acceptors in light-harvesting going all the way back to the Tang Cell [21], fullerene acceptors in BHJ plastic PV based on polymer/fullerene combinations were primarily viewed to serve simply as efficient electron acceptor and electron conductor in the blend. As a consequence, the mainstream of materials research in plastic PV has invariably been focused on the development of new and better oligomeric or polymeric donor materials donors with optimized optical bandgap for the AM 1.5 spectrum, with the a hole mobility similar to the electron mobility of [60]PCBM for balanced charge transport, with an optimized LUMO-LUMO offset between that of the polymer and that of [60]PCBM (i.e. Δ_L), good processability, and chemical stability. Nevertheless, with the introduction of [70]PCBM, ten years ago, it was already proven that there is only one fundamental difference between donor and acceptor materials in functioning in a donor/acceptor molecular solar cell: the transport of the type of charge carriers. [70]PCBM (available only as a mixture of isomers, in contrast to [60]PCBM, which is a single compound) is a versatile and strongly blue and green light absorbing acceptor with an electron mobility only slightly less than that of [60]PCBM. The absorption spectrum of [70]PCBM makes it a complementary (to the donor polymer) absorber in almost every world record efficiency plastic solar cell of the past ten years. Hence, under AM 1.5 illumination, absorption and exciton diffusion take place in both phases, leading to both hole and electron transfer processes at the D/A interface [33,34].

The key feature of fullerenes and their solution processable derivatives in the PV active layer is their low internal reorganization energy in every relevant process in which they are involved. This low reorganization energy, the high polarizability of the molecule [35], and the relatively high dielectric constant of the solid [36] ($\varepsilon_r = 4$) are closely related properties that stem from the spherical shape and the size of the π-conjugated system. Hence, the spherical shape, albeit a nightmare to the chemists who try to design efficient (supra)molecular architectures for highly efficient PV action between donor and acceptor molecular systems, is a unique and highly beneficial property for OPV application. While [60]PCBM and [70]PCBM have almost identical and quite versatile optical bandgaps for standard PV application, [84]PCBM is a real low bandgap material that can be employed in IR-sensitive PV devices [37].

As is evident by the challenges surrounding polymer acceptors [38,39], designing superior alternatives to fullerenes is far from trivial, as they will have to surpass a whole set of strong features of [70]PCBM. Nevertheless, especially in the search for ultimately green and high dielectric constant active layer ingredients, non-fullerene acceptors are potentially more viable candidates, at least in the long run.

Hybrid organic–inorganic solar cells

Hybrid photovoltaic devices based on blends of semiconducting polymers and colloidal semiconductor nanocrystals (NCs) [40] represent an emerging technology able to combine the advantages of the two classes of materials the high optical absorbance of conjugated polymers and the high conductance, tunable optical band gap and high dielectric constant of nanocrystals ($\varepsilon = 17$ for PbS and $\varepsilon = 23$ for PbSe) [41–43]. Among the many semiconductor nanocrystals under investigation for photovoltaic applications (CdSe [44,45], CdS [46,47], CdTe [48], PbSe [49–51]), lead sulfide (PbS) NCs [52] have emerged as one of the most promising candidates, because of their high electron mobility [53,54], broad absorption and stability [55,56]. In particular, the synthetic control over the PbS diameter allows for the precise tuning of the quantum confined energy gap [57] enabling solar energy conversion in the near-infrared (NIR) [58]. Moreover, the high quality of PbS NCs allows power conversion efficiencies above 4% with a simple Schottky junction solar cells (metal semiconductor junctions) [59,60]. While hybrid OPV devices are relatively new compared to polymer/fullerene blends, they are rapidly gaining ground.

The stringent requirements for the realization of efficient hybrid blends have limited the performance of the PbS/polymer system until now. Only very recently the Prasad group [61] showed that it is possible to meet all these criteria and to achieve high efficiency in hybrid devices based on PbS NCs. By selecting a suitable narrow band-gap polymer, poly(2,6-(*N*-(1-octylnonyl)dithieno[3,2-*b*:20,30-*d*]pyrrole)-*alt*-4,7-(2,1,3-benzothiadiazole)) (PDTPBT) [62], and performing a post deposition ligand exchange, they realized an energetically favorable type II heterojunction with broad spectral response and a PCE of 2%. Optimization of the devices, by selecting the suitable nanoparticle size and by inserting a titania (TiO_2) interlayer before the cathode deposition, allowed reaching 3.78%. Prasad and co-workers showed the importance of the energy levels matching between the polymer and the nanoparticles, and the efficacy of the post-deposition ligand exchange treatment.

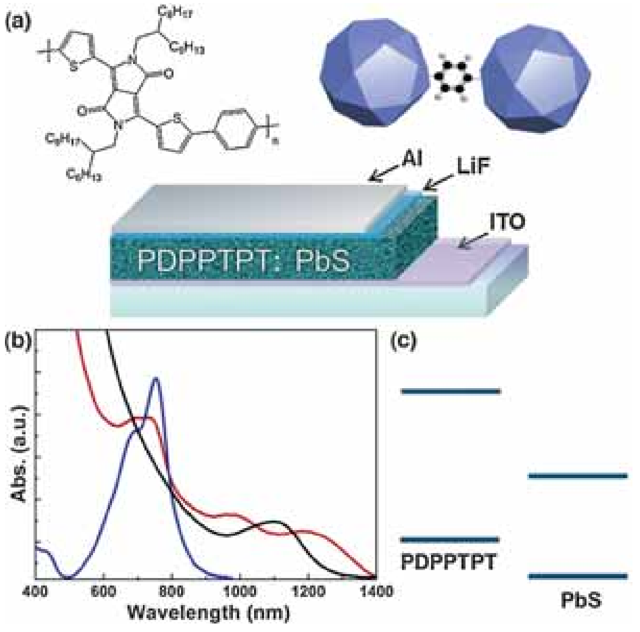

FIGURE 4

Molecular structure of the PDPPTPT polymer, schematic of the BDT crosslinked PbS nanocrystals and of the device structure. [63] Reproduced by permission of the Royal Society of Chemistry

Using a simpler device structure Piliego *et al*. realized efficient bulk heterojunction solar cells with PbS NCs and a narrow band gap polymer, PDPPTPT (poly[{2,5-bis(2-hexyldecyl)-2,3,5,6-tetrahydro-3,6-dioxopyrrolo[3,4-*c*]pyrrole-1,4-diyl}-*alt*-{[2,2′-(1,4-phenylene)bisthiophene]-5,5′-diyl}]) [63].

Using this bulk heterojunction blend produced a simple and efficient hybrid solar cell, as shown in the schematic device configuration in Figure 4. A thin layer of PDPPTPT:PbS-OA (10:90 wt%) blend was deposited on the top of the ITO substrate by spin-coating, followed by the ligand exchange treatment. Optical measurements performed on the blend indicate that the combination of the PbS nanoparticles with this narrow band gap polymer form a type II heterojunction (i.e. Figure 1a) and is expected to provide good photovoltaic performance. Figure 5a shows the *I–V* characteristic of the best PDPPTPT:PbS blend device measured under AM 1.5 illumination at 100 mW/cm^2. The device exhibits a J_{SC} of 12.5 mA/cm^2, V_{OC} of 0.47 V, and a FF of 49% resulting in an overall PCE of 2.9%. This value is remarkable considering the absence of interlayers at the interface with the electrodes. It has been shown that the insertion of a thin hole blocking buffer layer, such as TiO_2 or ZnO [64], on top of the active layer could dramatically improve the performance. Figure 5b compares the incident photon-current conversion efficiency (IPCE) spectrum of the device from the PDPPTPT:PbS blend and the absorption spectrum of the BDT treated blend film. The IPCE spectrum obtained from the device is consistent with the film absorption showing the combined contribution of PDPPTPT and PbS. This proves that blending the narrow band gap polymer and the NIR absorbing PbS NCs gives rise to a broad response covering from the UV to the NIR spectral range.

Progress in device physics

The importance of charge transport in OPV has been widely recognized [65]. If charges cannot be transported out of the active layer sufficiently quickly, there is a real possibility for them to

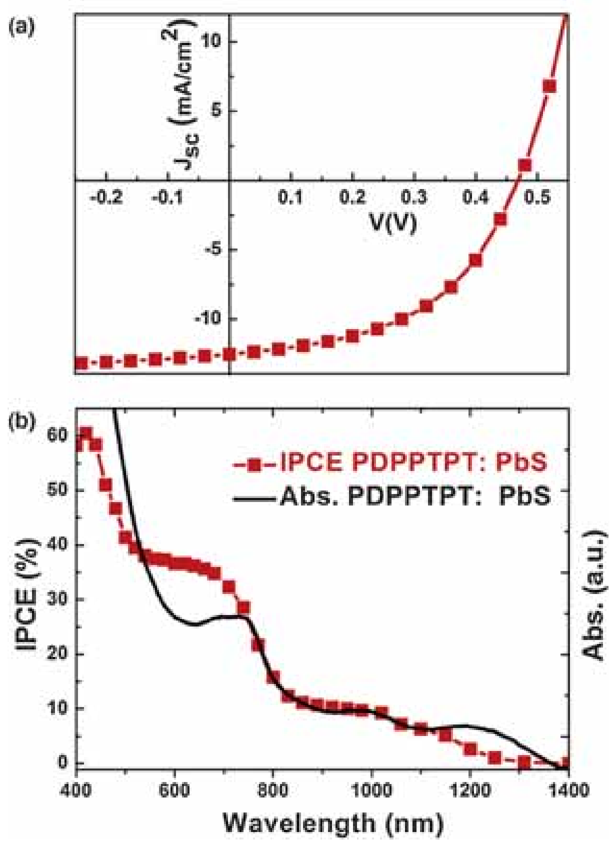

FIGURE 5

(a) *I–V* characteristics of the PDPPTPT:PbS (10/90 wt%) blend under AM 1.5 G (100 mW/cm^2), and (b) plots of the IPCE of the blend device and the absorption spectrum of the BDT-treated blend film. [63] Reproduced by permission of the Royal Society of Chemistry

recombine. Additionally, if one carrier species is much slower than the other one a net space-charge will be built-up in the active layer [65,66]. This space-charge distorts the electric field such that the extraction of the slower species is aided, at the cost of slowing down the extraction of the faster species. The overall process limits the fill-factor and efficiency of solar cells with unbalanced electron and hole mobilities.

Organic materials are characterized by both energetic and positional disorder. Charge transport involves a sequence of hopping events, whereby carriers hop from one localized site to another. Clearly, this is very different from band-type transport in high-quality inorganic semiconductors. It is well known that the mobility of charge carriers in organic materials is a strong function of electric field and carrier density [67]. While there exist several techniques to measure charge transport in one form or another, not all of them are equally suited to OPV materials. To reflect charge transport in OPV devices, the electric field and carrier density need to be representative of real devices. It is therefore not straightforward to use field-effect transistor (FET) data to describe the transport in organic solar cell materials as FETs operate at much higher carrier densities than solar cells do.

Another important realization regards charge transport was the discovery that a donor/acceptor blend can have very different transport properties than their pristine constituents [65]. For example, in PPV/PCBM blends the hole mobility is found to be several orders of magnitude higher than in the pristine PPV material. This behavior is indicative of the ability of interactions between fullerenes and the pendant groups of conjugated polymers to affect π-stacking in the backbone [65].

Charge transport is but one side of the charge-extraction coin. Bimolecular recombination is the other. Whereas bimolecular recombination in organic LEDs follows standard Langevin theory [68], which implies that it is governed by the sum of the mobilities, large deviations have been found in several donor–acceptor blends [69]. Surprisingly, recombination processes are much slower in these blends, which greatly improves the efficiency.

One of the central parameters of organic solar cells is the open-circuit voltage (V_{OC}). Broadly speaking, it is determined by the work functions of the contacts [70], the energy levels of the materials [71] and the carrier generation and recombination processes [71,72]. In 2006, these insights in the device physics of organic solar cells culminated in the prediction that PCEs over 10% could be reached [7,73]. At the time, the highest reported efficiencies were in the 3–4% range and the 10% efficiency mark was far away. However, provided the energy levels of the donors could be tuned to make the combination with fullerenes more favorable, while at the same time improving the overlap with the solar spectrum, it was predicted that organic solar cells could be much more efficient. With the benefit of hindsight, one can safely say that these are indeed key factors in the steady progress in efficiencies that have been reported since.

Electronic structure theory in organic photovoltaic materials

The description of OPV devices is a perfect example where multi-scale modeling is required. It ranges from microscale modeling, with accurate calculations on the individual constituent molecules, to device modeling, where macroscopic properties are used as input, to determine the efficiency of the actual device. The macroscopic properties used here as input can be derived from high-level calculations or from experiment. Complete modeling at the microscopic level of OPV devices is far from straightforward [74] for example, the structures of the devices are usually not known precisely, the size of the system hampers the application of many computational methods, and accurate descriptions of the ground state and the excited states are required, which limits the applicability of computational methods even further. The current strategy is to combine macroscale modeling molecular dynamics with quantum chemical calculations on the molecular scale.

Nowadays, the most studied features are the properties of the electronic ground and excited states of the polymers and oligomers, the morphology and structure of the donor–acceptor interface, the charge-transfer states at the donor–acceptor interface, and the transition rates for different decay pathways. The morphology of the donor–acceptor interface is usually studied using (course grained) molecular dynamics simulations of polymer/PCBM blends. Especially interesting is the morphology as a function of the polymer:PCBM ratio, to find the optimal blending ratio [75]. This optimal blending ratio appears to be quite dependent on the polymers for a P3HT:PCBM blend [75] a phase separation was found for a low PCBM weight percentage, while for a PBTTT:PCBM (PBTTT is a donor/acceptor co-polymer) blend [76] the optimal blending ratio had higher PCBM concentrations because of substantial intercalation of PCBM in PBTTT [77], leading to a PBTTT-plus-PCBM phase. Also, periodic DFT calculations have been performed to study P3HT/C_{60} interface, and in particular to gain insight in the interfacial charge-transfer mechanism [78]. In this study, it was found that an efficient adiabatic electron transfer is highly probable, because of the presence of an electronic state that extends across the interface in the lowest excited state.

Calculations on molecular systems have been performed to study the rates of electron transfer (see, e.g. [79–83]). The estimation of these rates is based on Marcus and related models [84,85]. Here, the governing matrix element is the electronic coupling between the diabatic initial and final states. One way to calculate this coupling matrix elements is the procedure of Kawatsu *et al.* [86] using the ZINDO/CISD approximation. Another way to evaluate these matrix elements is the use of nonorthogonal CI [87]. The competing singlet–triplet intersystem crossing rate can be estimated using a time-dependent approach [88]. The relative rates of the various possible processes can be used to predict whether charge-separation or recombination is favored at the donor/acceptor interface, guiding the design of new materials for OPV devices.

Combination of molecular dynamics and first principle calculations is nowadays the tool to study the charge-transfer states. Molecular dynamics simulations are performed to generate suitable geometries on which more accurate quantum chemical studies are performed, as has been done in some recent studies [89–91]. This combination of QM/MM was used to rationalize the good electron-hole separation at the P3HT/PCBM interface [90]. It turned out that near the interface, the P3HT chains are more disordered, which led to an increase in the band gap. This enlarged band gap has as a consequence that excitons and holes are repelled by the interface. In another study, the charge-transfer rates as a function of the variations in structure have been studied [89]. One interesting result is that two different interface geometry groups exist, one that supports charge transfer states with complete charge while the other group supports charge bridging states.

Because of size limitations, only DFT and semi-empirical calculations are computationally feasible at the moment. The excitation energies of the donor molecules are frequently calculated using the TDDFT approach, however, current popular functionals are usually not suitable for the calculation of the energies of the charge-transfer states [92,93]. Solutions to overcome this problem are the use of long-range corrected functionals [94,95–97], or constrained DFT calculations [98,99].

The environment can have a significant influence on the energetics of the excitation energies and the energies of the CT and CS states. These effects can be accounted for by using a QM/MM approach: a relatively small part of the system (one PCBM molecule and one oligomer) is treated using a quantum chemical approach, which is embedded in polarizable charges. Different schemes exist, like the Discrete Reaction Field (DRF) approach [100,101], and the polarizable embedding density functional theory scheme [102], which has been used to calculate one- and two-photon absorption in green fluorescent protein [103].

Computational studies on only the polymers are also valuable for investigating the electronic and optical properties of the copolymers [104]. Interestingly, in a study of donor/acceptor polymers, a correlation between the efficiency of OPV devices and the change in dipole moment upon excitation has been found [105]. These dipole moments for ground- and excited states have been calculated at the semi-empirical AM 1 level, using the CIS approach. An alternative way to calculate the dipole moment of excited states is with response theory [106], which may give more reliable results.

Future directions in multi-scale modeling

The advances in computer technology and linear scaling techniques [107,108–110], together with the development of more accurate functionals, make the treatment of large systems at an accurate level computationally realistic. This means that in the near future accurate predictions of the CT states of the molecules are within reach and, that, for the prediction of the electron transfer rates, more accurate electronic couplings together with the Franck-Condon factors can be evaluated using more advanced methods. Embedding techniques with QM/MM methods ensure that influences of the environment are properly taken into account, so that accurate predictions at the micro-scale level can be made. The embedding should be dynamic which means that changes that occur in the environment upon excitation/electron transfer can be taken into account. This will lead to deeper knowledge of the processes that take place at the interface, and will provide detailed information on how the molecular properties of the individual molecules affect the efficiency of the device.

Conclusion

Over the past 25 years, the field of organic photovoltaics has grown from scientific curiosity to viable technology, with both startups and large companies increasingly working to bring ‘plastic solar cells’ to market. In this short review we touched on bulk heterojunction and hybrid OPV architectures, but there are others, for example, small-molecule, tandem, and bi-layer. However polymer-based, bulk heterojunction OPV devices have already been commercialized and are the most likely to see large-scale production in the near-future, not because they have the highest power conversion efficiencies, but because they can be fabricated reproducibly, roll-to-roll, and without vacuum steps. The principal challenges lie in lowering costs by, for example, finding cheaper printable cathodes and more efficient encapsulation methods to extend the service lifetime of the devices. Current research efforts in interfacial materials and inverted architectures (i.e. that do not require air-sensitive cathode materials) may very well solve some problems, but there is a bright future for all forms of OPV. In the next 25 years, we will probably see myriad OPV architectures in myriad form factors, to fill small, niche applications all the way to large-scale energy production plants.

Acknowledgements

This work is part of the research program of the Foundation for Fundamental Research on Matter (FOM), which is part of the Netherlands Organization for Scientific Research (NWO). This is a publication by the FOM Focus Group ‘Next Generation Organic Photovoltaics’, participating in the Dutch Institute for Fundamental Energy Research (DIFFER). RWAH acknowledges Prof. Dr. R. Broer (RUG, NL) and Drs. H.D. de Gier (RUG, NL) for fruitful discussions. The authors acknowledge the Zernike Institute for Advanced Materials (‘Dieptestrategie’ program) for financial support. LJAK acknowledges support by a grant from STW/NWO (VENI 11166).

References

[1] B. Walker, C. Kim, T.-Q. Nguyen, Chem. Mater. 23 (2011) 470–482.
[2] Y. Sun, G.C. Welch, W.L. Leong, C.J. Takacs, G.C. Bazan, A.J. Heeger, Nat. Mater. 11 (2011) 44–48.
[3] B.E. Lassiter, J.D. Zimmerman, A. Panda, X. Xiao, S.R. Forrest, Appl. Phys. Lett. 101 (2012) 063303 (4 pages).
[4] G. Dennler, M.C. Scharber, C.J. Brabec, Adv. Mater. 21 (2009) 1323–1338.
[5] J.H. Seo, A. Gutacker, Y. Sun, H. Wu, F. Huang, Y. Cao, U. Scherf, A.J. Heeger, G.C. Bazan, J. Am. Chem. Soc. 133 (2011) 8416–8419.
[6] C. Piliego, M.A. Loi, J. Mater. Chem. 22 (2012) 4141.
[7] M.C. Scharber, D. Mühlbacher, M. Koppe, P. Denk, C. Waldauf, A.J. Heeger, C.J. Brabec, Adv. Mater. 18 (2006) 789–794.
[8] B. Kippelen, J.-L. Brédas, Energy Environ. Sci. 2 (2009) 251–261.
[9] L.J.A. Koster, et al. Phys. Rev. B 72 (2005) 085205.
[10] C.M. Martin, et al. J. Appl. Phys. 102 (2007) 104506.
[11] K. Maturová, et al. Nano Lett. 9 (2009) 3032.
[12] M. Gruber, et al. Org. Electron. 12 (2011) 1434.
[13] B. Ray, P. Nair, M. Alam, Solar Energy Mater. Solar Cells 95 (2011) 3287.
[14] L.J.A. Koster, et al. Adv. Eng. Mater. 3 (2013) 615–621. http://dx.doi.org/10.1002/aenm.201200787.
[15] P.K. Watkins, A.B. Walker, G.L.B. Verschoor, Nano Lett. 5 (2005) 1814.
[16] R.A. Marsh, C. Groves, N.C. Greenham, J. Appl. Phys. 101 (2007) 083509.
[17] J.D. Servaites, M.A. Ratner, T.J. Marks, Appl. Phys. Lett. 95 (2009) 163302.
[18] L.J.A. Koster, S.E. Shaheen, J.C. Hummelen, Adv. Eng. Mater. 2 (2012) 1246.
[19] A. Pochettino, Accad. Lincei Rend. 15 (1906) 171.
[20] H. Kallmann, M. Pope, J. Chem. Phys. 30 (1959) 585.
[21] C.W. Tang, Appl. Phys. Lett. 48 (1986) 183–185.
[22] N.S. Sariciftci, L. Smilowitz, A.J. Heeger, F. Wudl, Science 258 (1992) 1474–1476.
[23] G. Yu, J. Gao, J.C. Hummelen, F. Wudl, A.J. Heeger, Science 270 (1995) 1789–1791.
[24] J.J.M. Halls, et al. Nature 376 (1995) 498–500.
[25] R.D. McCullough, R.D. Lowe, M. Jayaraman, D.L. Anderson, J. Org. Chem. 58 (1993) 904–912.
[26] M. Leclerc, J.-F. Morin, Design and Synthesis of Conjugated Polymers, John Wiley & Sons, 2010.
[27] H. Zhou, L. Yang, W. You, Macromolecules 45 (2012) 607–632.
[28] J. You, L. Dou, K. Yoshimura, T. Kato, K. Ohya, T. Moriarty, K. Emery, C.-C. Chen, J. Gao, G. Li, Y. Yang, Nat. Commun. 4 (2013) 1446.
[29] C.E. Small, et al. Nat. Photonics 6 (2011) 115–120.
[30] C.M. Amb, et al. J. Am. Chem. Soc. 133 (2011) 10062–10065.
[31] W. Li, A. Furlan, K.H. Hendriks, M.M. Wienk, R.A.J. Janssen, J. Am. Chem. Soc. 135 (2013) 5529–5532.
[32] G. Li, R. Zhu, Y. Yang, Nat. Photon. 6 (2012) 153–161.
[33] M.M. Wienk, J.M. Kroon, W.J.H. Verhees, J. Knol, J.C. Hummelen, P.A. van Hal, R.A.J. Janssen, Angew. Chem. Int. Ed. Engl. 42 (2003) 3371–3375.
[34] A. Bakulin, J.C. Hummelen, M.S. Pshenichnikov, P.H.M. van Loosdrecht, Adv. Funct. Mater. 20 (2010) 1653–1660.
[35] R. Antoine, P. Dugourd, D. Rayane, E. Benichou, M. Broyer, F. Chandezon, C. Guet, J. Chem. Phys. 110 (1999) 9771.
[36] S.L. Ren, et al. Appl. Phys. Lett. 59 (1991) 2678–2680.
[37] A.P. Zoombelt, M. Fonrodona, M.M. Wienk, A.B. Sieval, J.C. Hummelen, R.A.J. Janssen, Org. Lett. 11 (2009) 903–906.
[38] C.R. McNeill, Energy Environ. Sci. 5 (2012) 5653–5667.
[39] E. Zhou, J. Cong, Q. Wei, K. Tajima, C. Yang, K. Hashimoto, Angew. Chem. Int. Ed. 50 (2011) 2799–2803.
[40] D.V. Talapin, J.-S. Lee, M.V. Kovalenko, E.V. Shevchenko, Chem. Rev. 110 (2010) 389.
[41] R. Debnath, O. Bakr, E.H. Sargent, Energy Environ. Sci. 4 (2011) 4870.
[42] P. Reiss, E. Couderc, J. De Girolamo, A. Pron, Nanoscale 3 (2011) 446.
[43] I. Kang, F.W. Wise, J. Opt. Soc. Am. B 14 (1997) 1632.
[44] N. Yaacobi-Gross, M. Soreni-Harari, M. Zimin, S. Kababya, A. Schmidt, N. Tessler, Nat. Mater. 10 (2011) 974.
[45] J.N. de Freitas, I.R. Grova, L.C. Akcelrud, E. Arici, N.S. Sariciftci, A.F. Nogueira, J. Mater. Chem. 20 (2010) 4845.
[46] L.X. Reynolds, T. Lutz, S. Dowland, A. MacLachlan, S. King, S.A. Haque, Nanoscale 4 (2012) 1561.
[47] H.C. Leventis, S.P. King, A. Sudlow, M.S. Hill, K.C. Molloy, S.A. Haque, Nano Lett. 10 (2010) 1253.
[48] W. Yu, H. Zhang, Z. Fan, J. Zhang, H. Wei, D. Zhou, B. Xu, F. Li, W. Tian, B. Yang, Energy Environ. Sci. 4 (2011) 2831.
[49] C.Y. Kuo, M.S. Su, Y.C. Hsu, H.N. Lin, K.H. Wei, Adv. Funct. Mater. 20 (2010) 3555.
[50] W.L. Ma, S.L. Swisher, T. Ewers, J. Engel, V.E. Ferry, H.A. Atwater, A.P. Alivisatos, ACS Nano 5 (2011) 8140.
[51] K.M. Noone, N.C. Anderson, N.E. Horwitz, A.M. Munro, A.P. Kulkarni, D.S. Ginger, ACS Nano 3 (2009) 1345.
[52] H. Fu, S.-W. Tsang, Nanoscale 4 (2012) 2187.
[53] S.-J. Lee, M.V. Kovalenko, J. Huang, D.S. Chung, D.V. Talapin, Nat. Nanotechnol. 6 (2011) 348.
[54] S.Z. Bisri, C. Piliego, M. Yarema, W. Heiss, M.A. Loi, Adv. Mater. (2013), http://dx.doi.org/10.1002/adma.201205041.
[55] J. Tang, K.W. Kemp, S. Hoogland, K.S. Jeong, H. Liu, L. Levina, M. Furukawa, X. Wang, R. Debnath, D. Cha, K.W. Chou, A. Fischer, A. Amassian, J.B. Asbury, E.H. Sargent, Nat. Mater. 10 (2011) 765.
[56] M. Sykora, A.Y. Koposov, J.A. McGuire, R.K. Schulze, O. Tretiak, J.M. Pietryga, V.I. Klimov, ACS Nano 4 (2010) 2021.
[57] F.W. Wise, Acc. Chem. Res. 33 (2000) 773.
[58] M.A. Hines, G.D. Scholes, Adv. Mater. 15 (2003) 1844.
[59] K. Szendrei, W. Gomulya, M. Yarema, W. Heiss, M.A. Loi, Appl. Phys. Lett. 97 (2010) 203501.
[60] K. Szendrei, M. Speirs, W. Gomulya, D. Jarzab, M. Manca, O.V. Mikhnenko, M. Yarema, B.J. Kooi, W. Heiss, M.A. Loi, Adv. Funct. Mater. 22 (2012) 1598.
[61] J. Seo, M.J. Cho, D. Lee, A.N. Cartwright, P.N. Prasad, Adv. Mater. 23 (2011) 3984.
[62] W. Yue, Y. Zhao, S. Shao, H. Tian, Z. Xie, Y. Geng, F. Wang, J. Mater. Chem. 19 (2009) 2199.
[63] C. Piliego, M. Manca, R. Kroon, M. Yarema, K. Szendrei, M. Andersson, W. Heiss, M.A. Loi, J. Mater. Chem. 22 (2012) 24411.
[64] W. Yu, H. Zhang, Z. Fan, J. Zhang, H. Wei, D. Zhou, B. Xu, F. Li, W. Tian, B. Yang, Energy Environ. Sci. 4 (2011) 2831.
[65] P.W.M. Blom, et al. Adv. Mater. 19 (2007) 1551.
[66] V.D. Mihailetchi, J. Wildeman, P.W.M. Blom, Phys. Rev. Lett. 94 (2005) 126602.
[67] W.F. Pasveer, et al. Phys. Rev. Lett. 94 (2005) 206601.
[68] A. Pivrikas, et al. Phys. Rev. B 71 (2005) 125205.
[69] A. Pivrikas, et al. Prog. Photovolt.: Res. Appl. 15 (2007) 677.
[70] V.D. Mihailetchi, L.J.A. Koster, P.W.M. Blom, Appl. Phys. Lett. 85 (2004) 970.
[71] L.J.A. Koster, et al. Appl. Phys. Lett. 86 (2005) 123509.
[72] A. Maurano, et al. Adv. Mater. 22 (2010) 4987.
[73] L.J.A. Koster, V.D. Mihailetchi, P.W.M. Blom, Appl. Phys. Lett. 88 (2006) 093511.
[74] J.-L. Brédas, J.E. Norton, J. Cornil, V. Coropceanu, Acc. Chem. Res. 42 (2009) 1691–1699.
[75] C.-K. Lee, C.-W. Pao, C.-W. Chu, Energy Environ. Sci. 4 (2011) 4124–4132.
[76] C.-K. Lee, C.-W. Pao, J. Phys. Chem. C 116 (2012) 12455–12461.
[77] A.C. Mayer, M.F. Toney, S.R. Scully, J. Rivnay, C.J. Brabec, M. Scharber, M. Koppe, M. Heeney, I. McCulloch, M.D. McGehee, Adv. Funct. Mater. 19 (2009) 1173–1179.
[78] Y. Kanai, J.C. Grossman, Nano Lett. 7 (2007) 1967–1972.
[79] V. Lemaur, M. Steel, D. Beljonne, J.-L. Brédas, J. Cornil, J. Am. Chem. Soc. 127 (2005) 6077–6086.
[80] T. Liu, A. Troisi, J. Phys. Chem. C 115 (2011) 2406–2415.
[81] B.P. Rand, D. Cheyns, K. Vasseur, N.C. Giebink, S. Mothy, Y. Yi, V. Coropceanu, D. Beljonne, J. Cornil, J.-L. Brédas, J. Genoe, Adv. Funct. Mater. 22 (2012) 2987–2995.
[82] Y. Yi, V. Coropceanu, J.-L. Brédas, J. Mater. Chem. 21 (2011) 1479–1486.
[83] Y. Li, T. Pullerits, M. Zhao, M. Sun, J. Phys. Chem. C 115 (2011) 21865–21873.
[84] P.F. Barbara, T.J. Meyer, M.A. Ratner, J. Phys. Chem. 100 (1996) 13148–13168.
[85] J.-L. Brédas, D. Beljonne, V. Coropceanu, J. Cornil, Chem. Rev. 104 (2004) 4971–5003.
[86] T. Kawatsu, V. Coropceanu, A. Ye, J.-L. Brédas, J. Phys. Chem. C 112 (2008) 3429–3433.
[87] R.W.A. Havenith, H.D. de Gier, R. Broer, Mol. Phys. 110 (2012) 2445–2454.
[88] M. Etinski, J. Tatchen, C.M. Marian, J. Chem. Phys. 134 (2011) 154105.
[89] T. Liu, D.L. Cheung, A. Troisi, Phys. Chem. Chem. Phys. 13 (2011) 21461–21470.
[90] D.P. McMahon, D.L. Cheung, A. Troisi, J. Phys. Chem. Lett. 2 (2011) 2737–2741.
[91] S.R. Yost, L.-P. Wang, T. van Voorhis, J. Phys. Chem. C 115 (2011) 14431–14436.
[92] A. Dreuw, M. Head-Gordon, J. Am. Chem. Soc. 126 (2004) 4007–4016.
[93] L. Goerigk, S. Grimme, J. Chem. Phys. 132 (2010) 184103.
[94] T. Körzdörfer, J.S. Sears, C. Sutton, J.-L. Brédas, J. Chem. Phys. 135 (2011) 204107.
[95] L. Pandey, C. Doiron, J.S. Sears, J.-L. Brédas, Phys. Chem. Chem. Phys. 14 (2012) 14243–14248.
[96] D. Jacquemin, V. Wathelet, E.A. Perpete, C. Adamo, J. Chem. Theory Comput. 5 (2009) 2420–2435.
[97] R. Peverati, D.G. Truhlar, Phys. Chem. Chem. Phys. 14 (2012) 11363–11370.
[98] Q. Wu, T. van Voorhis, Phys. Rev. A 72 (2005) 024502.
[99] A.M.P. Sena, T. Miyazaki, D.R. Bowler, J. Chem. Theory Comput. 7 (2011) 884–889.

[100] A.H. de Vries, P.T. van Duijnen, A.H. Juffer, J.A.C. Rullmann, J.P. Dijkman, H. Merenga, B.T. Thole, J. Comput. Chem. 16 (1995) 37–55.

[101] P.T. van Duijnen, M. Swart, L. Jensen, in: S. Canuto (Ed.), Solvation Effects on Molecules and Biomolecules, Springer, 2008, pp. 39–102.

[102] J.M. Olsen, K. Aidas, J. Kongsted, J. Chem. Theory Comput. 6 (2010) 3721–3734.

[103] A.H. Steindal, J.M.H. Olsen, K. Ruud, L. Frediani, J. Kongsted, Phys. Chem. Chem. Phys. 14 (2012) 5440–5451.

[104] L. Pandey, C. Risko, J.E. Norton, J.-L. Brédas, Macromolecules 45 (2012) 6405–6414.

[105] B. Carsten, J.M. Szarko, H.J. Son, W. Wang, L. Lu, F. He, B.S. Rolczynski, S.J. Lou, L.X. Chen, L. Yu, J. Am. Chem. Soc. 133 (2011) 20468–20475.

[106] Y. Luo, D. Jonsson, P. Norman, K. Ruud, O. Vahtras, B. Minaev, H. Ågren, A. Rizzo, K.V. Mikkelsen, Int. J. Quantum Chem. 70 (1998) 219–239.

[107] C. Yam, Q. Zhang, F. Wang, G. Chen, Chem. Soc. Rev. 41 (2012) 3821–3838.

[108] D.R. Bowler, T. Miyazaki, Rep. Prog. Phys. 75 (2012) 036503.

[109] S. Coriani, S. Høst, B. Jansík, L. Thøgersen, J. Olsen, P. Jørgensen, S. Reine, F. Pawlowski, T. Helgaker, P. Salek, J. Chem. Phys. 126 (2007) 154108.

[110] T. Kjærgaard, P. Jørgensen, J. Olsen, S. Coriani, T. Helgaker, J. Chem. Phys. 129 (2008) 054106.

Materials Today • Volume 16, Numbers 7/8 • July/August 2013

Imparting the unique properties of DNA into complex material architectures and functions

Phyllis F. Xu[1,†], Hyunwoo Noh[1,2,†], Ju Hun Lee[1,2], Dylan W. Domaille[2], Matthew A. Nakatsuka[1], Andrew P. Goodwin[2,*] and Jennifer N. Cha[1,2,*]

[1] Department of Nanoengineering and Materials Science and Engineering Program, University of California, San Diego, 9500 Gilman Dr. MC 0448, La Jolla, CA 92093-0448, USA
[2] Department of Chemical and Biological Engineering, University of Colorado, Boulder, 3415 Colorado Avenue, 596 UCB, Boulder, CO 80303, USA

While the remarkable chemical and biological properties of DNA have been known for decades, these properties have only been imparted into materials with unprecedented function much more recently. The inimitable ability of DNA to form programmable, complex assemblies through stable, specific, and reversible molecular recognition has allowed the creation of new materials through DNA's ability to control a material's architecture and properties. In this review we discuss recent progress in how DNA has brought unmatched function to materials, focusing specifically on new advances in delivery agents, devices, and sensors.

Introduction

DNA is a remarkable biopolymer with molecular recognition properties far surpassing any synthetic analog. The predictability and ease of DNA–DNA binding, the creation of algorithms for the *de novo* design of new assembled structures, and the ability to synthesize DNA oligonucleotides with an almost unlimited range of sequences and functional end-groups has allowed the production of frameworks for the rational design of materials with programmable shape, size, and function. In this review, we examine some key examples in which the unique qualities of DNA have enabled the creation of an entire new set of devices and sensors with previously unmatched complexity and function. For example, not only have numerous 2D and 3D nano- and mesoscale DNA architectures been designed and synthesized to highlight the power and generality of DNA self-assembly; these architectures have also been employed for the delivery of therapeutics and the study of chemical reactions. In addition, the creation of nanoparticle–oligonucleotide conjugates can serve as building blocks for controlled nanoparticle assemblies ranging from simple dimers to complex 3D heterostructures as a framework for fabricating new device architectures. Finally, the reversible, single-molecule interactions of DNA aptamers and DNAzymes with specific analytes can be transduced into a variety of detection signals for new materials for sensors and *in vivo* imaging agents.

Assembly of DNA into programmed discrete structures in two and three dimensions

DNA is composed of four nucleotide bases, adenosine (A), guanine (G), thymine (T), and cytosine (C), where hybridization between A–T and C–G produces a double helix consisting of anti-parallel complementary strands. Once hybridized, the persistence length increases from $\sim$1 nucleotide for single stranded DNA (ssDNA) to about 100 bases for double stranded DNA (dsDNA), and this rigidity allows self-assembled DNA structures to hold their shape upon assembly. The optimization of solid-phase synthesis has facilitated the production of synthetic oligonucleotides with almost any sequence, providing materials engineers with an unlimited selection of designs for different self-assembled 2- and 3D DNA architectures. In more recent years, the expansion of design rules into computer algorithms has led to a virtual explosion in the number of DNA scaffolds that can be created for a wide variety of applications that include nanomaterial assembly, biosensors [1], drug delivery [2], computation [3,4], and biomolecular actuation [5–7]. In their pioneering work, Seeman

---

*Corresponding author:. Goodwin, A.P. (Andrew.Goodwin@colorado.edu), Cha, J.N. (Jennifer.Cha@colorado.edu)

[†] These authors contributed equally to this work.

1369-7021/06/$ - see front matter http://dx.doi.org/10.1016/j.mattod.2013.07.001

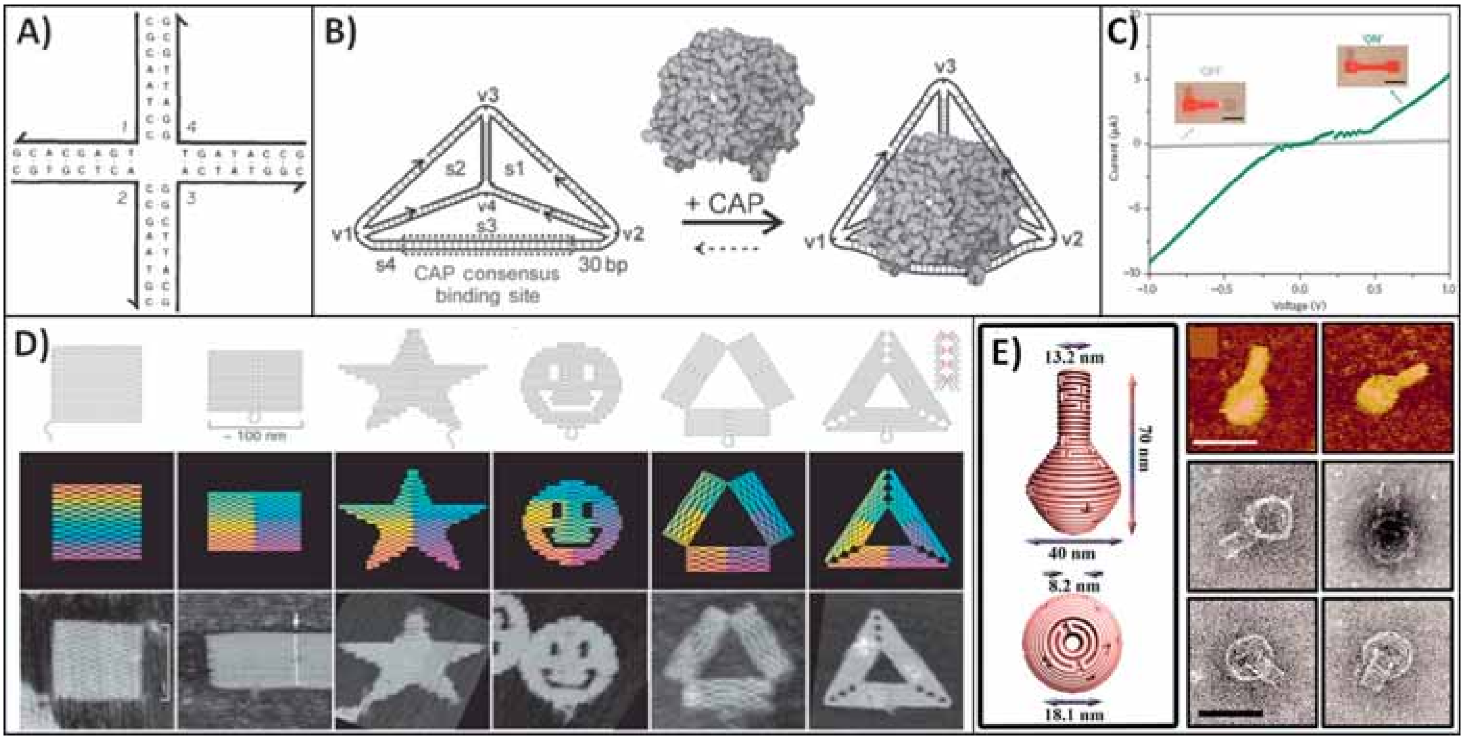

FIGURE 1

(a) Schematic of a branched DNA unit [9]. (b) DNA tetrahedron structure with captured CAP protein [10]. (c) Electrical switch operated by DNA meta-hydrogels [16]. (d) Design of DNA origami, folding path, and AFM images [17]. (e) Schematic of 3D DNA structures with complex curvatures and TEM images [20].

and co-workers provided the initial guidelines for forming tetrameric complexes in solution from immobile DNA junctions [8,9]. Four different strands of DNA cooperated to form a junction in which each arm contained free ssDNA that could hybridize to an adjacent junction, resulting in a square-like, branched-DNA unit (Fig. 1a). A key aspect of this assembly is the design of DNA strands that each bind simultaneously to different complementary partners, allowing the joining of multiple strands into complex architectures.

This basic motif has since been elaborated into larger and more complex 2- and 3D assemblies tuned toward addressing specific applications in materials science. For example, targeted delivery of bioactive cargo is of importance for treating cancer and other diseases, but monodisperse vehicles with predictable delivery profiles have been difficult to create. A 3D DNA tetrahedron has been demonstrated as a potential carrier for this application: the precisely sized scaffold can encapsulate proteins [10] (Fig. 1b) or peptides [11], while the superstructure can be easily transported to the target thanks to its innate biocompatibility. These multivalent DNA structures can also be easily modified with additional functional oligonucleotides [12] added to their exteriors or can be specifically shaped [13] to provide resistance to nuclease degradation and facilitate cell uptake. Because of these unique attributes, the DNA tetrahedron structure has been successfully used for the *in vivo* delivery of siRNA for cancer targeting and therapy; a truly remarkable achievement [14]. Mimicking the well-defined and homogeneous structure of these DNA carriers with synthetic systems is difficult, but DNA allows for the specific programming of the orientation and number of modifications per delivery platform for optimal delivery efficacy, whereas polymer particles and assemblies typically created through bulk emulsification or precipitation lack the same precise control over size and surface.

DNA nanostructures have also been incorporated into and used to form active hydrogels, which can be applied as novel biomaterials for tissue engineering and scaffolds for 'smart' delivery and sensing. For example, simple, branched DNA nanostructures ligated together under controlled conditions to form cross-linked structures exhibit the familiar viscoelastic mechanical properties of hydrogels, allowing facile programming of such properties over the degree of crosslinking, strength of crosslinking, and length between junctions [15]. Control over hydrogel properties is extremely important for tissue engineering in particular, as the cellular growth scaffold must mimic that of the desired tissue or growth environment. By tuning the initial DNA branched structure, gel-loading (e.g. with DNA-binding drugs, insulin, and even mammalian cells), and environmental conditions, the material's swelling profile, tensile modulus, and degradation rate (drug release rate) may be controlled accordingly. In addition, an exciting variation of DNA hydrogels, 'meta-hydrogels,' has been engineered to act as a mechanical metamaterial that can exhibit liquid-like properties when outside of water but solid-like properties when immersed in water, acting as a water-induced switch (Fig. 1c) [16].

Another significant breakthrough in DNA nanotechnology, called 'DNA origami,' was made by Rothemund, in which ssDNA isolated from the M13 bacteriophage was folded into compact 2D DNA architectures [17]. Rather than assembling many short strands into a larger structure, the long viral ssDNA is allowed to react with many short oligonucleotides, or 'staples', producing a vast library of different DNA configurations ranging from simple geometrical shapes to complex maps of the world (Fig. 1d) in only a few steps. Following Rothemund's initial work, a diverse range of DNA origami structures have been synthesized and applied as active materials or templates for various research areas. For example, Sugiyama and co-workers applied 'window'-shaped DNA origami as a platform to study the interaction of EcoRI protein with DNA strands placed under tension [18]. Similarly, Gothelf and co-workers used rectangular DNA scaffolds as breadboards for running different chemical reactions for nanoscale combinatorial chemistry [19]. DNA origami has also been applied toward engineering complex 3D systems; for example, Yan and co-workers recently created exquisite 3D DNA shapes with large curvature (Fig. 1e) [20]. Highly novel examples of 3D origami systems designed for biological applications include the fabrication of stimuli-responsive DNA boxes and cages. These 3D structures can be controlled to 'lock' and 'unlock' the accessibility of oligonucleotide [21] or protein [22] targets, allowing the controlled release of a payload from within the heart of the structure. Similar to the aforementioned DNA tetrahedron, the ability to engineer multivalent 3D, stimuli-responsive origami structures that can be easily modified with nanoscale precision may have a significant impact on applications such as controlled release or active transport in both *in vitro* and *in vivo* settings.

DNA-mediated assembly of nanomaterials for device fabrication

The advent of nanotechnology has brought to existence a diverse set of nanomaterials possessing unique electronic, optical, or magnetic properties. One of the grand challenges associated with engineering functional materials or devices from such nanoscale objects has been how to integrate and assemble them into hierarchical arrays with minimal defects. However, as demonstrated in initial groundbreaking work by Alivisatos and Mirkin [23,24], these particles and surfaces are generally easily modified with oligonucleotides that can direct the organization of nanomaterials into different packing densities and arrangements for a variety of applications. By varying the length and sequence of the DNA on the nanoparticles, core-satellite structures [25] or discrete geometrical organizations [26,27] have been formed in which the DNA controls not only the distance between particles [28] but also the angle of packing [29]. Particle distances may also be adjusted within an already assembled structure through dynamic hybridization schemes such as hairpin structures [30]. Beyond discrete nanoparticle clusters, Mirkin and Gang recently reported methods to create well-ordered bulk nanoparticle solids (Fig. 2a) [31,32]. Specifically, tuning hybridization between two particles led to gold nanoparticle (AuNP) superlattices with either face-centered-cubic (FCC) or body-centered-cubic (BCC) orientation. Since their first demonstration, further studies have clarified the effect of particle size, hydrodynamic size, and length of DNA on assembly [33], and similar techniques have been applied to create mixed-particle systems of AuNPs and quantum dots [34]. It is worth noting that this degree of tunability in nanoparticle ordering, relative distance, and packing cannot be easily achieved with synthetic polymers or small molecule systems, nor is it trivial to obtain thermodynamically stable nanoparticle superlattices through simple thermal annealing.

Anisotropic nanomaterials may also be organized with similar tools. The size and shape of metal nanostructures determine their plasmon behavior, and an understanding of the different facets on a given structure can allow face-selective DNA functionalization for engineering new optically active materials. For example, Mirkin and co-workers recently created a hexagonal close-packed superlattice of Au nanorods by using different DNA sequences and lengths (Fig. 2b) [35], and Mann and co-workers described a similar example in which nanorods were assembled in 2D along their long axes to maximize DNA overlap and hybridization [36].

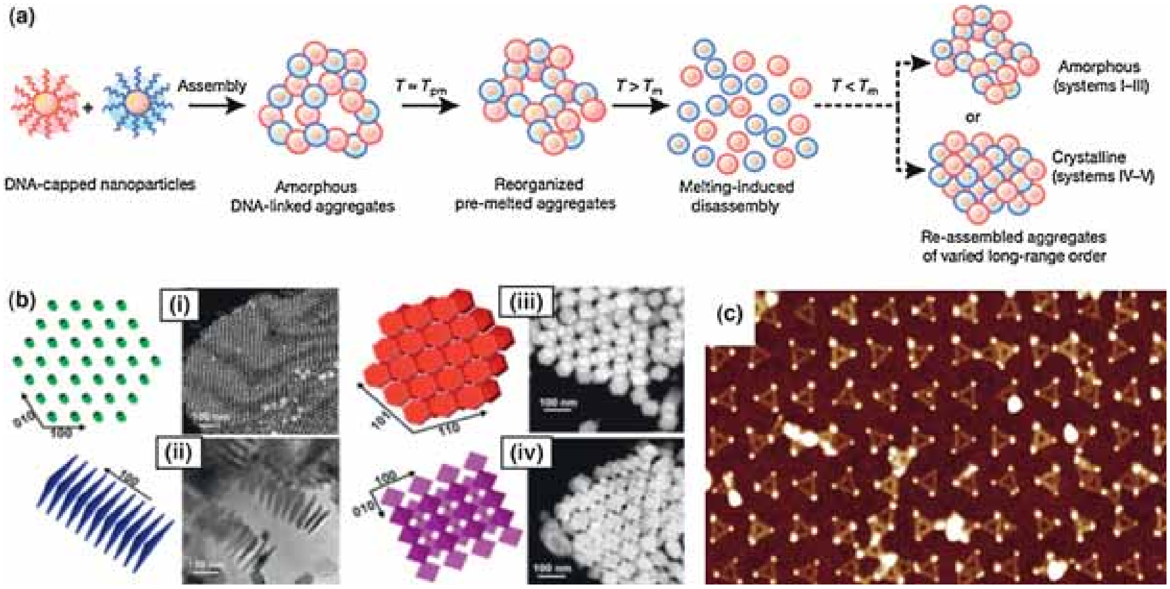

FIGURE 2

(a) Amorphous and crystalline 3D gold nanoparticle arrays assembled through DNA interactions. T_{pm} and T_m encode for DNA premelting and melting temperatures, respectively [32]. (b) Schematic illustration and TEM image of superlattices with ordered (i) nanorod (55 nm length, 14 nm width), (ii) nanoprism (140 nm edge length), (iii) rhombic (64 nm diameter) and (iv) octahedra (83 nm diameter) nanoparticles [35]. (c) DNA origami mediated assembly of gold nanoparticles on lithographically patterned surfaces [43].

DNA has also guided the assembly of various anisotropic nanoparticles such as nanoprisms and rhombic dodecahedra. In these cases, the inherent difference in surface energies in anisotropic colloidal particles allowed selective functionalization of the sides of the particles for building unique hybrid structures [37,38]. Furthermore, since DNA hybridization is thermally reversible, the plasmon responses of DNA-nanorod assemblies can be easily and controllably tuned through simple temperature changes [39].

DNA-guided assembly directly on surfaces has also been shown as a promising method for the creation of nanoelectronic, nanophotonic, or optoelectronic solid-state devices, as such materials often require control over nanomaterial placement, organization, and orientation in both two and three dimensions. The overall strategy of these methods is to use complementary and/or orthogonal sequences in both surface-bound and particle-bound DNA to direct the assembly of particles both to a surface and to each other. DNA is deposited onto a surface through either physical interaction with a hydrophilic surface (typically patterned from a hydrophobic resist) or covalent conjugation through an end group on the DNA. For example, 2D DNA origami has been deposited onto areas etched by either e-beam lithography or photolithography, followed by hybridization and deposition of DNA-AuNPs onto the etched surface [40–42]. Because of the mesoscale size regime of DNA origami, methods to merge top-down lithography with bottom-up self-assembled DNA have been developed to produce precise ordered arrays of 5 nm AuNPs (Fig. 2c) [43,44]. These DNA origami can also in principle be extended to organizing other nanomaterials on surfaces, including carbon nanotubes (CNTs) [45] or biomolecules (Fig. 3a,b) [46–48]. Although CNTs are typically very difficult to disperse in aqueous media without the addition of surfactants [49] or chemical modification of the nanotube surface [50], ssDNA can solubilize CNTs through π–π stacking of the DNA bases to the CNT sidewall [51]. Specific DNA oligonucleotides have also been shown to bind to specific CNT widths and chiralities [52], empowering DNA for both CNT purification and assembly (Fig. 3c,d) [53,54].

In addition, cost-effective printing methods have been developed to produce patterned domains of large-area close-packed nanoparticle films on substrates. For example, nanoparticle superlattices with long range order were obtained within DNA arrays patterned by traditional micro-contact printing or inking-subtraction-printing [55], by use of thermal annealing to promote hybridization between the DNA-AuNPs and the surface DNA [56]. Similar techniques have been applied to create 3D particle assemblies on substrates with surface strands used to promote interparticle hybridization [57]. The ability to organize nanoparticle arrangements on surfaces through simple tuning of DNA hybridization exemplifies the power of a self-recognizing polymer such as DNA for controlling particle packing in multiple dimensions. The typical approaches for engineering ordered thin films of nanoparticles on substrates to date have been to use electrostatic interactions [58], spatial confinement [59], or air–liquid interfaces [60]. Using DNA interactions to drive particle ordering provides a framework to assemble a diverse set of nanoparticle sizes and compositions while circumventing barriers to manufacturing such as needing high nanoparticle concentrations or slow evaporation. Furthermore, because DNA interactions can be programmed to include flexible, compressible sections, polydisperse nanoparticle batches may also be assembled into well-ordered arrangements [33–35].

Tunable DNA switches as general platforms for sensitive and specific analyte detection

The unique ability of DNA to bind to itself or other analytes has also been employed to create powerful new diagnostics. A typical clinical sample contains only a minute amount of a particular

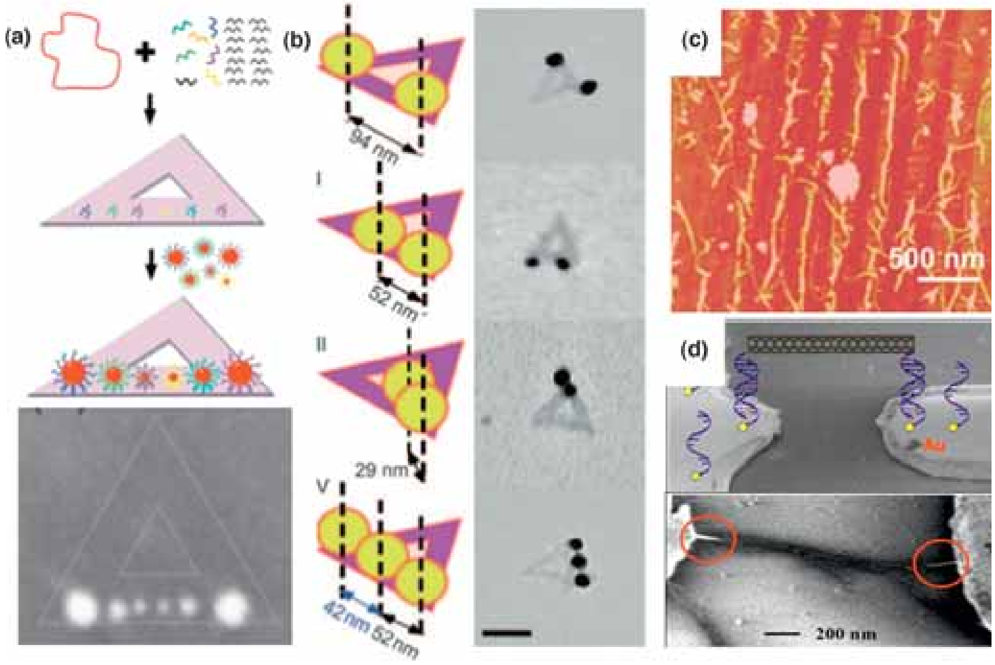

FIGURE 3

DNA origami is used to pattern (a) gold nanoparticles of different sizes [47] and (b) silver nanoparticles in specified locations [48]. Carbon nanotubes aligned by DNA on (c) Si substrates [53] and (d) across gold electrodes [54].

biomarker in the presence of many other proteins, peptides, small molecules, and cells, so sensors are needed that boast high sensitivities and specificities, stability in a range of conditions, and favorable cost-to-benefit ratios. DNA has already been utilized heavily in oligonucleotide detection and gene sequencing, and DNA's self-complementarity and library of different sequences have made it an ideal choice for labeling and identifying particular biomarkers through a 'biobarcode' that can be amplified and sequenced for multiplexed detection [61–63]. However, in this review we will focus specifically on the ways in which tuning the energies of DNA binding with itself or other analytes has made DNA a powerful tool for engineering sensors that actuate a unique response to analyte binding.

In the simplest scenario, one or more detection strands are made complementary to a nucleic acid analyte, and the act of binding causes the emission of a detectable signal or change in signal. In a common example, changes in fluorescence can be observed via quenching or Förster Resonance Energy Transfer (FRET) by utilizing the DNA-analyte exchange to change the distance between a donor and acceptor dye or quencher. Other common detection schemes include colorimetric via plasmon shifts in aggregated nanoparticles (Fig. 4a) [64,65], electrochemical via changes in current and voltage [66], magnetic via changes in T2 relaxivity with iron oxide nanoparticles [67], and, more recently, Surface Enhanced Raman Spectroscopic (SERS), in which DNA recognition brings the Raman active reporter directly into the 'hot spot' between two metallic nanoparticles [68]. In order to sense analytes other than nucleic acids, aptamers of DNA or RNA have been found that bind with high specificity to substrates such as small molecules, peptides, or proteins. To generate a signal upon aptamer–ligand binding, a sensing strand is displaced from its complement to bind to a more strongly binding non-DNA analyte; this displacement mechanism has been employed for fluorescence sensing (Fig. 4b) [69], MRI contrast agents (Fig. 4c) [70], and SERS sensors (Fig. 4d) [71]. Another interesting use of this type of displacement mechanism is to change the properties of DNA–polymer networks. For example, Tan and co-workers have designed hydrogels composed of polymers crosslinked with hybridized DNA–aptamers, which become soluble after the analytes cause the decrosslinking of the network [72–74]. For *in vivo* applications, the aptamers' affinities for both soluble and bound biomarkers can bias the accumulation of contrast agents into diseased sites [75] or even actuate changes in imaging signal [76]. In one example of the latter, the presence of elevated levels of thrombin, such as those found in a growing blood clot, caused a gas-filled microbubble to change its response and contrast under ultrasound (Fig. 4e); an aptamer displacement mechanism similar to that described for the aforementioned hydrogels caused the decrosslinking of a stiff exterior shell then in turn changed the mechanical properties of the bubble [77].

Other DNA sequences known as DNAzymes are able to undergo structural conformational changes upon binding to induce catalytic covalent cleavage of specific substrates. DNAzymes are useful because they possess lower cost, higher thermal tolerance, and

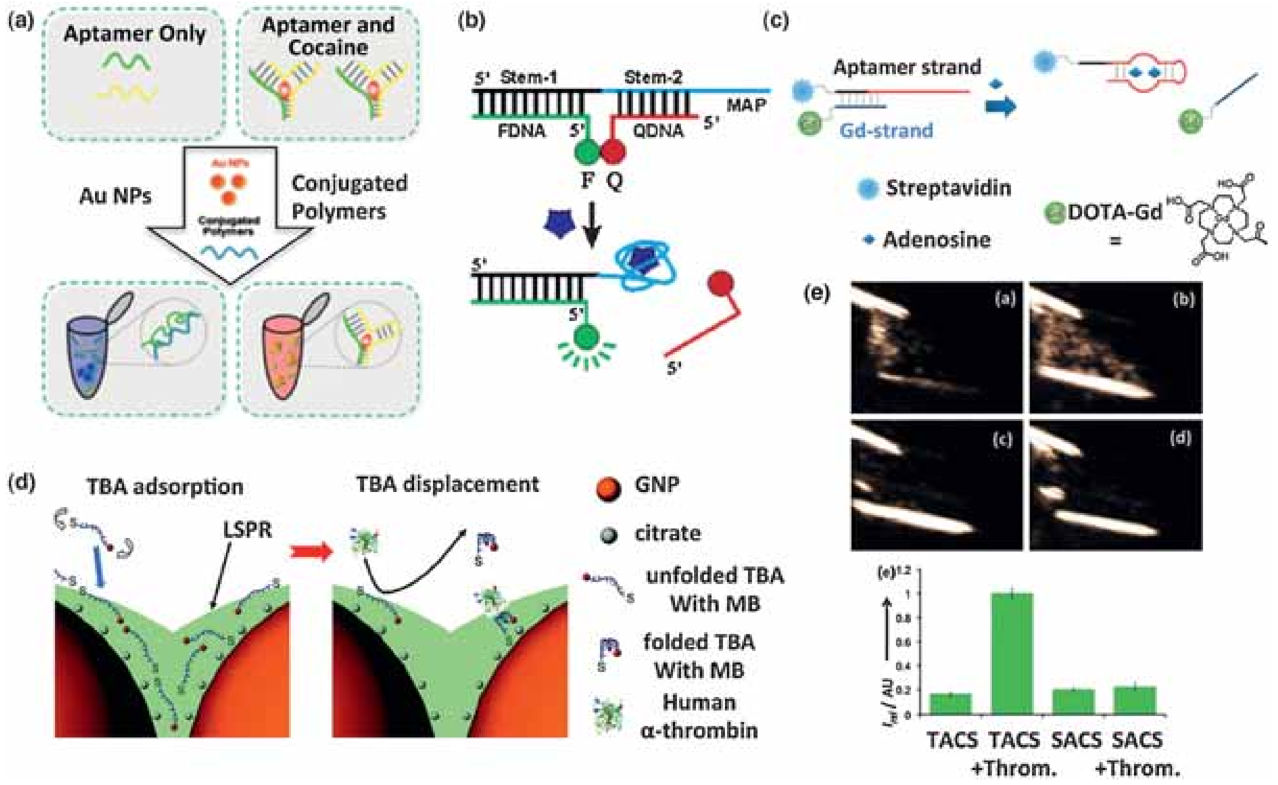

FIGURE 4

(a) Color changes are caused by aggregation of GNP aggregation or dispersion due to aptamer binding of cocaine [64]. (b) A triparite, fluorescence-quenching assembly [69]. (c) An adenosine-responsive gadolinium MRI contrast agent [70]. (d) Gold nanoparticles (GNP) with adsorbed thrombin binding aptamer (TBA) and SERS active dye will decrease their Raman signal in the presence of thrombin [71]. (e) Contrast enhanced sonography of TBA crosslinked microbubbles. Acoustic signal will increase in presence of thrombin as shell becomes more fluid [77].

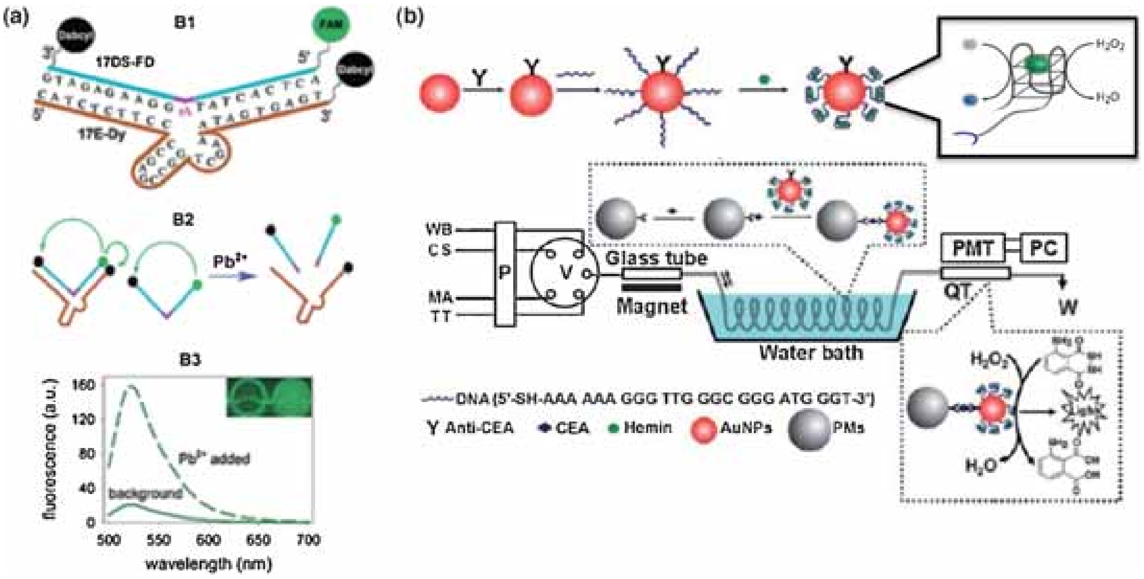

FIGURE 5

(a) A Pb(II)-dependent DNAzyme with both intra- and inter-strand fluorescence quenchers causes a fluorescence increase in the presence of Pb(II) [82]. (b) Gold nanoparticles decorated with an anti-CEA antibody and HRP-mimic DNAzymes are used in an ultrasensitive assay for carcinoembryonic antigen [91].

smaller size than their protein enzyme counterparts while preserving much of their efficacy. For example, researchers have also been able to isolate DNAzymes that require specific metal ions to catalyze hydrolysis of a ribonucleic acid bond. These DNAzymes can thus sense for their required ion cofactor; examples of which include Cu^{2+} [78], Mg^{2+} [79], Zn^{2+} [80], UO_2^{2+} [81], and Pb^{2+} (Fig. 5a) [82]. Liu and co-workers in particular have shown success with a Pb^{2+}-dependent DNAzyme with detection methods that include a fluorophore/quencher pair [83], electrochemical detection [84], and gold nanoparticle-based aggregation methods [85]. As with detection antibodies in ELISAs, DNAzymes can also be conjugated to a variety of different biomolecular or synthetic substrates to amplify signal generated from a detected analyte such as DNA [86], microRNA [87], or other biomolecules [88]. For instance, the horseradish peroxidase mimic DNAzyme (HRP-DNAzyme) folds into a stable G-quadruplex to complex a molecule of hemin, which in the presence of hydrogen peroxide generates a colorimetric or chemiluminescent signal from 2,2′-azino-bis(3-ethylbenothiazoline-6-sulfonic acid) (ABTS) or luminol, respectively [89,90]. This DNAzyme was utilized in an assay in which carcinoembryonic antigen (CEA) was captured to antibody-conjugated paramagnetic microspheres, followed by detection with gold nanoparticles decorated with both anti-CEA and HRP–DNAzyme complexes to produce a chemiluminescent signal detectable down to CEA concentrations of $4.1\ \mathrm{pg\,mL^{-1}}$ (Fig. 5b) [91]. In another example, proteins at the very tip of the filamentous M13 bacteriophage were designed to bind to an analyte, while the remainder of the phage was functionalized with many copies of HRP–DNAzyme; this methodology produced detectable signal down to 125 fmol with hydrogen peroxide and ABTS [66].

A major benefit of employing DNAzymes and aptamers for sensing materials is that they are able to do much of the work of enzymes and antibodies but with more favorable cost and thermal stability. In addition, the substantial degree of control over analyte or substrate binding, as well as the ability to switch binding on or off depending on the application, allows DNA-based sensing materials to be joined with many different types of assays and instruments, improving their utility further.

Conclusions and future prospects

The unique properties of DNA have enabled the generation of many different types of structures and materials with unprecedented design and function. Such materials include 2- and 3D nano- and mesoscale DNA architectures, precise assemblies of nanoparticles in solution and on surfaces, and switchable systems for biomolecule detection. The variability of DNA sequences and binding energies, its tunability in flexibility or stiffness, and the ease of synthesis and production have made it one of the most unique and exquisite macromolecular systems from which to build new materials. Moving forward, we imagine that DNA alone or in combination with other molecular structures will be engineered into new functional materials that demonstrate increasing complexity in structure and optimal function.

Acknowledgements

This work was supported by an NSF Career Award (DMR-1056808), Office of Naval Research (Award Number: N00014-09-01-0258), Department of Energy (DE-CS0004937), DOE Early Career Award (DE-SC0006398), NSF (CMMI-0856671), Alfred P. Sloan Fellowship, and NIH (R21 EB012758). A.P.G. is a recipient of a Pathway to Independence Award in Cancer Nanotechnology (K99/R00 CA153935).

References

[1] R.P. Goodman, et al. Nat. Nanotechnol. 3 (2008) 93.
[2] Y.-X. Zhao, et al. ACS Nano 6 (2012) 8684.
[3] G. Seelig, et al. Science 314 (2006) 1585.
[4] L. Qian, E. Winfree, Science 332 (2011) 1196.
[5] J. Shin, N.A. Pierce, J. Am. Chem. Soc. 126 (2004) 10834.
[6] B. Ding, N.C. Seeman, Science 314 (2006) 1583.
[7] T. Omabegho, R. Sha, N.C. Seeman, Science 324 (2009) 67.
[8] N.C. Seeman, J. Theor. Biol. 99 (1982) 237.
[9] N.R. Kallenbach, R.I. Ma, N.C. Seeman, Nature 305 (1983) 829.

[10] R. Crawford, et al. Angew. Chem. 125 (2013) 2340.
[11] J.D. Flory, et al. J. Am. Chem. Soc 135 (2013) 6985.
[12] J. Li, et al. ACS Nano 5 (2011) 8783.
[13] G.D. Hamblin, J. Am. Chem. Soc. 134 (2012) 2888.
[14] H. Lee, et al. Nat. Nanotechnol. 7 (2012) 389.
[15] S.H. Um, et al. Nat. Mater. 5 (2006) 797.
[16] J.B. Lee, et al. Nat. Nanotechnol. 7 (2012) 816.
[17] P.W.K. Rothemund, Nature 440 (2006) 297.
[18] M. Endo, et al. J. Am. Chem. Soc. 132 (2010) 1592.
[19] N.V. Voigt, et al. Nat. Nanotechnol. 5 (2010) 200.
[20] D. Han, et al. Science 332 (2011) 342.
[21] E.S. Andersen, et al. Nature 459 (2009) 73.
[22] S.M. Douglas, I. Bachelet, G.M. Church, Science 335 (2012) 831.
[23] A.P. Alivisatos, et al. Nature 382 (1996) 609.
[24] C.A. Mirkin, et al. Nature 382 (1996) 607.
[25] S. Pal, et al. Chem. Commun. 0 (2009) 6059.
[26] A.J. Mastroianni, S.A. Claridge, A.P. Alivisatos, J. Am. Chem. Soc. 131 (2009) 8455.
[27] A. Fu, et al. J. Am. Chem. Soc. 126 (2004) 10832.
[28] J. Lee, et al. Angew. Chem. Int. Ed. 46 (2007) 9006.
[29] Y. Wen, et al. Chem. Commun. 48 (2012) 3963.
[30] P.F. Xu, et al. Small 9 (2013) 228.
[31] S.Y. Park, et al. Nature 451 (2008) 553.
[32] D. Nykypanchuk, et al. Nature 451 (2008) 549.
[33] R. Macfarlane, et al. Science 334 (2011) 204.
[34] D. Sun, O. Gang, J. Am. Chem. Soc. 133 (2011) 5252.
[35] M.R. Jones, et al. Nat. Mater. 9 (2010) 913.
[36] E. Dujardin, et al. Chem. Commun. (2001) 1264.
[37] L. Xu, et al. J. Am. Chem. Soc. 134 (2012) 1699.
[38] J.E. Millstone, et al. Small 4 (2008) 2176.
[39] Z. Li, et al. J. Am. Chem. Soc. 134 (2012) 3322.
[40] K.E. Sapsford, et al. Langmuir 24 (2008) 10245.
[41] B. Kannan, R.P. Kulkarni, A. Majumdar, Nano Lett. 4 (2004) 1521.
[42] C.H. Lalander, et al. ACS Nano 4 (2010) 6153.
[43] A.M. Hung, et al. Nat. Nanotechnol. 5 (2010) 121.
[44] R.J. Kershner, et al. Nat. Nanotechnol. 4 (2009) 557.
[45] H.T. Maune, et al. Nat. Nanotechnol. 5 (2009) 61.
[46] N. Stephanopoulos, et al. Nano Lett. 10 (2010) 2714.
[47] B. Ding, et al. J. Am. Chem. Soc. 132 (2010) 3248.
[48] S. Pal, et al. Angew. Chem. Int. Ed. 49 (2010) 2700.
[49] M.S. Arnold, et al. Nat. Nanotechnol. 1 (2006) 60.
[50] F. Liang, et al. Nano Lett. 4 (2004) 1257.
[51] M. Zheng, et al. Nat. Mater. 2 (2003) 338.
[52] X. Tu, et al. Nature 460 (2009) 250.
[53] P.F. Xu, et al. Phys. Chem. Chem. Phys. 13 (2011) 10004.
[54] M. Hazani, et al. Chem. Phys. Lett. 391 (2004) 389.
[55] H. Noh, et al. ACS Nano 3 (2009) 2376.
[56] H. Noh, et al. ACS Nano 4 (2010) 5076.
[57] H. Noh, A.M. Hung, J.N. Cha, Small 7 (2011) 3021.
[58] E.V. Shevchenko, et al. Nature 439 (2006) 55.
[59] W. Cheng, et al. Nat. Nanotechnol. 3 (2008) 682.
[60] A. Dong, et al. Nature 466 (2010) 474.
[61] B. Schweitzer, S.F. Kingsmore, Curr. Opin. Biotechnol. 13 (2002) 14.
[62] S.I. Stoeva, et al. J. Am. Chem. Soc. 128 (2006) 8378.
[63] J.H. Lee, et al. ACS Nano 6 (2012) 5621.
[64] F. Xia, et al. Proc. Natl. Acad. Sci. U. S. A. 107 (2010) 10837.
[65] S.J. Park, et al. Science 295 (2002) 1503.
[66] D.W. Domaille, et al. Chem. Commun. 49 (2013) 1759.
[67] M.V. Yigit, et al. Chembiochem 8 (2007) 1675.
[68] D.K. Lim, et al. Nat. Mater. 9 (2010) 60.
[69] R. Nutiu, Y. Li, J. Am. Chem. Soc. 125 (2003) 4771.
[70] W. Xu, Y. Lu, Chem. Commun. 47 (2011) 4998.
[71] H. Cho, et al. Nano Lett. 8 (2008) 4386.
[72] L. Peng, et al. J. Am. Chem. Soc. 134 (2012) 12302.
[73] Z. Zhu, et al. Angew. Chem. Int. Ed. Engl. 49 (2010) 1052.
[74] H. Yang, et al. J. Am. Chem. Soc. 130 (2008) 6320.
[75] C.H. Wang, et al. Biomaterials 33 (2012) 1939.
[76] O.C. Farokhzad, et al. Proc. Natl. Acad. Sci. U. S. A. 103 (2006) 6315.
[77] M.A. Nakatsuka, et al. Adv. Mater. 24 (2012) 6010.
[78] J. Liu, Y. Lu, J. Am. Chem. Soc. 129 (2007) 9838.
[79] R.R. Breaker, G.F. Joyce, Chem. Biol. 2 (1995) 655.
[80] J. Li, et al. Nucleic Acids Res. 28 (2000) 481.
[81] J. Liu, et al. Proc. Natl. Acad. Sci. U. S. A. 104 (2007) 2056.
[82] J. Li, Y. Lu, J. Am. Chem. Soc. 122 (2000) 10466.
[83] J. Liu, Y. Lu, Anal. Chem. 75 (2003) 6666.
[84] X. Yang, et al. Chem. Commun. 46 (2010) 3107.
[85] J. Liu, Y. Lu, J. Am. Chem. Soc. 125 (2003) 6642.
[86] V. Pavlov, et al. Anal. Chem. 76 (2004) 2152.
[87] Y. Wen, et al. Anal. Chem. 84 (2012) 7664.
[88] G. Pelossof, et al. Anal. Chem. 82 (2010) 4396.
[89] P. Travascio, et al. Chem. Biol. 5 (1998) 505.
[90] J. Kosman, B. Juskowiak, Anal. Chim. Acta 707 (2011) 7.
[91] C. Wang, et al. Analyst 136 (2011) 4295.

Materials Today • Volume 16, Numbers 7/8 • July/August 2013

ELSEVIER

Uncovered

Ball of string

Warwar and Silverstein take a close look at porous shape memory polymers

Christine Warwar* **and Michael S. Silverstein**

Department of Materials Science and Engineering, Technion – Israel Institute of Technology, Haifa, Israel

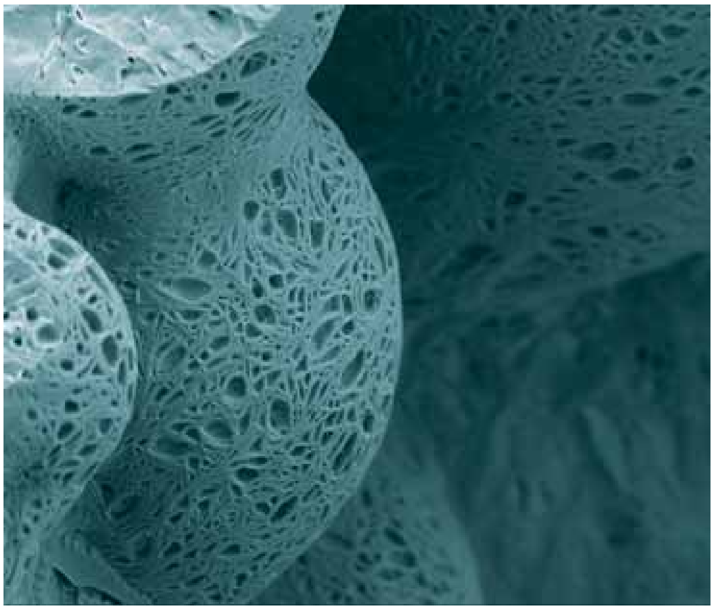

Shape memory polymers (SMPs) have the ability to return from an imposed deformed shape to their original shape when prompted by an external trigger such as temperature, pH, moisture, light, or magnetic field. Thermally activated SMPs usually contain two elements: a reversible transition which acts as a molecular switch and is responsible for maintaining the imposed deformed shape and a restoration mechanism which is responsible for restoring the original shape. The reversible transition could be a glass transition temperature or a melting point (T_m). The restoration mechanism could be physical or chemical crosslinking or could be a phase whose transition temperature is higher than the reversible transition temperature. Compared to fully dense SMPs, porous SMPs can achieve higher temporary deformations and exhibit higher deformations when they recover their permanent shape.

PolyHIPEs are crosslinked polymers with emulsion-templated porous structures that are synthesized within the continuous, external phase of high internal phase emulsions (HIPEs) [1,2]. In HIPEs, which are usually highly viscous, the dispersed, internal phase constitutes more than 74% of the volume. Mayonnaise, for example, is an oil-in-water HIPE. The HIPEs for polyHIPE synthesis are usually formed by the slow dropwise addition of the internal phase to the external phase under constant stirring. The HIPE is usually stabilized using an amphiphilic surfactant which is only soluble in the continuous, external phase. Pickering HIPEs are HIPEs that are stabilized using amphiphilic nanoparticles (NPs) which preferentially migrate to the oil-water interface, replacing the surfactant. The NPs used to stabilize Pickering HIPEs can also serve as crosslinking centers, replacing the crosslinking comonomer [3]. Typically, polyHIPEs are based upon the polymerization at elevated temperatures of hydrophobic monomers and crosslinking comonomers within the continuous phase of water-in-oil (w/o) HIPEs. A free radical polymerization (FRP) initiator is either added to the organic phase, for organic-phase initiation, or is added to the aqueous phase, for interfacial initiation. Both the structure and properties of polyHIPEs from Pickering HIPEs have been shown to be strongly dependent upon the locus of initiation [4,5]. Evacuating the internal phase through the multiple holes that develop in the polymer walls during polymerization leaves voids in place of the internal phase droplets and produces polymers with highly interconnected porous structures.

Recent work has shown that porous SMP polyHIPEs based on acrylates and methacrylates that bear long, crystallizable, aliphatic side-chains can be synthesized within NP-stabilized w/o Pickering HIPEs (where the NPs also serve as crosslinking centers) using organic-phase initiation [6]. PolyHIPEs based on stearyl acrylate (A18, $T_m \sim 33\ ^\circ C$) with crystallizable $C_{18}H_{37}$ side-chains were synthesized by heating the external phase to above the T_m before adding the internal phase in a dropwise fashion. The

---

*Corresponding author: Warwar, C. (chrisw@tx.technion.ac.il), Silverstein, M.S. (michaels@tx.technion.ac.il)

1369-7021/06/$ - see front matter © 2013 Elsevier Ltd. All rights reserved. http://dx.doi.org/10.1016/j.mattod.2013.07.006

A18-based polyHIPEs exhibited SMP properties of interest, maintaining the new shape imposed by a compressive strain of 70% and then exhibiting recoveries of around 90% for multiple cycles. The next stage in the investigation involved: (a) synthesizing polyHIPEs based on behenyl acrylate (A22, $T_m \sim 45\ ^\circ C$) with crystallizable $C_{22}H_{45}$ side-chains within almost identical NP-stabilized w/o Pickering HIPEs (where the NPs also serve as crosslinking centers); (b) synthesizing both A18- and A22-based polyHIPEs using interfacial initiation. The resulting porous structures of the A18- and A22-based polyHIPEs synthesized using interfacial initiation were quite unusual.

This month's cover shows a high-resolution scanning electron microscope image of spherical polymer protuberances ($\sim 40\ \mu m$ in diameter) with a thread-like ''ball of string'' texture. The spherical protuberances seem to have been exuded from the polyHIPE walls into the internal phase droplets. This exact structure was only found for A22-based polyHIPEs synthesized within NP-stabilized w/o Pickering HIPEs (where the NPs also serve as crosslinking centers) using interfacial initiation. In A18-based polyHIPEs synthesized using interfacial initiation, spherical polymer protuberances ($\sim 40\ \mu m$ in diameter) with smooth surfaces seem to have been exuded from the walls into the internal phase droplets. No such protuberances were found for A18- and A22-based polyHIPEs synthesized using organic-phase initiation. No such protuberances were found for similar polyHIPEs synthesized using interfacial initiation of acrylates whose T_m was below room temperature. Interestingly, no such protuberances were found for the A18- and A22-based polyHIPEs that were synthesized using interfacial initiation from an internal phase that was heated before its addition to the heated external phase.

The formation of these spherical protuberances seems to depend upon the presence of crystallizable side-chains with a T_m above room temperature, the use of interfacial initiation, and the addition of a room temperature internal phase to a heated external phase. These factors combine to create a situation in which the HIPE begins to destabilize before the polymerization and crosslinking have ''set'' the wall structure. The crystallization of the monomer surrounding the room temperature internal phase droplet seems to prevent interfacial initiation and delay polymerization and crosslinking. In addition, this crystallization seems to encompass the stabilizing NPs, reducing, if not eliminating, their mobility, and allowing a fluid instability to develop at the oil-water interface. The delay in the polymerization that ''sets'' the wall structure and the generation of a fluid instability do not occur when a monomer with a T_m below room temperature is used or when a heated internal phase is used. Since the monomer does not crystallize in these cases, the initiator and the stabilizing NPs can perform their respective functions. The delay in the polymerization that ''sets'' the wall structure does not occur when organic-phase initiation is used since the initiation occurs throughout the wall and is not restricted to the interface. The tendency towards phase inversion/phase separation of a system in which the continuous phase is only around 15% of the HIPE, the high interfacial tension, and the high interfacial curvature result in the exudation of spherical protuberances from the continuous external phase into the droplets of the dispersed internal phase. When polymerization finally does occur, the partially destabilized HIPE structure becomes ''set'' and the spherical polymer protuberances are the result.

Further reading

[1] M.S. Silverstein, et al., Encyclopedia of Polymer Science and Technology - Online, Wiley, 2010, http://dx.doi.org/10.1002/0471440264.pst571.

[2] M.S. Silverstein, Progress in Polymer Science, in press (2013). DOI:10.1016/j.progpolymsci.2013.07.003.

[3] I. Gurevitch, et al. Macromolecules 45 (2012) 6450.

[4] S. Livshin, et al. Macromolecules 41 (2008) 3930.

[5] T. Gitli, et al. Soft Matter 4 (2008) 2475.

[6] I. Gurevitch, et al. Soft Matter 8 (2012) 10378.

Events Diary

If you are organizing a future conference or workshop and would like to have it listed in *Materials Today* please contact Lucy Rodzynska – lucy.rodzynska@elsevier.com

---

MNE 2013
16 September 2013 – 19 September 2013
London

MNE is a major annual international conference, devoted to micro and nano fabrication and manufacturing, held in a European country every September.

http://www.mne2013.org/

Metamaterials 2013
16 September 2013 – 19 September 2013
Bordeaux, France

This Congress follows the success of Metamaterials 2007-2012 and continues the traditions of the highly successful series of International Conferences on Complex Media and Metamaterials (Bianisotropics) and Rome International Workshops on Metamaterials and Special Materials for Electromagnetic Applications and TLC.

http://congress2013.metamorphose-vi.org/
http://congress2013.metamorphose-vi.org/

AMWC 2013
16 September 2013 – 19 September 2013
Çesme, Turkey

Advanced Materials World Congress. The goal of congress is to provide a global platform for researchers and engineers coming from academia and industry to present their research results and activities in the field of materials science and engineering with a special attention on interdisciplinary research of advanced materials.

http://amwc2013.org/

NAP2013 International Conference "Nanomaterials: Applications & Properties' 2013"
16 September 2013 – 21 September 2013
Alushta, the Crimea, Ukraine

The conference is devoted to new actual problems of modern material science, such as technology of nanomaterial production and research; properties of nanoparticles and nanosystems. The conference is also focused on the applications of nanoobjects and nanostructured matters in hi-tech industry, biology, medicine, chemistry, etc.

http://www.nap.sumdu.edu.ua/index.php/nap/nap2013

CNPComp2013 6th International Conference on carbon nanoparticle based composites
22 September 2013 – 25 September 2013
Dresden, Germany

The conference shall gather the international scientific community working in the field of carbon nanotube, graphene, or other nanocarbon filled composites. The conference provides the forum where the latest results and findings in the field will be presented and offers researchers from both academic institutions and industry a great opportunity to exchange knowledge, make contacts and engage in discussions.

http://www.ipfdd.de/CNPComp2013.2320.0.html

Gettering and Defect Engineering in Semiconductor Technology (GADEST) XV
22 September 2013 – 27 September 2013
Oxford, UK

The GADEST conference series was established in 1985 by Hans Richter as a meeting of experts in the field of semiconductor technology, semiconductor devices and semiconductor defect physics.

http://www.gadest.org/

ICON 2013 5th International Conference on One dimensional Nanomaterials
23 September 2013 – 26 September 2013
Annecy, France

This conference aims to provide an overview of the most recent advances in one-dimensional nanostructures (nanowires, nanotubes...) made of semiconductor or metal materials. A broad range of subjects will be covered, from materials science to basic physics and device applications. Particular attention will be devoted, but not limited to: - Fabrication - Nanoelectronics - Photonics - Spintronics - Sensors - Hybrid structures - Energy storage and conversion. Transverse subjects such as modelling and advanced characterization techniques will also be address

http://www.icon2013.fr/

Optics of Liquid Crystals
29 September 2013 – 04 October 2013
Hololulu, Hawaii, U.S

As the world's leading conference in optics and photonics of liquid crystals, the 2013 Optics of Liquid Crystals (OLC 2013) in Honolulu, Hawaii, USA will provide a venue for intellectual and enlightening discussions of ideas at the emerging and frontier of liquid crystal science and technology in optics, photonics and displays

http://www.lcinet.kent.edu/conference/19/index.php

NDT 2013
07 October 2013 – 10 October 2013
Calgary, Alberta, Canada

The meeting will cover new developments of smart and nano materials properties, smart structures and systems; Structural Health Monitoring (SHM) with various types of sensors, actuators and control monitoring systems; NDE technologies; new applications and approaches for energy harvesting, vibration control and medical applications as well as new developments for dampers, transducers and ultrasonic techniques. Participants will include all the stakeholders of smart technologies, SHM and NDE in Canada from Research Centers to industries to Universities. There will be special focus on topics relating to the energy industry.

http://events.cinde.ca/

ICNNN 2013
19 October 2013 – 20 October 2013
Jeju, Korea

The 2nd International Conference on Nanostructures, Nanomaterials and Nanoengineering (ICNNN 2013) conference is an international forum for the presentation of technological advances and research results in the fields of Nanostructures, Nanomaterials and Nanoengineering.

http://www.icnnn.org/

MS&T 2013
27 October 2013 – 31 October 2013
Montreal, Quebec Canada

The MS&T partnership of ACerS, AIST, ASM, MetSoc and TMS brings together scientists, engineers, students, suppliers and more to discuss current research and technical applications, and to shape the future of materials science and technology.

http://www.matscitech.org/

ISIEM 2013
27 October 2013 - 31 October 2013
Rennes, France

The main aim of the 2nd International Symposium on Inorganic and Environmental Materials 2013 (ISIEM 2013) is to enhance the research collaboration and foster the newest research and technologies on inorganic materials related to the theme of global environment.

http://isiem2013.sciencesconf.org/NTRC/hamdiy/news/icnma2013.htm

---

ICPMSE 2013
14 November 2013 – 15 November 2013
Venice, Italy

The XXXIV. International Conference on Polymer Materials Science and Engineering aims to bring together leading academic scientists, researchers and scholars to exchange and share their experiences and research results about all aspects of Polymer Materials Science and Engineering, and discuss the practical challenges encountered and the solutions adopted.

https://www.waset.org/conferences/2013/italy/icpmse/

Materials Today Virtual Conference: Biomaterials
19 November 2013 – 21 November 2013
An online only event

At the interface between the life sciences and physical sciences, biomaterials is at the forefront of 21st century research; and so, Materials Today is delighted to announce that our next Virtual Conference will focus on biomaterials.

http://www.materialstoday.com/virtualconference/materials-today-virtual-conference-biomaterials-2013

MRS Fall Meeting & Exhibit 2013
01 December 2013 – 06 December 2013
Hynes Convention Center, Boston, MA, USA

The increasingly cross-disciplinary worldwide activity in materials research manifests itself every year in the MRS Fall Meetings. Featuring over 50 symposia and attended by as many as 6,000 researchers from every corner of the globe, the annual Fall Meeting in Boston's Hynes Convention Center and Sheraton Boston Hotel is the preeminent annual event for those in the field of materials research.

http://www.mrs.org/fall2013/

3rd Nano Today Conference 2013
08 December 2013 – 11 December 2013
Biopolis, Singapore

Organized by the Institute of Bioengineering and Nanotechnology and Nano Today, this international conference seeks to bring together researchers interested in nanoscience and nanotechnology. The conference will present the latest research at the multidisciplinary frontier of nanostructured materials and devices.

http://www.nanotoday2013.com/

Composites 2014
18 February 2014 – 18 February 2014
San Antonio, TX

COMPOSITES is the industry's premier event and the most diverse exhibition/convention of its kind in North America. As a unique, one-stop chance to do business, learn and network, it has a long track record of proven benefits for its participants. With a bottom-line emphasis on the future, all net revenues are reinvested back into the American Composites Manufacturers Association to fund its efforts to support you, your company and our industry.

http://www.eventsinamerica.com/events/composites-2014/ev5022b5522c1d1/

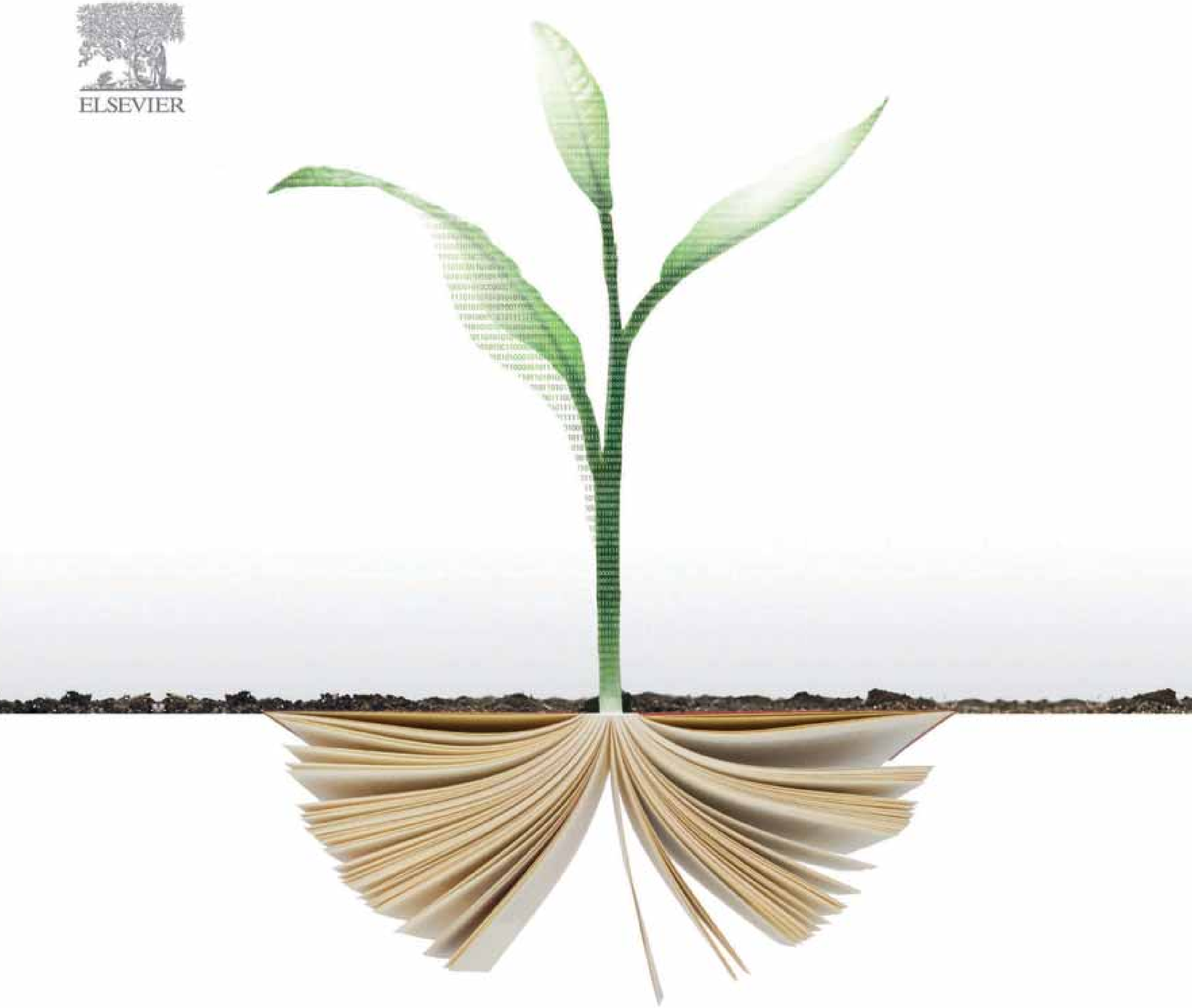

Need support with your English?

Elsevier Language Editing Services offer high-quality English language editing for researchers preparing articles for publication in international scientific and medical journals.

Elsevier's editorial expertise and long history of publishing peer-reviewed journals will ensure that the English language in your manuscript is clear and free of distracting errors before you submit.

visit us at **webshop.elsevier.com**

- Native English speakers from top universities
- Expert input from Ph.D.s or Ph.D. candidates matched to your field of study
- Your manuscript edited to professional scientific English (US or UK)
- Self-service website with easy article upload and retrieval
- Short turn-around time of 5 business days

ELSEVIER
WebShop

Customer comments

"...I am very grateful to you for helping me. The manuscript which you revised for me is excellent. Thanks a lot!" PhD. Qingyu Guan

Journal Editors' comments

"...my current view is that the author should take as many steps as possible to make their article right before it is submitted..."

"Poor English is a worrying problem, especially when the scientific work is novel and deserves publication."

"... authors have to be responsible for ensuring at least reasonable language."

ELSEVIER


materialstoday
materialstoday
materialstoday
materialstoday


the latest information direct to your desktop...
materialstoday

ELSEVIER

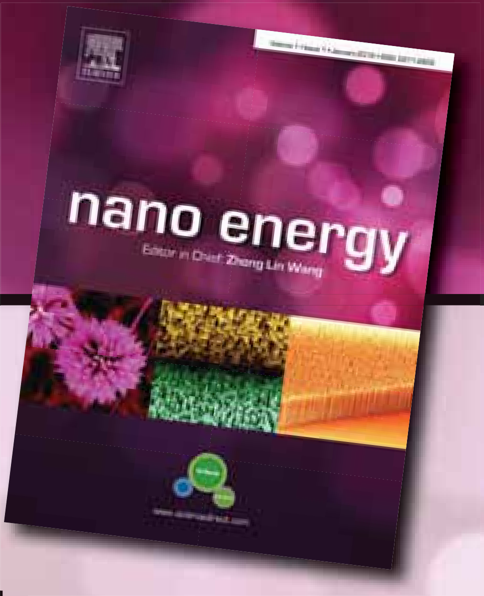

Nano Energy

publishes original experimental and theoretical research on all aspects of energy-related research which utilizes nanomaterials and nanotechnology. Manuscripts of four types are considered: review articles which inform readers of the latest research and advances in energy science; rapid communications which feature exciting research breakthroughs in the field; full-length articles which report comprehensive research developments; and news and opinions which comment on topical issues or express views on the developments in related fields.

The editors welcome contributions on a variety of topics such as:
Batteries | Fuel Cells | Hydrogen generation and storage | Light emitting diodes | Optoelectronic devices for efficient energy usage | Photovoltaics | Piezoelectric nanogenerators | Policy and perspectives in energy | Self-powered nanodevices/nanosystems | Supercapacitors | Thermoelectrics

'Research in energy will be at the core of science and technology for decades to come, and will affect the quality of life for every one of us. My intention is that the journal of Nano Energy will become a leading platform to communicate global research in green and sustainable energy using nanomaterials and nanotechnology.'

Z.L. Wang, *Editor-in-Chief*
School of Materials Science & Engineering,
Georgia Institute of Technology, 500 10th Street NW,
Atlanta, GA 30332, USA, Email: zhong.wang@mse.gatech.edu

Submit your paper today

www.nanoenergyjournal.com